Schweizerische Eidgenossenschaft
Confédération suisse
Confederazione Svizzera
Confederaziun svizra

Federal Department of the
Environment, Traffic, Energy and Communications DETEC

Swiss Federal Office of Energy

Final report 1 May 2014

SOL-HEAP
Solar and Heat Pump Combisystems

SOL-HEAP
Solarthermie-Wärmepumpen-Kombisysteme

Contracting body:

Swiss Federal Office of Energy SFOE
Research Programme Solar Heat and Heat Storage
CH-3003 Bern
www.bfe.admin.ch

Contractor:

Institut für Solartechnik SPF
Hochschule für Technik Rapperswil HSR
Oberseestrasse 10
CH-8640 Rapperswil
www.solarenergy.ch

Authors:

Michel Yves Haller, Institut für Solartechnik SPF, michel.haller@solarenergy.ch
Robert Haberl, Institut für Solartechnik SPF, robert.haberl@solarenergy.ch
Daniel Carbonell, Institut für Solartechnik SPF, dani.carbonell@solarenergy.ch
Daniel Philippen, Institut für Solartechnik SPF, daniel.philippen@solarenergy.ch
Elimar Frank, Institut für Solartechnik SPF, elimar.frank@solarenergy.ch
Mit Beiträgen von Andreas Reber, Hauke Hirsch, Simon Zimmermann, Sabrina Gemperle, und Félix Hantzsche

Acknowledgements:

The collaboration with Elektrizitätswerke Rapperswil-Jona AG , Hoval AG , Energie Solaire SA, Viessmann Werke GmbH & Co KG, H+S Solar, and Soltop Schuppisser AG within this project is gratefully acknowledged.

SFOE Head of domain: Andreas Eckmanns
SFOE Programme manager: Jean-Christophe Hadorn
SFOE Contract number: SI/500494-01

Zusammenfassung

Im Projekt SOL-HEAP wurden von 2010 bis 2014 Solarthermie-Wärmepumpen-Kombisysteme für die Bereitstellung von Raumwärme und Warmwasser in Einfamilienhäusern untersucht. Die Aufgaben beinhalteten: Eine systematische Klassifizierung und Kennzahlen für die Effizienz der verschiedenen Systemkonzepte zu erarbeiten; Den Nutzen der Verwendung von Solarwärme für den Verdampfer der Wärmepumpe (serielle Wärmenutzung) zu untersuchen; Komponenten im Labor zu testen und Simulationsmodelle weiter zu entwickeln; Und die energetische Effizienz verschiedener Solar-Wärmepupen-Systeme mittels Jahressimulationen zu vergleichen. Ein wesentlicher Bestandteil war zudem die Entwicklung und Anwendung von Systemtest-Verfahren mit dem Hardware-in-the-Loop Konzept (Concise Cycle Test Methode). Die Arbeiten des SOL-HEAP Projektes waren zudem Bestandteil des Solar Heating and Cooling Task 44 / Heat Pump Programme Annex 38 (Task 44 / Annex 38) "Solar and Heat Pump Systems" der Internationalen Energieagentur (IEA).

Die systematische Klassifizierung und die Definition von Effizienz-Kennzahlen für Solar-Wärmepumpen-Systeme wurden in enger Zusammenarbeit mit anderen europäischen Forschungsinstitutionen ausgearbeitet. Diese Arbeiten sind in den Task 44 / Annex 38 eingeflossen, und haben inzwischen international breite Anwendung gefunden.

Mit der thermodynamische Analyse der seriellen Kollektorwärmenutzung konnte auf mathematischem Weg gezeigt werden, dass die serielle Kollektorwärmenutzung nicht generell vorteilhaft ist für die Effizienz von Solar-Wärmepumpen Systemen mit zwei Quellen Wärmepumpen.

Messungen an unabgedeckten Absorbern haben gezeigt, dass der Einfluss der Neigung auf die Wärmegewinne bei Betrieb unterhalb der Umgebungstemperatur bei Nacht signifikant sein kann. Der Einfluss war jedoch nicht auf eine Erhöhung der konvektiven Wärmegewinne bei stärkerer Neigung zurückzuführen, sondern auf eine Erhöhung der langwelligen Gegenstrahlung der Umgebung. Modelle für die Simulation von Solarkollektoren wurden erweitert, um Kondensationswärmegewinne zu berücksichtigen, wenn die Absorbertemperatur unterhalb des Taupunkts der Luft ist. Für die Simulation von Wärmepumpen wurden sowohl ein semi-physikalisches Modell als auch ein Parameter-Fit Modell weiter entwickelt und angewendet.

Systemsimulationen zeigten die sehr grosse Abhängigkeit der Systemeffizienz von vielen beeinflussenden Faktoren. Wie zu erwarten war sind unter diesen Einflussfaktoren das Klima, insbesondere die im Winter verfügbare Solarstrahlung, sowie das Temperaturprofil des Wärmebedarfs. Weitere, weniger offensichtliche, Einflussfaktoren sind die hydraulische Integration und Regelung der Wärmepumpe, insbesondere in Kombination mit Kombispeicher, Zeitfenster für die Warmwasser-Nachheizung durch die Wärmepumpe, Thermostatventile in der Raumheizungsverteilung, Legionellenschaltungen, und andere. Die Simulationen zeigen, dass die System-Jahresarbeitszahl einer Wärmepumpen-Heizung massiv erhöht werden kann durch die Kombination mit einer Solaranlage mit Kombispeicher, wenn die Hydraulik und Regelung richtig ausgeführt wird. Luft-Wasser Wärmepumpen erreichten in Kombination mit Solarwärme Jahresarbeitszahlen welche in der Grössenordnung von Erdsonden-Wärmepumpen ohne Solaranlagen liegen. Erdsonden-Wärmepumpen mit Solaranlagen wiesen die höchste Effizienz auf. Ein System mit nur Solarkollektoren in Kombination mit einem grossen Eisspeicher als Wärmequelle für die Wärmepumpe erreichte Jahresarbeitszahlen in der Grössenordnung von Erdsonden-Wärmepumpen mit paralleler Solarwärmenutzung. Für dieses serielle Konzept konnte gezeigt werden, dass die Effizienz durch die Berücksichtigung von Wettervorhersagen für die Regelung der Speicherbe- und entladung signifikant erhöht werden kann.

Die Weiterentwicklung der Concise Cycle Test Methode für die Anwendung auf Wärmepumpen-Systeme ermöglichte das Testen von insgesamt elf Solar-Wärmepumpen-Systemen im Labor. Diese beinhalteten sowohl parallele Konzepte mit Erdsonden oder mit Luft als Wärmequelle der Wärmepumpe, als auch parallel/serielle Konzepte welche Solarwärme zusätzlich oder als einzige Quelle verwendeten. Die Resultate dieser Tests ermöglichten eine energetisch end exergetische Analyse der Effizienz dieser Systeme, welche den Herstellern kommuniziert wurde und zu Verbesserungen und Weiterentwicklung von Speichern, Hydraulik, und Regelkonzepten führten.

Abstract

Within the SOL-HEAP project solar thermal and heat pump combinations for space heating and domestic hot water supply of single family homes were investigated from 2010 to 2014. The tasks that were performed included systematic analysis and classification of system concepts, the definition of performance indicators, analysis of solar heat as a source for heat pump evaporators (series heat use), analysis of components for solar and heat pump systems by laboratory measurements, further development of component models for annual performance simulations, solar and heat pump system simulations, and further development and application of whole system test methods based on a hardware-in-the-loop concept (Concise Cycle Test method). Results of the SOL-HEAP project contributed to a large extent to the success of the International Energy Agency's Solar Heating and Cooling Programme's Task 44 / Heat Pump Programme Annex 38 (Task 44 / Annex 38).

The systematic classification and the definition of performance figures for solar and heat pump systems has been elaborated in close collaboration with other European research institutes, and has also been adopted by Task 44 / Annex 38 and has thus become a state of the art for the analysis of solar and heat pump systems.

The thermodynamic analysis of series collector heat use provided for the first time a mathematically sound explanation for the fact that series heat use is not always advantageous for the overall performance of systems with dual source heat pumps.

Measurements that were performed on uncovered solar absorbers showed that the influence of absorber inclination on heat gains at night may be significant, but must be attributed to differences in long wave irradiance rather than to the natural convection on the absorber surface. Collector models were adapted in order to include heat gains from water vapour condensation when the absorber surface is below the dew point of the air, and both grey-box semi-physical heat pump models as well as parameter-fit heat pump models were further developed in order to include additional physical phenomena and possibilities for annual simulations.

System simulations showed above all the high dependency of the energetic performance of solar and heat pump systems on many boundary conditions. Among the more obvious influencing boundary conditions are the climate, in particular solar irradiation in winter months, the temperature level of the heat demand, and the share of domestic hot water in the total heat demand. Other boundary conditions that may be of equal importance (but less obvious) are the hydraulic integration and control of the heat pump, in particular in combination with solar combistorage tanks, time-windows for charging of domestic hot water by the heat pump, the control of the space heat distribution, legionella safety heater settings, and others. For well-designed systems with combistorage, it is shown that the seasonal performance factor increases substantially when solar collectors are added to a heat pump system. Air source and solar heat pump combinations reach seasonal performance factors in the same range as ground source heat pumps without solar, while the ground source heat pump and solar combinations are the most efficient solution that was found. An exclusively solar source system with large collector areas and large ice storage may reach seasonal performance factors in the same range as ground source and solar systems. For these series systems with large ice storage it was shown that the system performance may be improved significantly using weather forecast for the control of storage charging and discharging.

The further development of the Concise Cycle Test method was the base for testing a total of eleven solar and heat pump systems in the laboratory, including parallel system concepts for ground source and air source systems, as well as parallel/series system concepts that used solar as the only source, and a combination of parallel/series solar thermal heat use with an additional air source heat exchanger. The test results provided valuable insights into the energetic and exergetic performance of the system concepts that were communicated to the manufacturers of the systems and lead to improvements and further developments of storage tanks, hydraulic solutions, and control of the systems.

Table of Contents

1 Introduction

1.1 Solar and heat pump systems

Solar thermal systems and heat pumps are increasingly used throughout Europe for the preparation of domestic hot water (DHW) and space heat. With the combination of both technologies it is possible to cover heat demand over the whole year with a low primary energy effort that goes along with a substantial reduction of CO_2 emissions in comparison to systems that are operated with fossil fuels or with direct electric heating. The remaining demand of electricity for the operation of the heat pump and other components of the system is generally also the main contributor to the residual primary energy demand and CO_2-intensity of these systems. Therefore, the main target for system optimization is to further reduce the demand for electricity and to increase the seasonal performance factor, i.e. the ratio of heat delivered divided by electricity used. A combined system with solar thermal collectors and heat pumps may increase the seasonal performance factor of the system - compared to a system with only a heat pump - substantially, because solar thermal collectors are able to deliver about ten times more heat per electric input as heat pumps. However, solar thermal collectors rely on the solar resource that is abundant in summer, but insufficient for covering the full heat load in winter, whereas heat pumps can provide heat reliably over the whole year and independent from the temporal distribution of sunshine. Therefore, it is easy to cover the heat demand with a heat pump alone, but a 100% solar coverage is only possible with large collector fields and larger thermal energy storage, and the respective costs for these components.

In a classical combination of solar thermal collectors and heat pumps either solar collectors or the heat pump deliver heat to a warm storage for DHW and/or space heating, or directly to the heat distribution system. The two components are thereby arranged in a parallel manner, which means that it is not possible to use heat from solar collectors also as a source for the evaporator of the heat pump. In recent years, a number of systems have been introduced into the market in which solar heat is additionally or even exclusively used for the evaporator of the heat pump, or solar heat is used for de-icing of air source units of heat pumps.

Based on the knowledge that was available at the beginning of this project, it was difficult to make reliable performance estimations for parallel concepts, and there was no knowledge for the performance estimation of series concepts where solar heat is used as a heat source for the heat pump. For this reason, several research institutes together with industry have collaborated within the IEA SHC Task 44 / HPP Annex 38[1] (T44A38, http://task44.iea-shc.org/), in order to investigate solar and heat pump systems systematically from a theoretical and practical point of view. Results presented in this report were carried out by the Institut für Solartechnik SPF within the SOL-HEAP project as a contribution to T44A38.

[1] International Energy Agency (IEA) Solar Heating and Cooling Programme (SHC) Task 44 and Heat Pump Programme (HPP) Annex 38 "Solar and Heat Pump Systems", from 2010 – 2013, see http://task44.iea-shc.org/

1.2 Goals of the present study

The goal of the present work was to contribute to a better understanding of solar combisystems that are combined with heat pumps, and to create knowledge in particular about parallel system concepts and how these can be further improved and exploited. The following tasks were defined at the beginning of the project:

1. Creating a ***systematic classification*** for solar and heat pump systems from a technical point of view.
2. Developing a ***TRNSYS simulation environment*** for solar and heat pump systems with a semi-physical heat pump model that is able to simulate the refrigerant cycle.
3. Carrying out ***dynamic system simulations*** for solar and heat pump systems, and creating recommendations for the hydraulic connections and requirements for components within the system (collectors, heat pumps, storage, and control).
4. Developing a ***test method and test bench*** for carrying out hardware in the loop tests of solar and heat pump systems based on the Concise Cycle Test (CCT) method that has been developed at SPF.
5. Carrying out ***system tests*** with the CCT method for the determination of seasonal performance factors (SPF) of the whole system that reflect the performance of real-life installations.

1.3 Structure and content of the report

This report starts with the introduction of classification schemes that are used later for distinguishing between different system concepts for the combination of solar thermal collectors with heat pumps (section 2.1). The definitions of performance factors for the systems given in section 2.3 are in agreement with T44A38 and are equally used in other chapters of this report. Section 3 contains a thermodynamic analysis of the option to use solar heat for the evaporator of the heat pump in systems where the heat pump may also use another heat source than solar, and where the solar heat may also be used directly at the temperature level of the final heat demand. Measurements performed on heat pumps, on solar collectors, and on a small ice-storage laboratory prototype are reported in section 4, together with the work on simulation models for heat pumps and solar thermal collectors. The analysis of monitoring results from an air source and solar heating system in Rapperswil/Switzerland carried out by the authors are presented in section 5. Several simulation studies have been performed for different system concepts and with different objectives. The results provide valuable information on the integration of solar combistorages into systems with heat pumps (6.3), on the performance of parallel systems for DHW and space heating in different climates (6.5, 6.5.2), on the potential for series heat use evaluated based on simulations (6.6), on systems that use solar collectors as the only heat source in combination with a large, ground buried, ice-storage (6.7) and on the use of weather forecast for the control of these systems (6.8). Test methods and results from whole system hardware in the loop testing with the CCT method are presented in section 7, and section 8 summarizes the conclusions of the overall project. A list of dissemination activities that were carried out within the project, mainly conference papers and oral presentations, can be found in the Annex.

2 Systematic classification and performance figures

A systematic classification of solar and heat pump system concepts has been elaborated together with international experts from T44A38 and presented at the ISES EuroSun 2010 conference in Graz (Frank et al. 2010). A short summary is given here, details can be found in the cited reference. Performance figures for the evaluation of solar and heat pump systems were also elaborated with partners from T44A38 (Malenkovic 2013).

2.1 Energy flow charts, letter codes, and P/S/R classification

2.1.1 The energy flow chart

The energy flow chart of T44A38 is based on similar flow charts that are frequently used in building energy engineering. Instead of a whole building, only the heating system is illustrated (see Figure 2.1). Final energy flows (that have to be purchased, like electricity or natural gas) are shown at the system boundary to the left, useful energy flows like space heating and domestic hot water (DHW) to the right. Environmental energy sources such as ambient air are shown at the upper part (green fields). Losses may or may not be shown leaving the system downwards. A label for the manufacturer's name and the system type is introduced in the lower left part.

Any components or energy sources/sinks that are not present or used in a system are also displayed via placeholders, but not highlighted. The different colours are used to distinguish between final (grey), environmental (green) and useful (red) energy as well as energy converters (orange) and storages (blue).

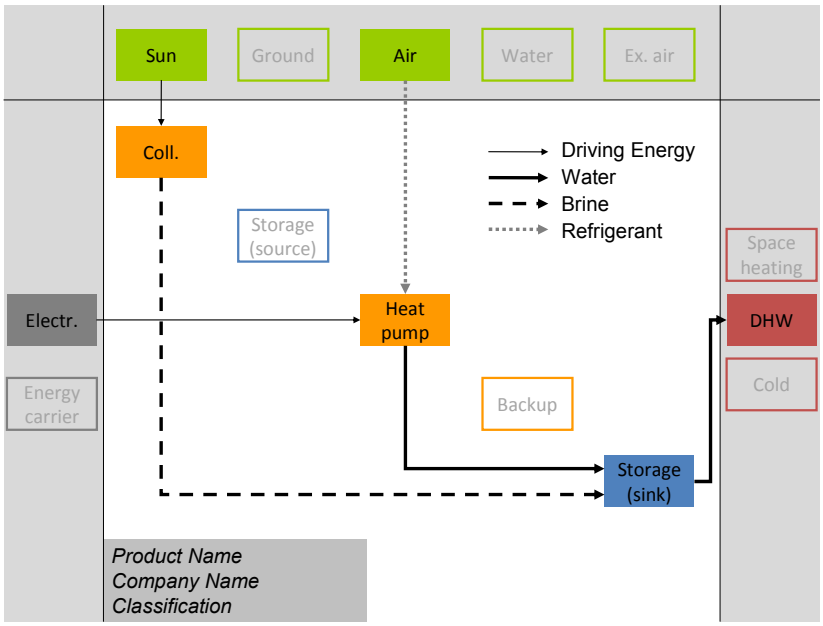

Figure 2.1: Energy flow chart scheme of the IEA SHC Task 44 / HPP Annex 38.

Lines with arrow-heads are introduced to visualize the energy flows that may occur in the depicted system. Each line style refers to the energy carrier. The line widths are indifferent, and thus not representing for example the quantity of transported energy. Finally, it is of

great importance to understand that any system is represented by exactly one flow chart. This means that no specific operating mode is shown but all operating modes that occur within the represented system are depicted simultaneously. Figure 2.2 and Figure 2.3 present energy flow charts for different system concepts.

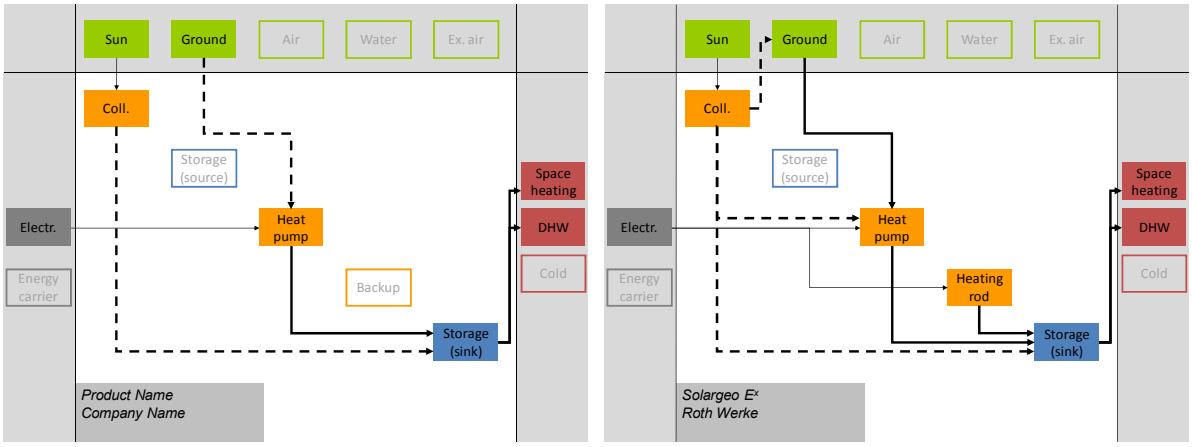

Figure 2.2: Typical energy flow charts with combi-store (left) and "Solargeo E^x" by Roth Werke (right).

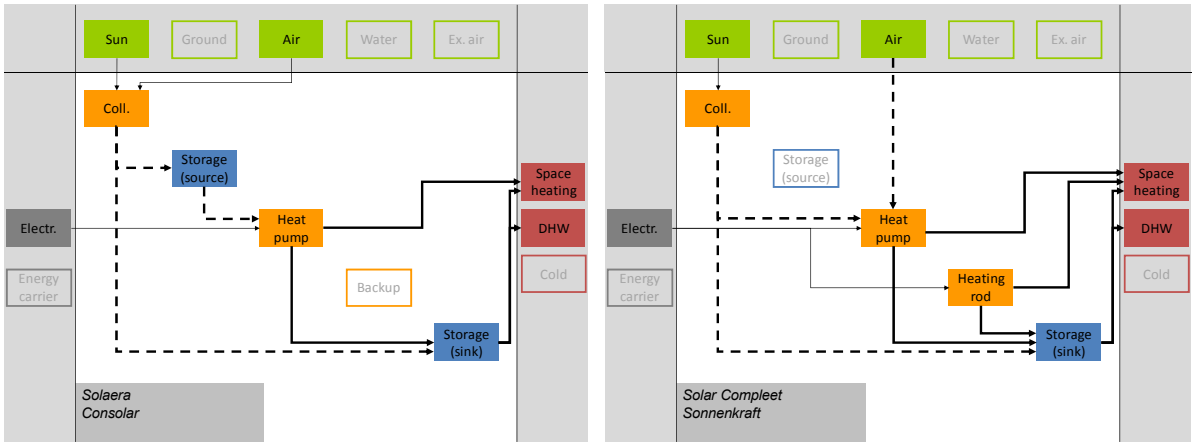

Figure 2.3: Energy flow charts for "Solaera" by Consolar (left) and "Solar Compleet" by Sonnenkraft (right).

2.1.2 The letter code

With the exception of backup heating, the information comprised in the schematics presented in Figs. 1 to 3 can also be denoted in letters with the abbreviation code shown in Table 2 and the convention that the sources and sinks of the solar collector (S) and the heat pump (HP) are indicated with superscripts (sources) and subscripts (sinks) around the abbreviation SHP which stands for *solar and heat pump*:

$$ {}^{sources}_{sinks}SHP^{sources}_{sinks} $$

Table 2.1: Abbreviations used for transferring the system information into a letter code.

S	solar collector	Air	air	srS	source storage (usually cold)
HP	heat pump	G	ground	skS	sink storage (usually hot)
Sol	solar irradiation	W	ground water	SH	space heat (directly)

With this way of notation, the systems shown in Figure 2.1 to Figure 2.3 would be denoted as follows:

Figure 2.1:	${}^{Sol}_{skS}SHP^{Air}_{skS}$		
Figure 2.2 (left):	${}^{Sol}_{skS}SHP^{G}_{skS}$	Figure 2.2 (right):	${}^{Sol}_{skS,G,HP}SHP^{G,S}_{skS}$
Figure 2.3 (left) :	${}^{Sol,Air}_{srS,skS}SHP^{srS}_{skS,SH}$	Figure 2.3 (right):	${}^{Sol}_{skS,HP}SHP^{Air,S}_{skS,SH}$

2.1.3 Parallel, series, and regenerative (P/S/R), single and dual source heat pumps

The interaction between collector and heat pump has been used for a general classification as “parallel” or “series” system concepts already in previous studies (Freeman et al. 1979; Trinkl et al. 2004; Citherlet et al. 2008). After analysing many systems that combine solar collectors and heat pumps, and considering these previous classification approaches, the following classification scheme has been introduced for T44A38 and is used in this report:

- ***Parallel (P)***: Solar collectors and the heat pump are hydraulically connected in a parallel manner, i.e. it is not possible to use solar heat for the evaporator of the heat pump, and consequently the heat pump always uses a heat source other than the solar collectors.
- ***Series (S)***: The heat pump uses solar heat for the evaporator.
- ***P/S:*** In a ***Parallel/Series*** concept, both ways of using collector heat are possible, either directly to serve the load or for storage on the hot side of the heat pump (P), or for the evaporator of the heat pump (S).
- ***Regenerative (R)***: if the main source of the heat pump is a ground heat exchanger, solar heat can be used to regenerate the ground or another heat source of the heat pump.
- ***P/R:*** in a ***Parallel/Regenerative*** system, both direct collector heat use as well as ground regeneration are possible.

Other combinations of P/S and R exist. For systems that e.g. include a series (S) operation mode, a further classification can be made according to the ability of the heat pump to use only one heat source or two different heat sources:

- ***Single source*** heat pumps use only heat from one source. In a series system this is the solar collector, and the concept may also be called a "***solar only***" heat source concept. Although some collectors do not only use solar heat directly but also heat from the ambient air when operated below the temperature of the ambient air, this is still considered to be a single source concept.
- ***Dual source*** heat pumps use two different heat sources, one of them usually being the solar collectors. The other heat source may be ambient air, ground heat or another heat source.

System concepts may feature more than one of these options as the options do not exclude each other. This non-hierarchical or exclusive structure is the main reason why a tree structure is regarded unsuitable for classification.

2.2 Identical boundary conditions for system comparison

Performance figures of solar and heat pump (SHP) systems, such as seasonal performance factors (SPF) or electricity consumption, are quite dependent on the boundary conditions for the climate, as well as on the temperature levels of the heat sources and heat sinks of the system. Both the collector efficiency as well as the COP of the heat pump decrease with increasing temperature levels of the heat demand. When the irradiance is high on the collector field (e.g. 800 W/m^2), the decrease of the energetic yield of the collectors is typically below 1% (relative) per K increase of temperature. The COP of a heat pump is reduced by about 2 - 3% per K increase of sink temperature. Thus, it can be concluded that under normal conditions the heat pump performance is more sensitive to changes in sink temperatures than the solar collector performance. However, the lower the irradiance on the collector field, the larger the relative loss of energy gain from the collector field. Thus, the performance of flat plate collectors is usually more sensitive to changes in sink temperatures than the heat pump when the irradiance on the collector field is below 300 W/m^2.

A direct comparison of the energetic performance of different SHP systems is only valid for identical boundary conditions for climate, available source temperatures, share of DHW load, as well as temperature levels and distribution over the year for DHW and space heating demand.

Identical boundary conditions are typically not found in field studies. Differences between different climates, different years for the evaluation, different quality of buildings and distribution systems for DHW and space heating, and last but not least different user behaviour, make a comparison of field test results extremely difficult. The possibility to define and apply identical boundary conditions for laboratory testing and for system simulations make these highly valuable for the comparison of different SHP systems.

Identical boundary conditions for system simulations were defined within the IEA SHC Task 44 / HPP Annex 38 (T44A38) and reported in Dott et al. (2013b) and Haller et al. (2013a). The climate of Strasbourg was used as a main reference, with a DHW demand of 2076 kWh/a. Three different building standards were defined and classified according to the need for space heating in the climate of Strasbourg:

- SFH15 with roughly 15 kWh/(m^{2}a) space heat demand (Strasbourg),
- SFH45 with roughly 45 kWh/(m^{2}a) space heat demand (Strasbourg), and
- SFH100 with roughly 100 kWh/(m^{2}a) space heat demand (Strasbourg).

Design flow and return temperatures of the heating system were 35/30 °C for SFH15 and SFH45, and 55/45 °C for SFH100. Table 2.2 shows the total amount of space heat needed (floor surface area 140 m^2) for the three buildings in Strasbourg.

Table 2.2: Space heat and DHW load for the different buildings in Strasbourg.

Q_{SH} SFH15	2474	kWh
Q_{SH} SFH45	6476	kWh
Q_{SH} SFH100	14031	kWh
Q_{DHW}	2076	kWh

Temperature levels of the space heat supply and return are shown in Figure 2.4. The plot shows the accumulated energy transferred with temperatures *below* the temperature plotted on the x-axis in the supply and return line, respectively. Thus, it can be seen that for the SFH45 in Strasbourg (solid lines in left part of the Figure) 6.5 MWh in a year are supplied over the whole year with supply temperatures in the range of 25 °C to 32 °C and return temperatures between 20 °C and 25 °C. For the SFH100 in Helsinki (dotted lines in right diagram) supply temperatures were between 30 °C and 50 °C, and mor than 25 MWh was supplied.

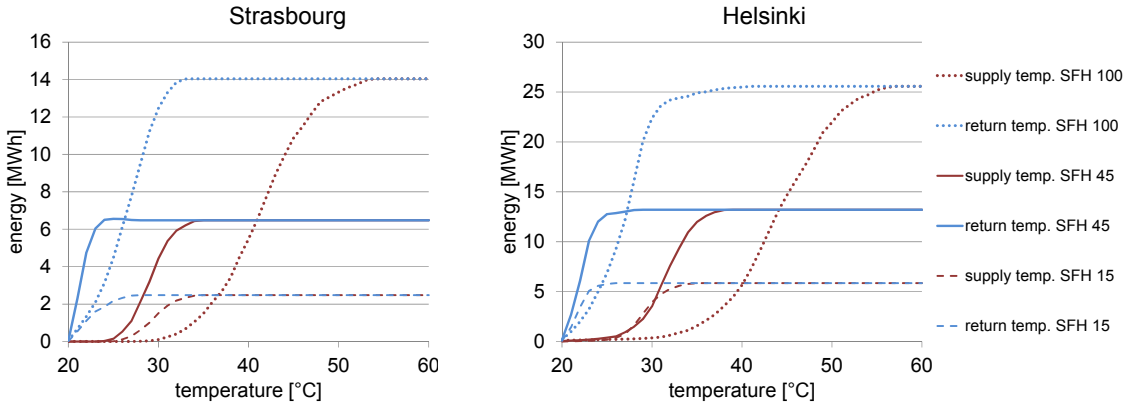

Figure 2.4: Energy-temperature-plots showing cumulative energy demand of the building vs. maximum supply and return temperatures for the two locations Strasbourg and Helsinki.

More details can be found in the cited literature and in Annex B.

2.3 Performance figures and comfort criteria

For the comparison of systems with identical heat load, the most important energetic performance figures are the amount of electricity used to run the system $W_{el,SHP+}$, and the overall system seasonal performance factor SPF_{SHP+}, i.e. the amount of useful heat delivered divided by the amount of electricity used. Different definitions are possible for these values. E.g., the SPF of the system may be based on different points of energy metering in the system (different system boundaries).

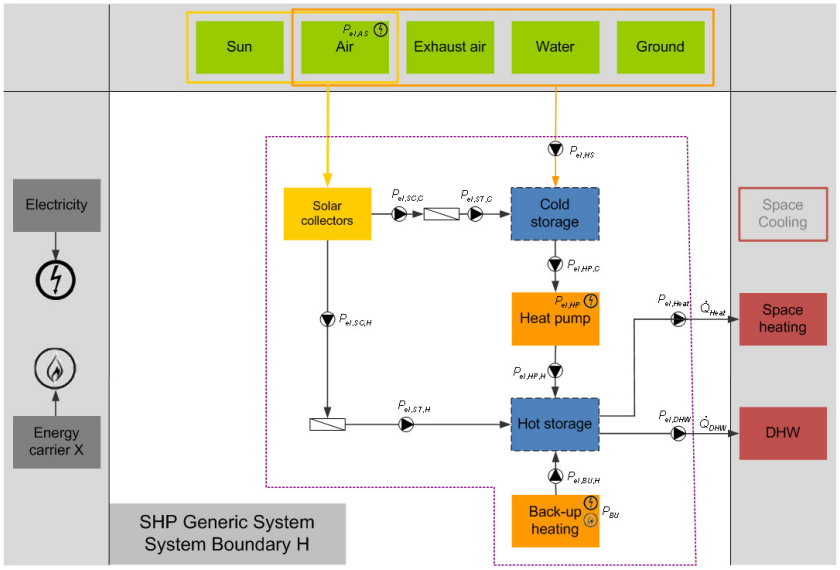

Figure 2.5: System boundary conditions for the calculation of SPF_{SHP+}. Source: Malenkovic 2011.

According to the definitions of T44A38, the SPF of the solar and heat pump system is defined once including the electric work for the space heat distribution pump (SHP+) and once not including the electric work of this pump (SHP):

Eq. 2.1 $$SPF_{SHP} = \frac{\int \left(\dot{Q}_{SH} + \dot{Q}_{DHW} \right) \cdot dt}{\int P_{el,SHP} \cdot dt}$$

Eq. 2.2 $$SPF_{SHP+} = \frac{\int \left(\dot{Q}_{SH} + \dot{Q}_{DHW} \right) \cdot dt}{\int P_{el,SHP+} \cdot dt}$$

with

$\dot{Q}_{SH}$ space heating power

$\dot{Q}_{DHW}$ domestic hot water power

No losses are simulated for the space heat distribution loop and the domestic hot water distribution outside of the technical room[2].

[2] i.e. eventual losses of the space heating loop occur only during the heating season and inside the heated building envelope and are thus not lost and must not be simulated. It can be assumed that they are already part of the heat load. No circulation line is used for the domestic hot water distribution of

Eq. 2.3 $$P_{el,SHP} = P_{el,HP} + P_{el,SC} + P_{el,EH} + P_{el,PU} + P_{el,Ctr}$$

$P_{el,SHP+}$ additionally includes the electric consumption of the space heat distribution pump, i.e.

Eq. 2.4 $$P_{el,SHP+} = P_{el,SHP} + P_{el,PU,SH}$$

With

HP heat pump – anything needed to run the heat pump (compressor, air ventilator, source pump(s), sink pump(s), heating elements, controllers, etc.)

SC Solar circuit – anything needed to run the solar circuit (pumps, controller - if additional to heat pump controller, valves, air ventilators for hybrid collectors, etc.)

EH electric heater elements (direct electric heating) that are not included yet in HP or SC

PU pumps that are not included yet in HP or SC, also including a primary DHW pump for an external DHW heat exchanger if present, but not the space heat distribution pumps

PU,SH space heat distribution pump

Ctr additional controllers that cannot be attributed to HP or SC alone.

Additional energy consumers are included if they are present within the SHP system boundaries defined.

Some systems may not at all times provide domestic hot water at the required temperature level or they may not be able to maintain the room temperature of the building at all times above 19.5 °C. In order to allow for a fair comparison between the simulation results of these systems and the simulation results of systems that maintained the defined comfort level of T44A38 at all times, penalties are added to the energy consumption, with a similar approach as in the IEA SHC Tasks 26 and 32 (Jordan et al. 2003; Heimrath & Haller 2007).

Eq. 2.5 $$SPF_{SHP+,pen} = \frac{\int\left(\dot{Q}_{SH} + \dot{Q}_{DHW}\right)\cdot dt}{\int\left(P_{el,SHP+,pen}\right)\cdot dt}$$

with

Eq. 2.6 $$P_{el,SHP+,pen} = P_{el,SHP+} + P_{el,DHW,pen} + P_{el,SH,pen}$$

For solar and heat pump combinations, the penalties are added as if missing energy would have to be provided by direct electric heating with a penalty factor. The purpose of this punishment factor is to avoid giving an advantage for substituting direct electric heating elements in the system that would normally be present by the penalty function that does the same job without heat losses. For domestic hot water production, the penalty factor is 1.5 (see Eq. 2.7 to Eq. 2.9), and for space heating the penalty factor is introduced by the exponent x=2 (see Eq. 2.10 to 2.12).

Eq. 2.7 $$P_{el,DHW,pen} = 1.5 \cdot \dot{m}_{DHW,loc} \cdot cp_{wat} \cdot \Delta T_{DHW,pen}$$

Eq. 2.8 $$\Delta T_{DHW,pen} = MAX\left(0; \vartheta_{DHW,set} - \vartheta_{DHW,sim}\right)$$

---

the reference system, since a circulation line is considered to be an energy-wasting luxury in a single family house. Other losses of the DHW distribution are assumed to be included in the DHW load profile that is used.

Eq. 2.9 $cp_{wat} = 4.19\,kJ/kgK$

Eq. 2.10 $P_{el,SH,pen} = UA_{bui} \cdot \left(\Delta T_{SH,pen} + \left\{ \Delta T_{SH,pen} + 1 \right\}^{x} - 1 \right)$

Eq. 2.11 $\Delta T_{SH,pen} = MAX\left(0;19.5°C - \theta_{room}\right)$

Eq. 2.12 $x = 2$

The UA values that are to be used in Eq. 2.10 for the different buildings are listed in Table 2.3.

Table 2.3: UA-values of the different buildings.

Building	UA_{bui} [W/K]
SFH15	97
SFH45	168
SFH100	290

Fractional solar savings, fractional thermal energy savings, etc. can be computed straightforward based on $P_{el,SHP+,pen}$, if the electric power consumption of a comparable reference system is known. These values depend significantly on the efficiency of the assumed reference heat pump system without solar thermal collectors for which a wide range of values may be assumed according to the differences in price and quality of heat pumps on the market. Thus, the resulting fractional solar savings may reflect the difference in the quality of the simulated heat pumps rather than the effect of the solar thermal installation. Therefore, such a reference system is not defined here.

2.4 Conclusion

With the approach presented to describe and classify combined solar thermal and heat pump systems it is possible to visualize such systems systematically and clearly simplified. With this approach, a basis is provided for the systematic description and comparison of combined solar thermal and heat pump systems, e.g. in the framework of IEA-SHC Task 44. The approach should be able to comprise both existing and newly developed system concepts. This systematic classification has been widely accepted and already used in numerous publications in the recent years.

3 Thermodynamics of series heat use

3.1 Introduction

The possibility of using solar thermal heat as a heat source for the heat pump in so called series connected systems has been discussed already decades ago (see e.g. Sporn & Ambrose 1955; Freeman et al. 1979). However, with the exception of the so called "solar heat pump water heaters" that is used for DHW in warmer climates with good solar resources over most of the year (Morrison 1994) series system concepts have not spread widely up to today. However, an increasing number of series solar and heat pump system concepts have been presented both in research as well as for market sale in recent years especially in Central Europe (Ruschenburg et al. 2013).

In comparison to the traditional concept where solar heat and e.g. an air source heat pump are providing heat in parallel configuration, a series heat use is expected to lead to higher temperatures on the evaporator side of the heat pump and lower temperatures for the collector, thus increasing both the COP of the heat pump COP_{HP} as well as the collector efficiency η_{coll}. It is tempting to assume that if both, COP_{HP} and η_{coll} increase, this will automatically lead to a better system performance. It is shown in this section that although this assumption is true for some specific cases, it is not true in general. It will also be shown that the boundary conditions under which this assumption is true are – for the investigated climates and applications – rather scarce (see also Haller & Frank 2011b; Haller & Frank 2011a).

3.2 Conditions for advantageous series operation

A parallel and series system concept (P/S) as shown in Figure 3.1 serves as an example for the derivation of conditions under which a better energetic performance can be expected from series operation mode compared to the parallel operation mode.

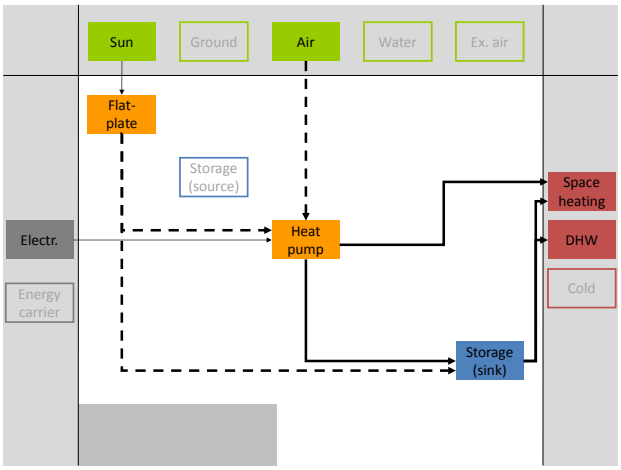

Figure 3.1: Energy flow chart of a parallel and series (P/S) solar and air source system concept.

As shown in Figure 3.2, heat from the solar collectors may be used parallel to the heat pump operation (left) or in a series configuration (right). The two operation modes can be compared only if they both deliver the same amount of useful heat at the same temperature level. In

this case, the series operation is only advantageous if the performance factor $PF_{sys} = Q_{sys} / W_{el,sys}$ for series operation is larger than for parallel operation:

Eq. 3.1 $$PF_{sys,ser} > PF_{sys,par}$$

The amount of useful heat that can be provided is limited by the serial mode of operation, where the available heat source is limited by the solar irradiation on the collector field ($Q_{sys} = Q_{HP,ser} = Q_{coll,par} + Q_{HP,par}$). Thus, Eq. 3.1 can be written as:

Eq. 3.2 $$\frac{Q_{HP,ser}}{W_{el,ser}} > \frac{Q_{coll,par} + Q_{HP,par}}{W_{el,par}}$$

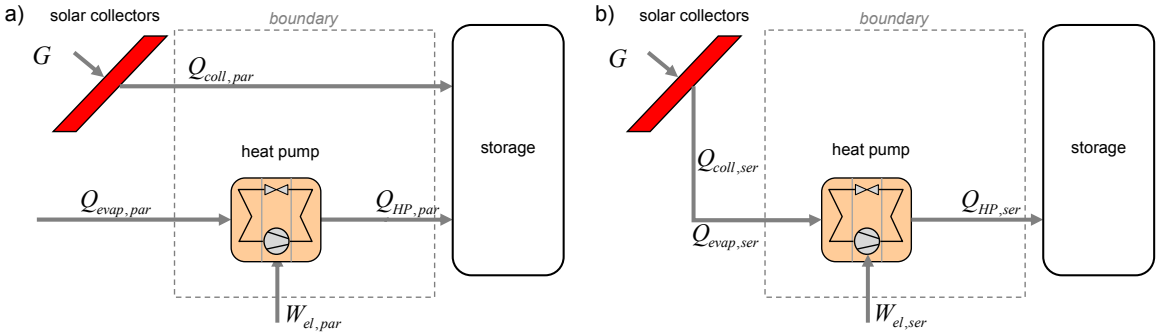

Figure 3.2: Energy flows in a P/S-type solar and heat pump system illustrating a) direct collector heat use and b) indirect collector heat use (adapted from Haller & Frank 2010).

Assuming that the electricity demand of the collector loop pump can be neglected since it is a minor contributor in both operation modes and it is identical for both operation modes, it follows from Eq. 3.2 with $COP_{HP} = Q_{HP} / W_{el}$ and $Q_{coll,par} + Q_{HP,par} = Q_{HP,ser}$ that:

Eq. 3.3 $$\frac{COP_{HP,ser}}{COP_{HP,par}} > \frac{Q_{HP,ser}}{Q_{HP,ser} - Q_{coll,par}}$$

With the definitions of $\Delta COP_{HP} = COP_{HP,ser} - COP_{HP,par}$ and $\Delta \eta_{coll} = \eta_{coll,ser} - \eta_{coll,par}$, and with some substitutions and rearrangements, the general criterion that has to be met in order to achieve an increased system performance factor for the series operation mode compared to the parallel operation mode can be written as:

Eq. 3.4 $$\frac{\Delta COP_{HP}}{\left(COP_{HP,par} - 1\right)} \cdot \frac{\Delta \eta_{coll}}{\eta_{coll,par}} > 1$$

The implication of this general condition can be demonstrated assuming e.g. a COP of 2.5 for the heat pump in parallel operation mode ($COP_{HP,par} = 2.5$). In this case, an advantage from using collector heat for the evaporator of the heat pump is possible if the COP of the heat pump increases by 1 ($\Delta COP_{HP} = 1$), and simultaneously the collector efficiency increases by +150% relative to the parallel collector operation mode (Figure 3.3). The curves of Figure 3.3 show for different values of $COP_{HP,par}$ the minimum increase of collector efficiency and of the COP of the heat pump in order to be able to increase the systems performance factor by using collector heat indirectly.

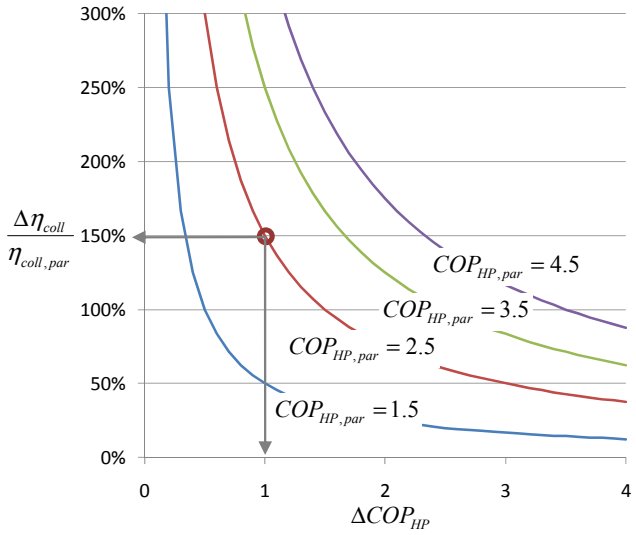

Figure 3.3: Limiting conditions for advantageous serial collector heat for different values of $COP_{HP,par}$ (Haller & Frank 2011b).

A direct consequence of Eq. 3.4 is that there is a limit for the irradiation on the collector field (G_{lim}) below which a serial operation mode has a positive effect on the system's performance factor. This limit depends on the characteristics of the heat pump and of the collector, as well as on the temperatures of the heat sink (heat use) of the different heat sources, and on the heat loss term of the collector:

Eq. 3.5 $$G_{lim} = \frac{\Delta COP_{HP}}{\left(COP_{HP,par} - 1\right)} \cdot \frac{x_{par} - x_{ser}}{\eta_0} + \frac{x_{par}}{\eta_0}$$

Where x are the losses of the collector in [W/m²] which depend on the temperature difference between the collector and the ambient:

Eq. 3.6 $$x = a_1 \cdot \Delta T_m + a_2 \cdot \Delta T_m \cdot \left|\Delta T_m\right|$$

With $\Delta T_m = \left(\vartheta_{coll,in} + \vartheta_{coll,out}\right)/2 - \vartheta_{amb}$.

The dependency of the irradiance limit G_{lim} on the ambient temperature (ϑ_{amb}) and on the temperature of the useful heat demand (ϑ_{supply}) is shown in Figure 3.4 for a typical solar and air source heat pump system of the P/S type. The performance characteristics that were assumed for the heat pump in air source and in brine source operation mode are shown in Figure 3.5, and the main performance coefficients for the solar collector were $\eta_0 = 0.8$, $a_1 = 3.5 W/\left(m^2 K\right)$, and $a_2 = 0.015 W/\left(m^2 K^2\right)$.

More details on this analysis can be found in Haller & Frank 2011b; Haller & Frank 2011a.

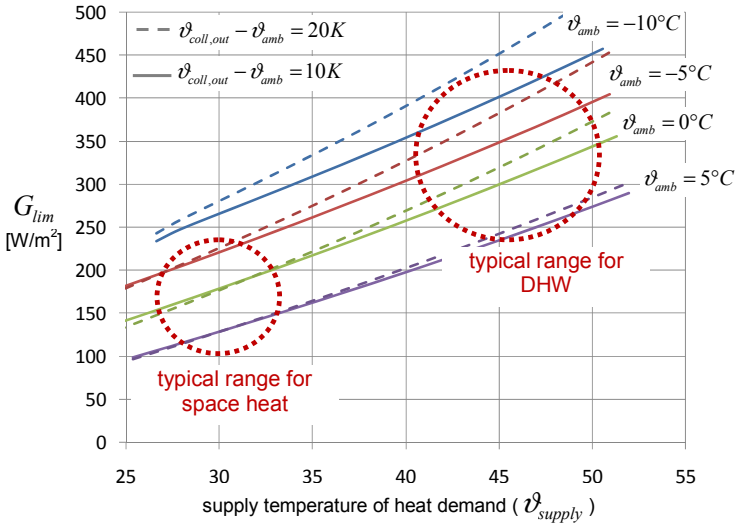

Figure 3.4: Irradiance limit (G_{lim}) below which a serial operation mode leads to an increase in the system's performance factor for a typical solar and air source heat pump system with covered flat plate collectors (Haller & Frank 2011b).

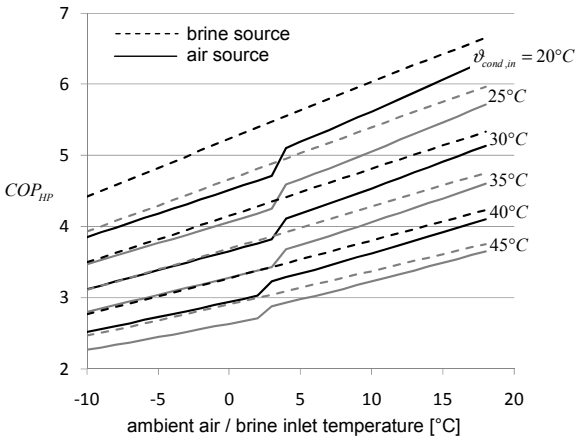

Figure 3.5: Coefficient of performance (COP) of the dual source heat pump at different inlet temperatures of the evaporator and the condenser of the heat pump.

3.3 Conclusion

The general mathematical relationship that determines under which circumstances the series operation mode is energetically more efficient than the parallel operation mode was presented with Eq. 3.4 and illustrated in Figure 3.3. These conditions are not easy to meet as both the COP of the heat pump and the collector efficiency must increase substantially in order to obtain a better performance from the series heat use. It was shown that there is a limit for the solar irradiance on the collector field above which the series operation is reducing the system's performance factor rather than increasing it. This irradiance limit depends on the characteristic performance curves of the solar thermal collector and of the heat pump. As could be expected, this limit is always higher for collectors with large heat losses to the ambient (e.g. uncovered collectors) than for collectors with low heat losses to the ambient (e.g. covered flat plate collectors). Based on example calculations it was shown that the irradiance limit also increases with increasing temperatures on the heat demand side, and with de-

creasing temperatures for the ambient air, that was in the used example case at the same time the alternative heat source for the heat pump.

In general, it can be concluded that an energetic advantage of the series heat use is only given for certain boundary conditions, and that this advantage is higher for higher temperatures on the demand side and for lower temperatures on the side of the heat source of the heat pump and the ambient air. The higher the irradiance on the collector field, the more the benefit of series operation decreases, down to the point where it is negative, i.e. where series operation is less efficient than the parallel operation. For a typical solar and air source heat pump system, depending on the heat source and heat sink temperatures, a series operation results in poorer performance than a parallel operation when the solar irradiance on the collector field is higher than 100 – 500 W/(m^2).

4 Components for solar and heat pump systems

4.1 Measurements on uncovered absorbers

The outdoor measurements reported in this section were also published in Philippen et al. (2011), the measurements in the climatic chamber in the Bachelor Thesis of Hantzsche (2011).

4.1.1 Introduction

When using uncovered (unglazed) collectors as heat source for heat pumps the temperature of the collector cycle can be operated below ambient temperature. This can be the case especially at night or when the sky is covered with clouds. For measuring and simulating uncovered collectors during these conditions more physical properties have to be taken into account compared to covered collectors, namely: long-wave radiative exchange and heat exchange due to convection, condensation, and precipitation. This chapter is about measurements of the dependencies of these physical properties on the absorber's inclination of uncovered flat plate collectors.

4.1.2 Theoretical background

Several models of the convective heat transfer between ambient and absorber surface of uncovered collectors can be found in literature (Palyvos 2008; Perers 2010). Most of these models show a linear or exponential dependency of the outer convective heat transfer coefficient from the wind speed in a certain distance from the absorber surface. No study could be found that analyses the influence of the collector's inclination on the outer convective heat transfer of uncovered collectors. However, this influence can be expected if wind speed and solar irradiation are low and the heat transfer hence is dominated by free convection. Due to the Nusselt correlations describing free convection (Cengel 2003, p. 467), a dependency of the heat transfer on typical inclinations of collectors can be expected especially if the temperature of the absorber is below ambient temperature.

The heat gain $\dot{Q}_{gain}$ of a collector with the absorber surface A_{coll} can be calculated with the area-related gains of absorption of short-wave solar irradiance ($\dot{q}_{abs,S}$), the long-wave radiative exchange with the surrounding ($\dot{q}_{rad,L}$), convective sensible ($\dot{q}_{conv,sens}$) and latent heat transfer ($\dot{q}_{conv,lat}$), and of heat conduction ($\dot{q}_{cond}$) according to[3]:

Eq. 4.1
$$\frac{\dot{Q}_{gain}}{A_{coll}} = \dot{q}_{gain} = \dot{q}_{abs,S} + \dot{q}_{rad,L} + \dot{q}_{conv,sens} + \dot{q}_{conv,lat} + \dot{q}_{cond}$$

As the measurements were conducted during night the absorption of short-wave radiation can be neglected. The heat conduction of the backside of the collector is also neglected as it was insulated (U = 0.3 W/(m^{2}K)).

The exchange of heat due to convection can be approximately expressed using the outer convective heat transfer coefficient, α_{conv}:

Eq. 4.2
$$\dot{q}_{conv,sens} = \alpha_{conv} \cdot \left(T_{amb} - T_m\right)$$

[3] In non-steady state conditions the heat capacity of the collector has to be taken into account, too.

The exchange of heat due to condensation of water vapour on the absorber surface can be expressed as a function of α_{conv} (Frank 2007) as condensation is dependent on convection that forces the mass flow of the humidity to the absorber surface:

Eq. 4.3 $$\dot{q}_{conv,lat} = \alpha_{conv} \cdot C_{cond} \left[p_{sat}\left(T_{DP}\right) - p_{sat}\left(T_m\right) \right]$$

with:

Eq. 4.4 $$C_{cond} = \frac{R_L \cdot r \cdot Le^{-0,66}}{R_D \cdot p_{amb} \cdot c_L}$$

and:

T_m = average temperature of absorber surface,

p_{sat} = saturation vapour pressure,

T_{DP} = dew point temperature,

T_{amb} = ambient temperature,

R_L = specific gas constant air,

R_D = specific gas constant water vapour,

r = phase change enthalpy,

Le = Lewis number,

p_{amb} = air pressure,

c_L = specific heat capacity air

After inserting into the energy balance, the outer convective heat transfer coefficient of a flat plate absorber can be expressed as follows:

Eq. 4.5 $$\alpha_{conv} = \frac{\dot{q}_{gain} - \dot{q}_{rad,L}}{\left|T_m - T_{amb}\right| + C_{cond} \cdot \left[p_{sat}\left(T_{DP}\right) - p_{sat}\left(T_m\right) \right]}$$

4.1.3 Measurements of the emissivity of selective uncovered absorbers

The emissivity of a sample of a black chrome coated steel plate from Energie Solaire SA was measured three times:

- dry measurement
- measurement with water droplets
- measurement with water film

Results are shown in Figure 4.1. While the emissivity of the dry surface showed the expected low value of ε = 0.13, the emissive properties with increasing amount of water on the surface approach the properties of water ($\varepsilon \approx 0.97$). Water droplets that can be expected from condensation while the absorber is operated below the dew point of the air increase the emissivity already to ε = 0.63, and a thin water film showed ε = 0.77.

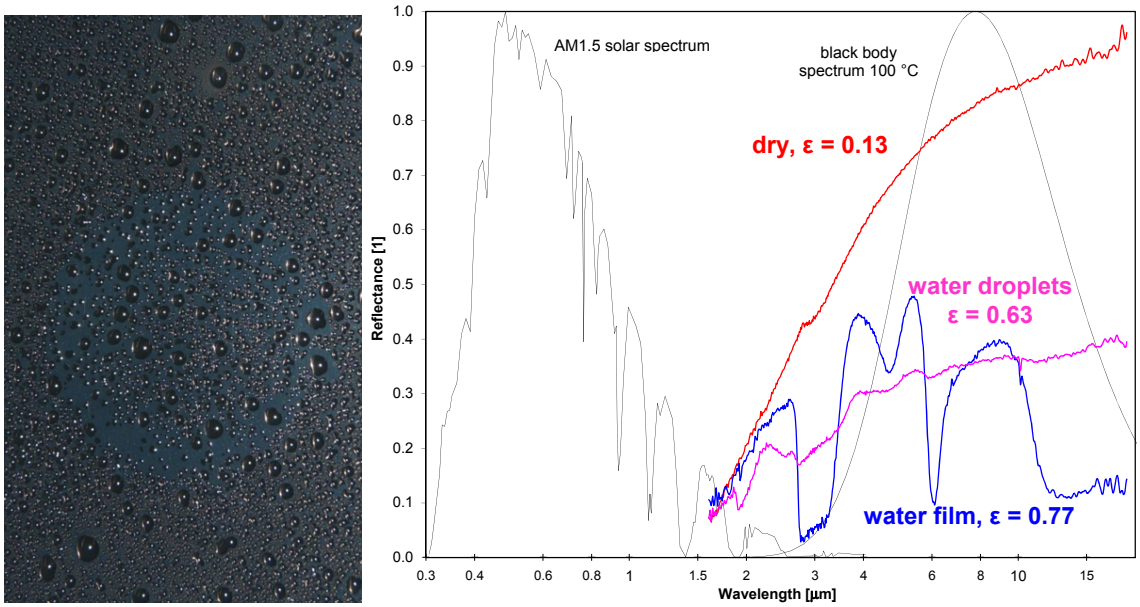

Figure 4.1: Selective absorber surface (black chrome on steel) with water droplets (left), and emissive properties under dry, water droplet, and water film conditions (right).

4.1.4 Outdoor measurements

Measurements were conducted during night on the roof of Hochschule für Technik Rapperswil with uncovered collectors with both selective and non-selective flat plate absorbers of 2.0 m^2 each, that were cushion absorbers made of steel. The performance of the absorbers was measured with different inlet temperatures below ambient temperature for different inclinations of the collectors. The inclination was automatically changed with a tracker.

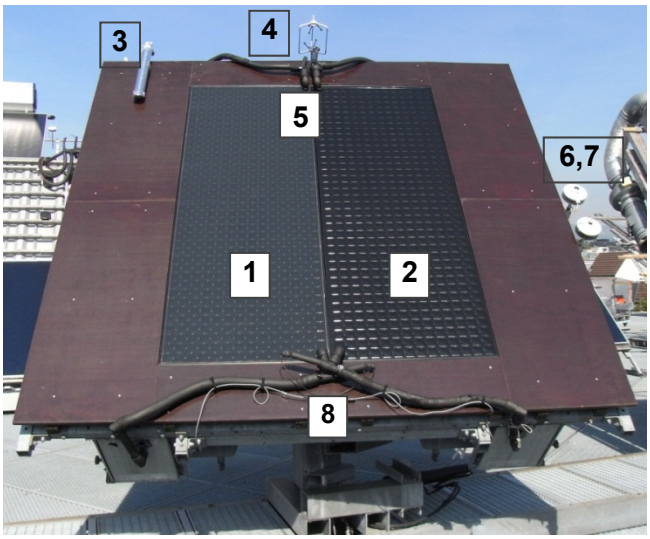

Figure 4.2: Set up on the tracker for the measurements of the selective (1) and non-selective (2) uncovered collectors from Energie Solaire SA. Measurement points: temperature of air above the collector plane (3), ultra sonic anemometer (4), pyranometer (6), pyrgeometer (7), collector inlet temperature (8), collector outlet temperature (5).

For each measurement the inlet temperature followed the temperature of the air above the absorber surface with a constant difference. The following meteorological quantities were measured in or parallel to the collector plane: wind speed, long-wave radiative exchange, short-wave radiation, humidity and temperature of the air. Measurement data was only used for the analysis if the conditions for the energy flows were relatively constant over time.

4.1.5 Measurements in the climatic chamber

An uncovered steel cushion absorber was installed in the climate chamber that was able to provide constant conditions for temperature (±0.1 K) and humidity (±1%). The absorber was insulated on the back side, in order to reduce the heat transfer relevant surface to one side. In order to reach a homogenous view temperature (long wave irradiance) for the absorbers, all surfaces with possibly different view temperatures (e.g. windows of the climatic chamber) were shielded. A pyrgeometer was installed with the same orientation as the uncovered absorber (accuracy ±3%). A thermostat bath with antifreeze was used to provide constant inlet temperatures to the absorber that were below the temperatures of the air. A gutter was installed below the absorber in order to collect condensate that is running off and to be able to measure the amount of condensate during the tests with a weighing scale (accuracy ±0.1 g). Inlet and outlet temperatures of the absorber and the temperature of the air were measured with 4-wire Pt100 sensors with an accuracy of ±0.04 K. Volumetric flow rates were measured with an in-house calibrated magnetic inductive device with an accuracy of ±0.5%. Humidity of the air was measured with an accuracy of ±1%.

The total heat transfer coefficients were calculated based on the absorber heat gain, the absorber surface area, and the temperature difference between the mean fluid temperature in the absorber and the ambient air. For the fully irrigated cushion absorber that was used, the fluid temperature is assumed to correspond closely to the surface temperature. The total heat transfer coefficient was split into different parts:

- Condensation gains were determined from the condensed water that was collected in the gully during steady state operation.
- Frost gains were determined by collection of water in the gully after the test was finished and the collector surface was de-iced.
- Long wave radiation heat exchange was calculated based on the long wave irradiation measured by the pyrgeometer, and the assumption of a surface emissivity of the absorber that corresponds to "absorber covered with dew".
- The remaining heat gain was attributed to sensible heat from the air by convection.

4.1.6 Results of the outdoor tests

After the entire absorber surface is covered with condensing water from the air (Figure 4.3, after 21:00) the thickness of the water on the absorber increases during the night to such a degree that the selective absorber loses its selectivity. This can be observed with the convergence of the specific heat gain of the selective absorber to the one of the non-selective absorber in Figure 4.3 (green and black line). If the temperature of the hemisphere above the absorber is colder than the absorber’s surface, this temporary loss of selectivity can lead to a net-loss of heat of the collector. It can be assumed that these losses are larger with low inclinations of the collector when it is faced against clear sky.

Figure 4.3 shows that the specific power of a non-selective absorber strongly dependents on the temperature of the hemisphere above the collector plane in times without solar irradia-

tion. This temperature though is normally influenced by the inclination and is lowest under the open sky (inclination 0°).

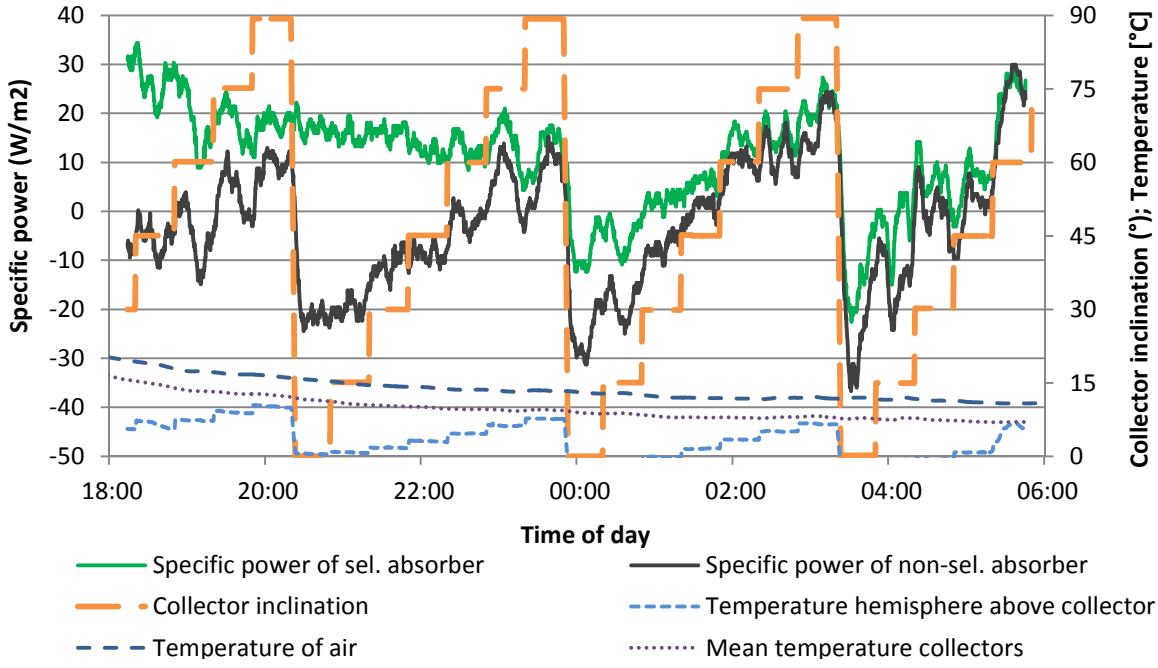

Figure 4.3: Specific power of the selective and the non-selective uncovered collector, and temperature of the hemisphere above the collector plane of a measurement during night with changing inclination of the collector (measurement from 21./22. October 2010, inlet temperature of collector 4 Kelvin below ambient air).

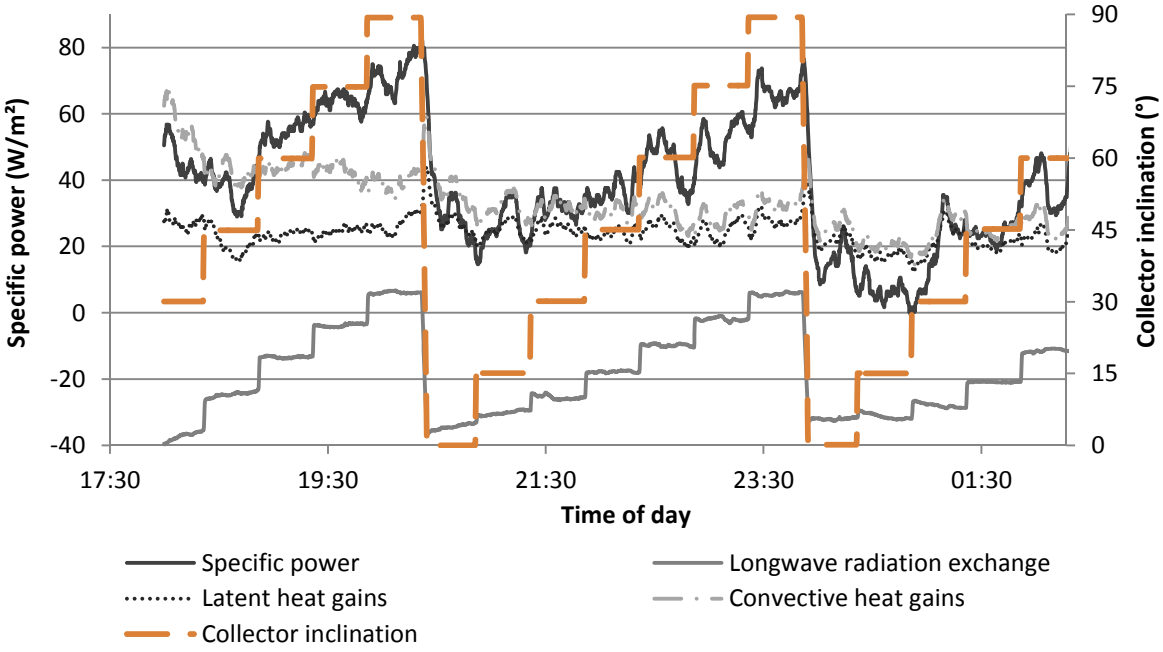

Figure 4.4: Share of the investigated energetic quantities at the non-selective absorber for different inclinations (measurement of 20./21. October 2010, inlet temperature of collector 8 Kelvin below ambient air).

The measurements show that the non-selective absorber could always gain heat only at inclination of 75° and 90° for inlet temperatures 4 K below ambient air.

The dependency of the heat gain of the collectors on the long-wave radiative exchange and hence on the inclination of the collector is also shown in Figure 4.4. In contrast to the long-wave radiative exchange no dependency on the inclination is show for the convective and for the latent heat gain.

No clear dependency of the outer convective heat transfer coefficient on the collector's inclination could be found for outdoor conditions. Increased gains for larger slopes are due to higher values for long wave irradiation on the collector surface.

Figure 4.5 shows the calculated outer convective heat transfer coefficient α_{conv} of a typical measurement during night with absorber temperatures below ambient. No clear dependency of α_{conv} on the collector's inclination at low wind speeds can be shown. Also with the analysis of several measurements during night the expected causal relationship could not be found. In particular the values for the horizontally orientated absorber are not the lowest but instead lie around the average of all values. The values at 60° inclination vary strongly. Only the order of priority of the values at 15°, 30°, 45°, 75°, and 90° show more or less the expected trend.

The observed maxima for the convective heat transfer at wind speeds below 0.5 m/s are in the range of 3 to around 6 W/(m²K) and therefore match with the values that can be expected according to literature (Cengel 2003).

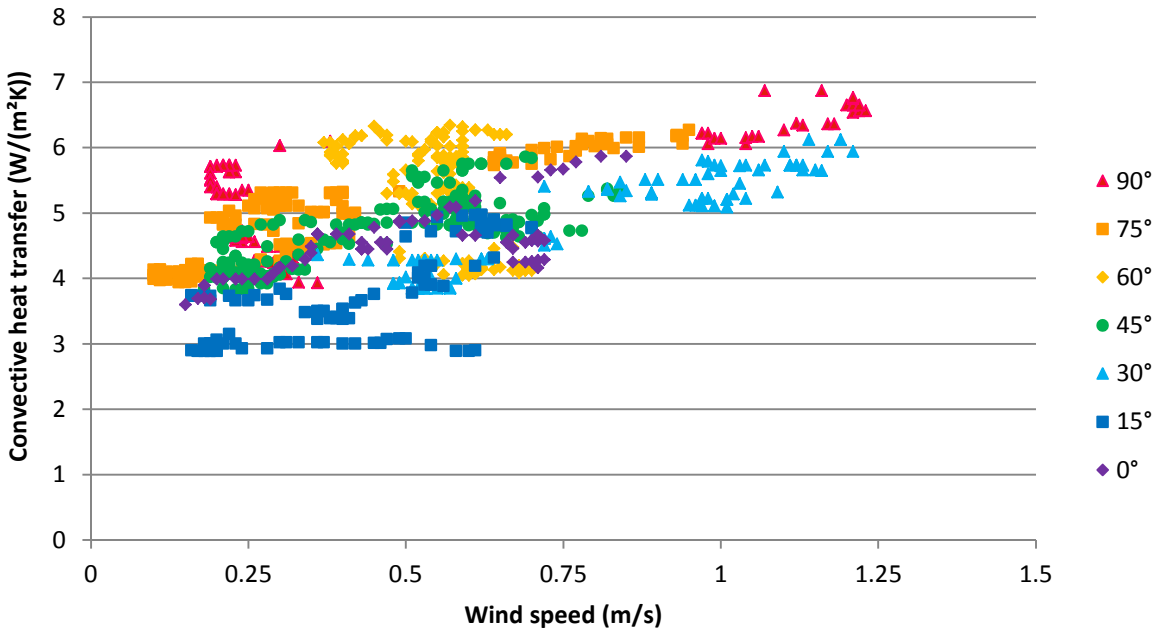

Figure 4.5: Calculated outer convective heat transfer coefficient α_{conv} of uncovered collectors versus wind speed in dependency of the collector's inclination (measurement of 17./18. February 2011, inlet temperature of collector 7 Kelvin below ambient air).

4.1.7 Results of the indoor tests

Figure 4.6 shows that the total heat transfer coefficient was in the range of 16 W/(m2K). For ambient air temperatures of 8 °C and a relative humidity of 94%, the heat transfer can be attributed to about one third each for condensation gains, long wave radiation exchange, and convective sensible heat gains from the air. Thus, each of the three phenomena contributed with about 5 W/(m^{2}K).

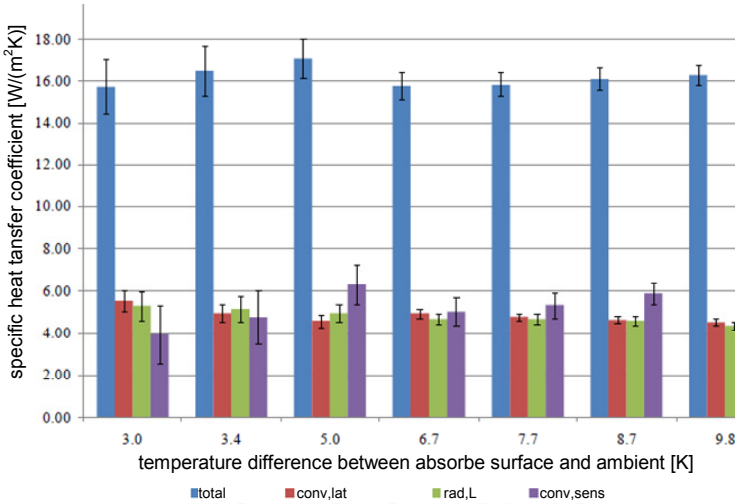

Figure 4.6: Total heat transfer coefficients per K temperature difference between air and absorber surface, and the parts that are attributed to condensation gains, long-wave radiation exchange, and convective sensible and latent heat gains from the air, for different temperature differences between the absorber and the ambient air, with air temperatures of 8 °C and 94% relative humidity (translated from Hantzsche 2011).

Figure 4.7 shows that for frost conditions with mean absorber temperatures of -1.1 °C and -2.6 °C slightly higher overall heat transfer coefficients of about 17 W/(m^{2}K) were measured. Frost heat gains were in the range of 8 – 10 W/(m^{2}K), while sensible heat gains from convection were reduced to 3 W/(m^{2}K). The significant increase of heat gains from water phase change compared to the results without frost is surprising, since the latent enthalpy of ice formation is only about 13% of the latent enthalpy of condensation. Further measurements would be needed to confirm this result, which could possibly also be an artefact of the test setup and evaluation procedures. Figure 4.8 shows the influence of the relative humidity of the air on heat gains from condensation. While these heat gains increase substantially with increasing humidity of the air, sensible convective heat gains are reduced only slightly.

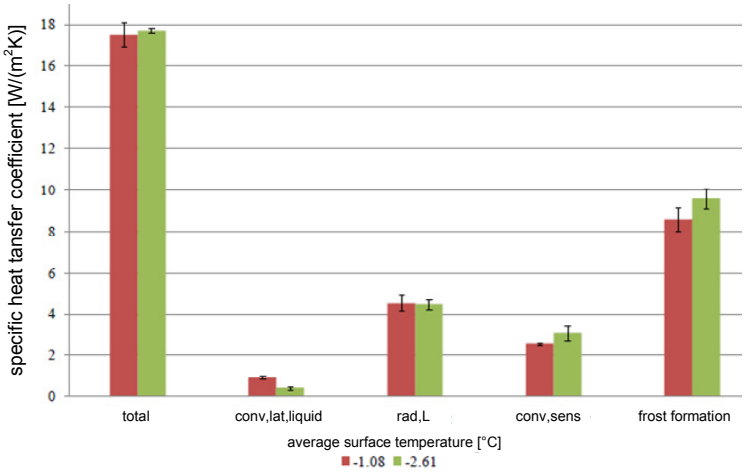

Figure 4.7: Total heat transfer coefficients and their origin under frost conditions (< 0 °C surface temperature). With air temperatures of 8 °C and relative humidity of 94% (translated from Hantzsche 2011).

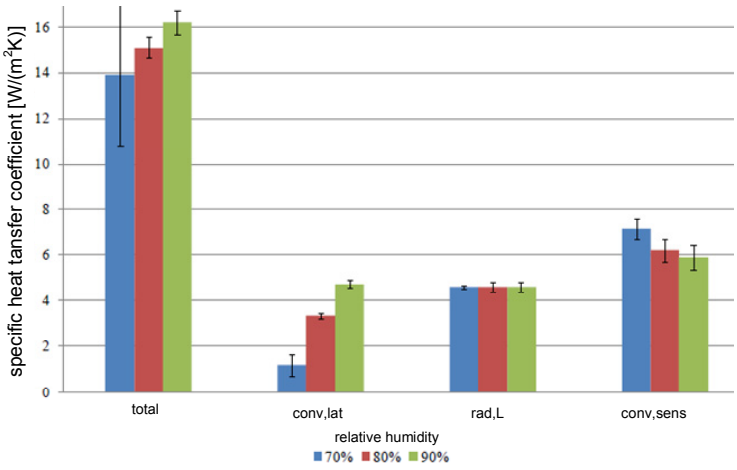

Figure 4.8: Total heat transfer coefficients and their origin with different relative humidity of the air, at air temperatures of 8 °C (translated from Hantzsche 2011).

4.1.8 Conclusion

A systematic influence of the inclination of uncovered collectors on the outer convective heat transfer for absorber temperatures below ambient and at low wind speeds could not be detected. Reasons for this could be that the investigated effect is smaller than it could be expected according to the theory of free convection, that the conditions during the measurements were too unstable (wind and temperature fluctuations), and the high measurement uncertainties in a range of 25 to 60%. The largest share of the total uncertainty is attributed to the long-wave radiative exchange with around 50%.

Nevertheless, the following findings for the operation of uncovered collectors with selective absorbers can be derived from the measurements:

- If humidity condensates on the absorber surface its selectivity is reduced or even eliminated temporarily. During the whole measurement period (October to February) dew was formed on the cold absorbers soon after dusk during the whole night (absorber surface temperatures 4 K or more below ambient). For that reason a decrease of selectivity of uncovered collectors at operation below dew point could have a relevant influence on the efficiency of solar heat pump systems if the collectors are used as heat source for the heat pump.
- It was shown that the specific energy gain of non-selective uncovered absorbers is dependent on the inclination of the collector. This is due to the dependency of the long-wave radiative exchange on the inclination. The dependency on the inclination is mainly given in nights with low wind speeds and with clear sky where the temperature of the hemisphere above the collector's plane changes strongly with changing inclination.

4.2 Measurements on heat pumps

Measurements were performed on three heat pump units in the laboratory. The purpose of these measurements was to:

- determine COP values that are outside of the range that is usually covered by standard test procedures,
- obtain information and data for the simulation of transient operating conditions,

- obtain additional data for parameterization of the semi-physical heat pump model (see section 4.5) and of the extended YUM model (see section 4.6).

The technical properties of the three heat pumps according to the manufacturer's declaration are shown in Table 4.1.

Table 4.1: Manufacturer specifications for the heat pump units evaluated in the test bench.

		I	II	III
Type		air/water (monobloc outdoor)	air/water (split)	brine/water
refrigerant		R404A	R410A	R407A
heating capacity[a)]	kW	9.4	3.1/8.3/7.2 [b)]	8.2
electric power[a)]	kW	2.6	0.8/2.5/2.0 [b)]	1.7
COP[a)]	-	3.7	3.8/3.4/3.7 [b)]	4.9

a) at A2W35 for air source and B0W35 for brine source.

b) values given are for min/max/nominal.

Unless stated differently in the respective sections, all measurements on heat pumps were performed as follows:

- immersed pair-wise calibrated 4-wire Pt100 temperature sensors were used for measuring of **inlet and outlet temperatures** of the condenser (water) or evaporator (brine). A general estimation for the uncertainty is 0.03 K for ΔT (provided the ΔT is low), and 0.1 K absolute.
- **flow rates** were measured with calibrated magnetic-inductive flow sensors. The estimated uncertainty is 0.5% for nominal or maximum flow rates measured for one heat pump, and up to 1 % for lower volume flow rates of 1/3 of the nominal or maximum measured volume flow rate.
- **temperatures in the refrigerant cycle** were measured using 4-wire Pt100 temperature probes attached to the copper tubes of the refrigerant cycle and well insulated against the ambient conditions. The estimated uncertainty is 0.1 K for the sensor itself, and up to 5 K for higher temperatures due to the non-ideal sensor placement
- **ambient air temperatures** were measured at the inlet of the air source heat exchanger with an estimated accuracy of 0.1 K
- **ambient air temperatures and humidity** were measured at the inlet of the air source heat exchanger with an estimated accuracy of 0.1 K and 1% rH respectively
- **electric power consumption** was measured with an accuracy of ±5%
- the technical room where indoor components were installed was conditioned to 20 ±1°C.

4.2.1 Heat pump I: air/water (monoblock)

The heat pump (outdoor unit) was installed in a climatic chamber and connected to the heat sink of the test bench. The control unit was mounted in the technical room. Temperature and humidity of the air source were controlled by the climatic chamber. Temperatures in the refrigerant cycle were measured at five positions (Figure 4.9).

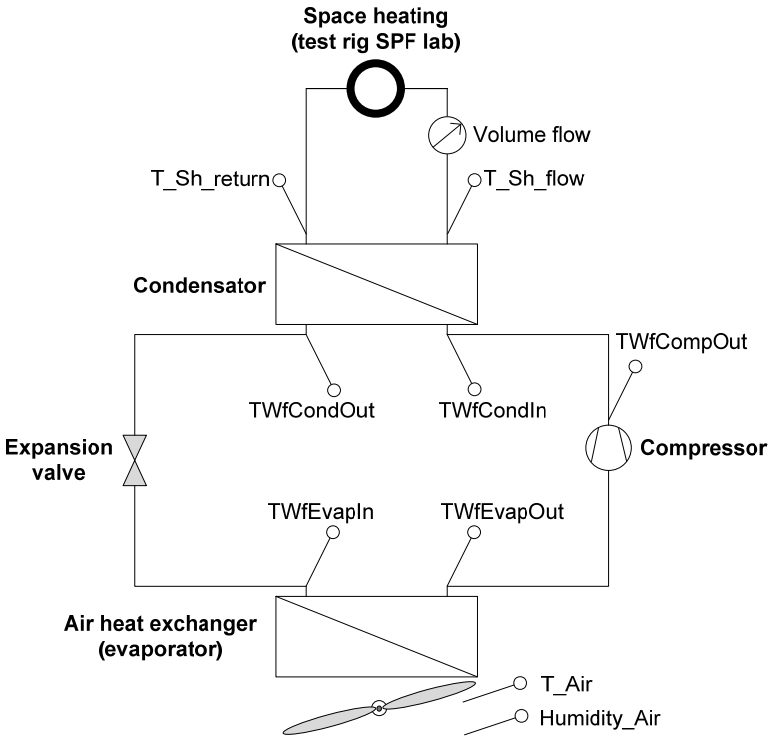

Figure 4.9: Measurement positions in the working fluid cycle and around the heat pump unit.

Mass flow rates and heating power were calculated based on measurements in 1 second time steps and power values were integrated to energies over time. All values were registered by the logging device at 1 minute time steps and the final data processing was based on these values.

The following conditions were applied:

- constant supply temperature of the heated water (dynamic quasi steady state with constant supply temperatures of the heat pump in times of normal operation, i.e. no defrosting).
- Cycling operation with average heating power below the nominal heating power of the heat pump.

For each test run the air source temperature and humidity was kept constant in a range of ± 0.8 K for the air source temperature and ± 20% for the humidity.

The COP of the heat pump was calculated as follows:

Eq. 4.6 $$COP = \frac{Q_{cond}}{W_{HP}} \approx \frac{\dot{Q}_{cond}}{P_{HP}}$$

Where Q_{cond} is the heat delivered by the condenser of the heat pump based on the temperature difference between inlet and outlet and the volume flow rate on the water side. W_{HP} includes only the electricity consumption of the outdoor unit (compressor, fan and control) without the circulation pump.

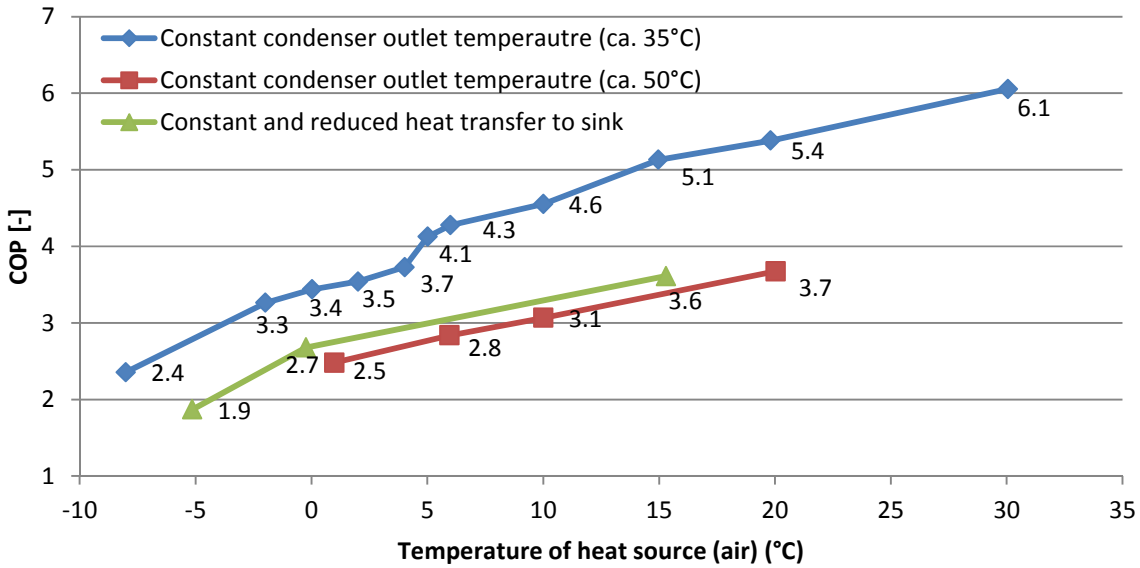

Figure 4.10: COP of the heat pump at different ambient air temperatures for condenser outlet temperatures of 35 °C (blue) and 50 °C (red) as well as for cycling on/off operation (green).

Table 4.2: Measurement results for +/- constant condenser outlet temperature 50 °C and varying air source temperature.

measurement point		***1***	***2***	***3***	***4***
temperature of the air source	°C	1	6	10	20
temperature condenser outlet	°C	47.9	49.5	49.9	51
rel. humidity	%	80	85	85	85
COP	-	2.48	2.84	3.07	3.67
volume flow rate condenser	L/h	1820	1820	1820	1820
ΔT outlet – inlet condenser (water)	K	4	4.8	5.2	6.3
heating power	kW	8.6	10.2	11.1	13.4
electric uptake	kW	3.5	3.6	3.6	3.6

Table 4.3: Measurement results for +/- constant condenser outlet temperature 35 °C and varying air source temperature.

measurement point		***1***	***2***	***3***	***4***	***5***	***6***	***7***	***8***	***9***
temperature of the air source	°C	-8	-2	0	2	4	5	15	19.8	30.1
temperature condenser outlet	°C	33.3	34.5	34.2	34.6	34.8	35.5	35.5	37.7	35.6
rel. humidity	%	80	80	86	89	80	80	80	90	85
COP	-	2.36	3.26	3.44	3.54	3.73	4.13	5.13	5.38	6.05
volume flow rate condenser	L/h	1820	1820	1820	1820	1820	1820	1820	1820	1820
ΔT outlet – inlet condenser (water)	K	1.3	4	4.2	4.3	4.6	5.1	6.3	6.9	7.6
heating power	kW	2.8	8.4	8.8	9.2	9.7	10.8	13.3	14.8	16.2
electric uptake	kW	1.2	2.6	2.6	2.6	2.6	2.6	2.6	2.7	2.7

Table 4.4: Measurement results for cycling on/off operation at different air source temperatures (volume flow rate 1820 l/h, rel. humidity 78%).

measurement point		***1***	***2***	***3***
temperature of the air source	°C	-5.1	-0.2	15.3
COP	-	1.87	2.68	3.61
condenser outlet temperature range from start to end of the on-phase	°C	35 - 52	25 - 51	24 - 53
temperature difference outlet – inlet condenser in the on-phase	K	2.3	3.1	3.9
heating power in the on-phase	kW	3.9	6.4	7.6
electric uptake in the on-phase	kW	2.6	2.6	2.7
duration of on-phase	min.	5	7	5
duration of off-phase	min.	15	13	15
number of measured cycles	-	31	7	6

The amount of superheating after the evaporation of the refrigerant was estimated based on the readings of the temperature sensors that were attached to the copper tubes of the refrigerant cycle before and after the evaporator. It was assumed that the temperature glide of the refrigerant (R404A) in combination with the pressure loss in the evaporator can be neglected in this analysis. Figure 4.11 shows that the amount of superheating is strongly dependent on the temperature of the air source for this heat pump that was equipped with a thermostatic expansion valve.

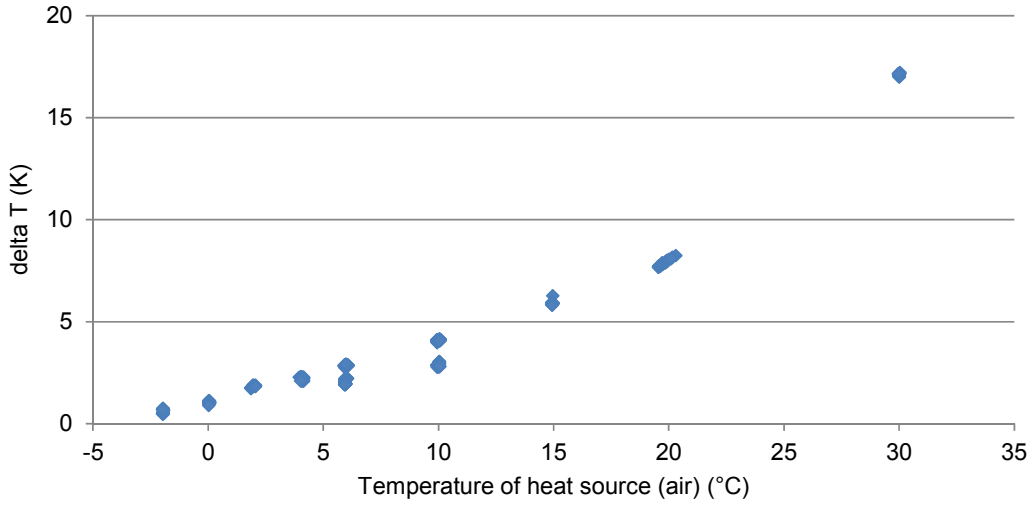

Figure 4.11: Temperature difference in the refrigerant cycle between evaporator inlet and evaporator outlet.

4.2.2 Heat pump II: air/water (split)

The outdoor unit of the heat pump was placed in the climatic chamber. This outdoor unit contained the evaporator and the expansion valve. The condenser was in an indoor unit that was connected with a twin refrigerant line of 8 m length for each line.

In order to obtain information on the thermodynamic state of the refrigerant six 4-wire Pt100 temperature sensors were attached to the copper tubes on both ends of the twin-refrigerant

line that connects the in- and the outdoor unit (in- and outlet of the condenser) and on the in- and outlet of the evaporator.

A total of 46 different measurement runs were performed with:

- Air source temperatures between – 15 °C and 30 °C.
- Condenser inlet temperatures between 20 °C and 50 °C.
- Mass flow rates between 250 kg/h and 1000 kg/h.
- Capacity between 25% and 100%.

Each measured point was kept for at least one hour, and for three hours for ambient air temperatures below 5 °C. Figure 4.12 shows an excerpt of the measurements on the heat pump at various ambient air temperatures. Because it is not possible to determine a COP of the heat pump with an 3 hour measurement period (due to de-icing of the evaporator) the measured data were not evaluated in detail but rather used as an input for the modelling of the heat pump.

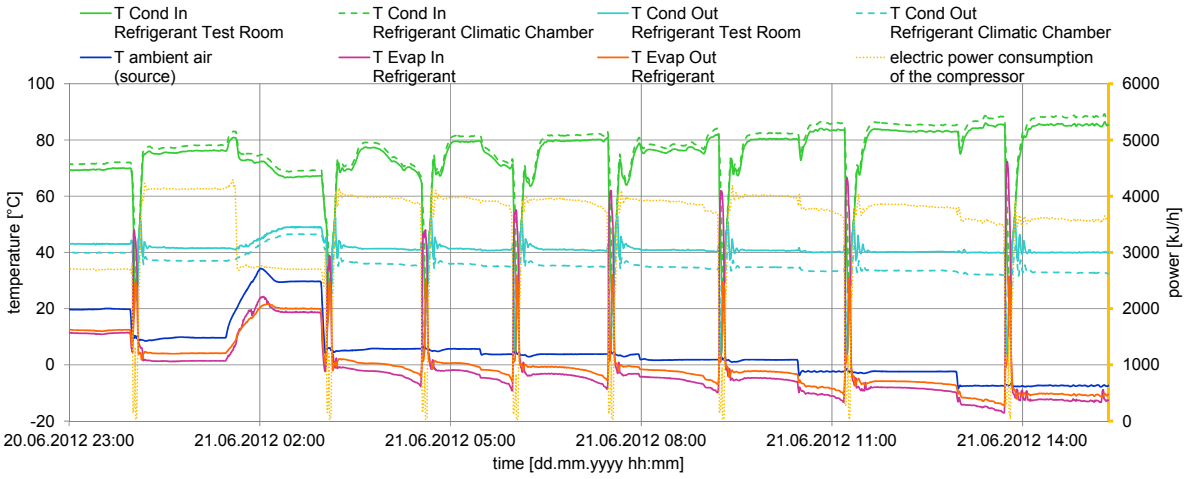

Figure 4.12: Excerpt of the measurements on the heat pump II: air/water.

4.2.3 Heat pump III: brine/water

A brine source heat pump was connected to a 500 l water storage tank. Before each measurement, the storage tank was conditioned to a temperature of 20 °C. No active heat extraction took place during storage charging with the heat pump. The brine source was conditioned to constant inlet temperatures in the range of -1.5 to +9.5 °C. The flow rate of the source side was 1050 kg/h and a mixture of 33.3% vol. Antifrogen N was used for the heat source fluid. Heat pump and storage were installed in the technical room. Measurements were performed while the heat pump was loading the water storage tank until it reached a temperature of 57 °C. Therefore the measurements were not steady state measurements. When the storage tank reached 57 °C, the heat pump was stopped and the tank was unloaded until it reached 20 °C.

In the COP calculation of this heat pump, the source and sink pump electric uptake is included in the electric uptake of the heat pump unit.

Different mass flow rates were applied on the sink side of the heat pump (condenser). Figure 4.13 shows the COP dependent on the mean temperature of the condenser for different heat

source temperatures (evaporator inlet). The figure shows the temperature dependency of the COP.

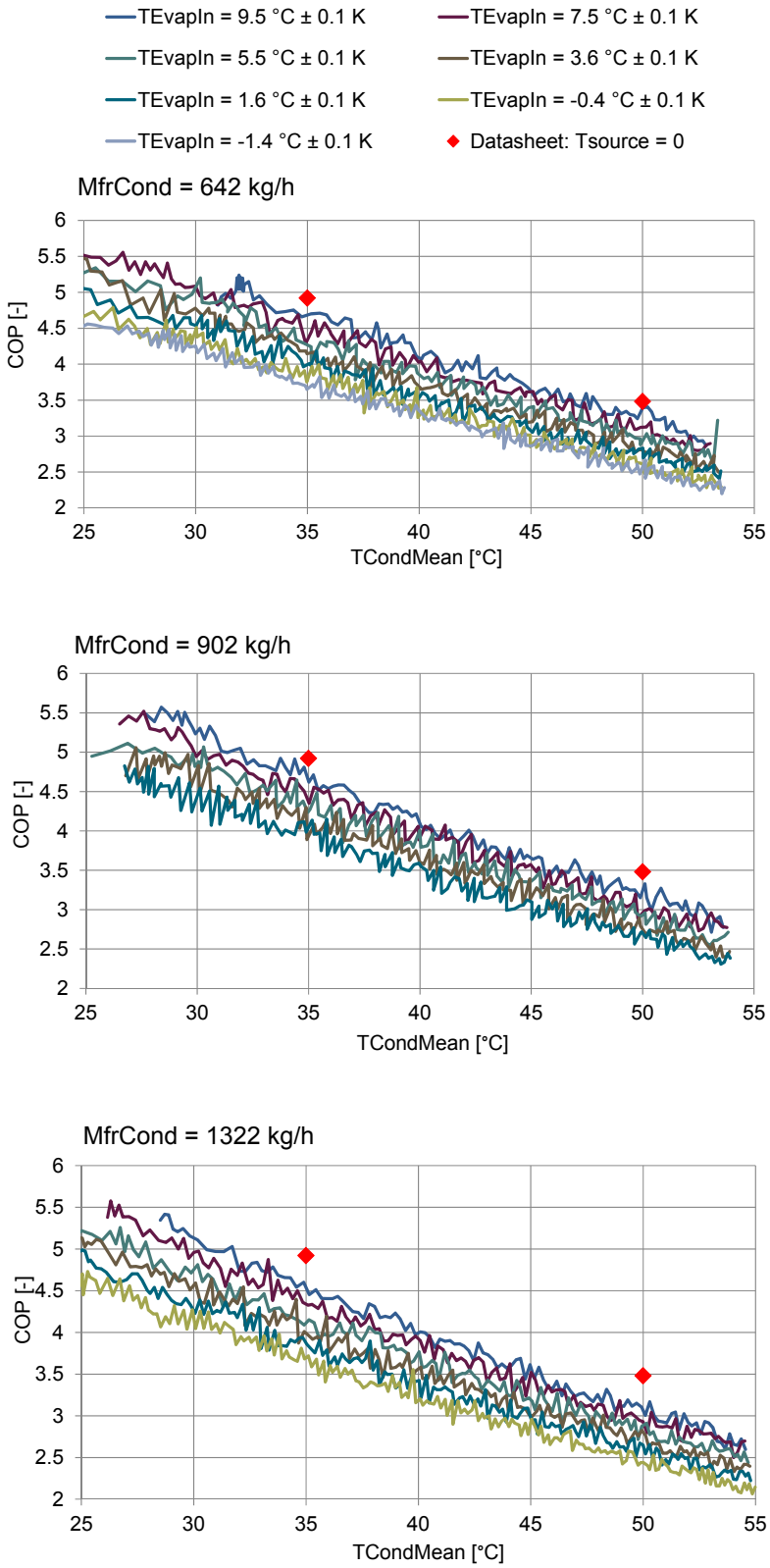

Figure 4.13: Temperature difference in the refrigerant cycle between evaporator inlet and evaporator outlet.

4.3 Measurements on a small de-iceable ice-storage heat exchanger

For some of the serial solar and heat pump concepts, ice storages are used in order to provide heat to the heat pump from the phase change enthalpy of the ice formation. The ice storage is regenerated with low temperature solar heat. Within the SOL-HEAP project, a small ice storage prototype with de-iceable heat exchangers was built and tested (Hirsch 2010). The conceptual idea of this ice storage unit was that the heat exchange surface area can be kept at low if the heat exchangers can be de-iced periodically. De-icing is achieved by temporarily providing heat to the heat exchanger that causes the melting of a thin layer of ice at the interface between the ice and the (flat plate) heat exchanger. Because of its lower density, buoyancy forces the ice to detach from the heat exchanger and the ice will float to the top of the water volume.

The copper-plate heat exchanger was built similar to a serpentine solar absorber and placed on the insulated bottom of a water filled glass-box (Figure 4.14). The iceable surface area was 64 x 30 cm. Heat extraction was provided by a cooling thermostat LAUDA RP 855 with integrated circulation pump, and a mixtures of 33.3% Antifrogen N ® was used as the heat carrier fluid.

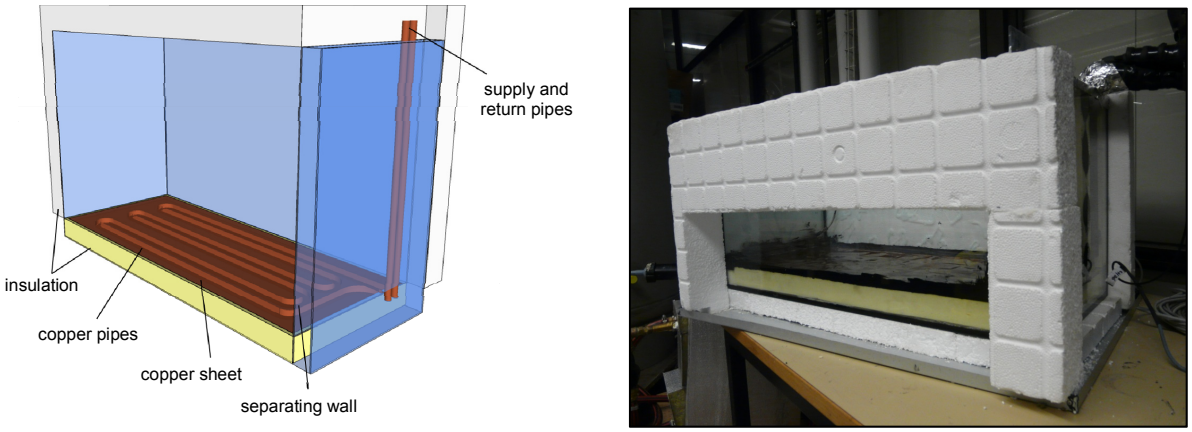

Figure 4.14: Schematic drawing of the heat exchanger in the glass water container (left) and photograph of the insulated container with removable pieces of insulation (right), (Hirsch 2010).

The temperatures of the heat carrier fluid were measured at the inlet and outlet of the pipes with pairwise calibrated 4-wire Pt100 temperature sensors, and the volume flow rate was measured with an in-house calibrated magnetic inductive flow sensor. From the Gauss'ian error propagation law, an uncertainty of 3% is estimated for the total heat extraction power, and an uncertainty of 5% for the UA-value calculated thereof. Figure 4.15 shows the measured specific heat extraction during ice formation for different inlet temperatures, and a comparison with estimated heat extraction rates when the ice-layer can be de-iced periodically. The de-icing was also tested and it showed that the automatic buoyancy driven detaching worked reliably, although the time-lags between the starting of the melting process and the detachment itself needed to be improved.

Based on this conceptual idea that was first evaluated in small scale in the SOL-HEAP project, the project HIGH-ICE was launched in order to upscale and further develop and improve the concept into a complete solar and heat pump system with ice storage.

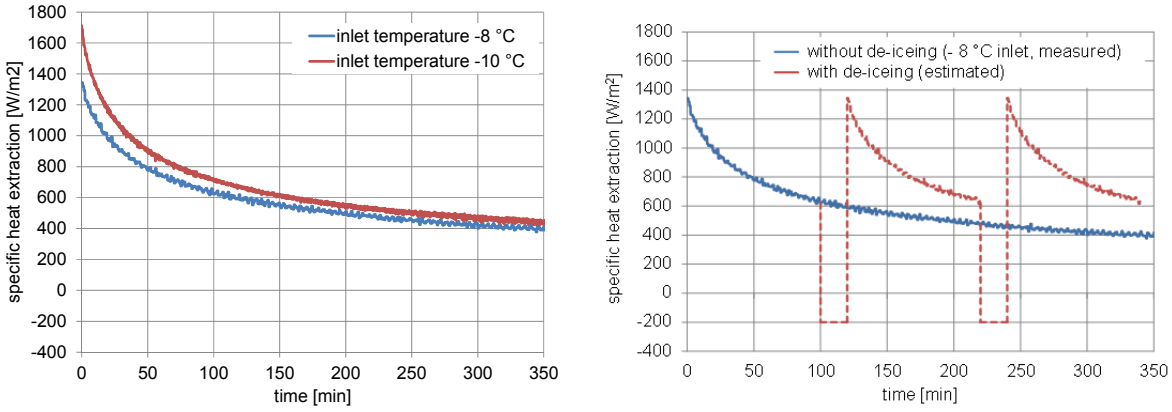

Figure 4.15: Specific heat extraction with a volume flow rate of 60 l/h without de-icing (left) and a comparison with the estimated specific heat extraction that can be achieved with de-icing (right), (Hirsch 2010).

4.4 Collector model adaptions for uncovered absorbers

Several changes have been introduced to the multinode collector model that was presented in Haller 2010, pp.59–60 which is based on the one-node ISO-model of Perers & Bales 2002:

- the number of nodes / segments has been increased from 10 to 100 and heat loss calculation of each node can now be based on the temperature of the respective node
- a stability criteria has been introduced to inform the user if the number of nodes for the collector capacitance has to be increased
- the quadratic heat loss term has been adapted
- a condensation term has been introduced

The increase in number of nodes / segments is important for simulating large unglazed collector fields because of two reasons:

1. in the type of model that is used, large thermal capacitance of the collector field combined with small time steps or small mass flow rates may cause instabilities in the calculation and unreasonable results (see also Haller 2010, pp.59–60). Increasing the number of nodes decreases the thermal capacitance of each node and thus improves both stability and accuracy of the model.
2. Uncovered collectors that are connected to heat pumps may be operated in absence of solar irradiation, serving as an air-to-brine heat exchanger. This operation may be characterized by small specific mass flow rates and heat gains that are not equal for the first and the last absorber in the fluid path, since the temperature difference to ambient may be quite different between these two collectors. Thus, heat gains have to be calculated based on the temperature difference to ambient for each collector element rather than based on an average collector field temperature that is taken as the average of the inlet and outlet temperature. In general, for any application it can be recommended that the number of nodes chosen should be equal to or greater than the number of collectors connected in series.

The stability criterion that was introduced is of the form $\left(\dot{m} \cdot c_p \cdot N_{seg} \cdot dt\right) \Big/ \left(C_{eff} \cdot A\right) \geq 0.5$. A warning is printed to the log-file if the stability criterion is not met.

The quadratic heat loss term of the collector efficiency equation is usually calculated as $a_2 \cdot (\vartheta_m - \vartheta_{amb})^2$ has been replaced by $a_2 \cdot (\vartheta_m - \vartheta_{amb}) \cdot |\vartheta_m - \vartheta_{amb}|$ in order not to increase heat losses (or reduce heat gains) when operated below the ambient temperature.

Two models for condensation gains have been implemented: one is based on Perers 2010. In this mode, the condensation gains are calculated as:

Eq. 4.7 $$\dot{q}_{lat} = \mathrm{c}_{cond} \cdot \Delta \mathrm{h}_{cond} \cdot u_{conv} \cdot \left[RH_{amb}/100 \cdot \nu_{sat}(\vartheta_{amb}) - \nu_{sat}(\vartheta_m) \right]$$

with

c_{cond} a parameter to be identified for the particular absorber, ideally it corresponds to $Le^{-2/3}/(cp_l \cdot \rho_l) = 0.916 \left[m^3 K/kJ \right]$, m³K/kJ

$\Delta \mathrm{h}_{cond}$ enthalpy of water condensation (depending on temperature 2400 – 2500 kJ/kg), for temperatures of the absorber fluid <-1°C, the enthalpy of solidification (+333.5 kJ/kg) is added to this value, kJ/kg

u_{conv} convective heat transfer coefficient between ambient air and absorber surface for condensation gain calculation, may be an input or calculated internally, W/(m²K)

$wf \cdot u_{w,0}$ meteorological wind speed multiplied with wind speed factor to account for mitigation effects that lead to lower wind speed on the absorber surface, m/s

$\nu_{sat}(\vartheta)$ saturated water load of air at temperature ϑ, kg/m³

The internal calculation of u_{conv} in the method of Perers is:

Eq. 4.8 $$\mathrm{u}_{conv} = 2.8 \frac{W}{m^2 K} + 3.0 \frac{J}{m^3 K} \cdot wf \cdot u_{w,0}$$

The second approach for modelling condensation gains is based on a method described by Bertram et al. 2010:

Eq. 4.9 $$\dot{q}_{lat} = \mathrm{u}_{conv} \cdot \Delta \mathrm{h}_{cond} \cdot \frac{R_L}{R_D} \cdot \frac{Le^{-2/3}}{cp_l \cdot p_{amb}} \cdot \left[RH_{amb}/100 \cdot p_{sat}(\vartheta_{amb}) - p_{sat}(\vartheta_{surf}) \right]$$

with $\vartheta_{surf} = \vartheta_m + \dot{q}_{gain}/u_{\mathrm{int}}$ and

R_L/R_D ratio of gas constant of air and water vapour, -

p_{amb} ambient pressure, bar

$p_{sat}(\vartheta)$ saturation water vapour pressure at temperature ϑ, bar

u_{int} internal heat transfer coefficient between fluid and absorber surface – to be found for each collector, W/m²K

The internal calculation of u_{conv} in this method is (units neglected):

Eq. 4.10 $$\mathrm{u}_{conv} = \sqrt[3]{\left(0.123 \cdot (\vartheta_{surf} - \vartheta_{amb}) + 2.7\right)^3 + \left(2.83 \cdot wf \cdot u_{w,0} + 4.3\right)^3}$$

The new version of this collector model including its source code and documentation is available for download from the homepage of SPF[4].

[4] www.solarenergy.ch -> Products.

4.5 Semi-physical heat pump model

The basis for the heat pump model Type 877 was an EES-model, that has originally been developed by Stefan Bertsch of NTB Buchs (Bertsch 2009), Switzerland and used the ARI model for the simulation of the compressor performance (ANSI/ARI 1999). Based on this EES model a TRNSYS model was programmed at Institut für Solartechnik SPF and further developed in cooperation between the Institute of Thermal Engineering, Graz University of Technology and SPF.

The compression heat pump model Type 877 is a semi-physical model based on a calculation of the thermodynamic refrigerant cycle and the thermal properties of the used refrigerant. A performance map of the compressor is used for the simulation of the compressor efficiency and the electricity consumption. Figure 4.16 shows a schematic view of the refrigerant cycle that can be simulated with the model. It includes the possibility to use air, brine or both as a heat source (two evaporators) and the possibility to use an extra desuperheater heat exchanger in addition to the condenser for e.g. the preparation of domestic hot water. A more detailed description can be found in Heinz & Haller (2013).

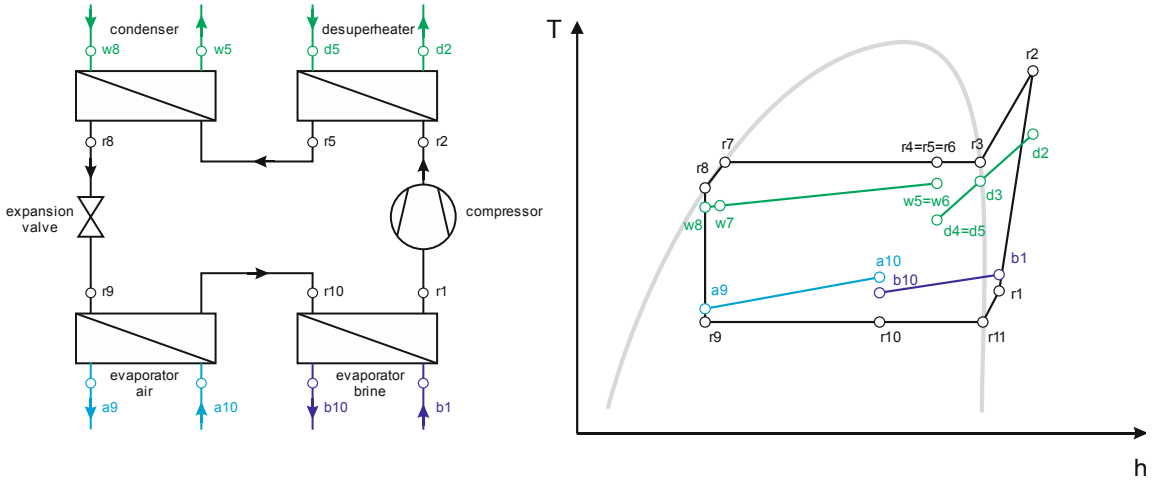

Figure 4.16: Left: Schematic of the heat pump cycle; Right: Schematic example process in the T-h-diagram with all heat exchangers active (Source: Heinz & Haller, Annex A3 of Dott et al. 2013a).

4.5.1 Modelling of the air/water (monoblock) heat pump I

The air/water heat pump measurements presented in section 4.2.1 were used to parameterize the semi-physical heat pump model using a compressor performance map as described in Heinz & Haller (2013). The first attempt to model the heat pump with a constant ΔT for superheating resulted in a considerable overestimation of the performance of the heat pump at high ambient air temperatures. In a second approach, the superheating was calculated as a function of the outdoor temperature, based on measurements of the temperature of the refrigerant loop before and after the evaporator (see Figure 4.17).

The parameters and constant inputs of the heat pump were fitted using GenOpt. The main parameters included:

- UA values of the evaporator and of the condenser
- parameters that determine the superheating as a function of the ambient air temperature
- amount of subcooling (a constant value was assumed)

- heat losses
- electricity uptake for the fan and the controller

The resulting deviation between measured and simulated COP of the heat pump, including control device and electricity for the fan, but excluding the pump for the heating water, was 0.045 COP-point on average (Figure 4.17). The measured point at -8°C ambient air temperature was excluded from the fit because of additional electric uptake of the control unit for heating the fan-casing during defrosting that was not observed for any other measured points. An extra deduction from the COP would have to be done for ambient air temperatures < -5 °C to take this extra electric uptake into account.

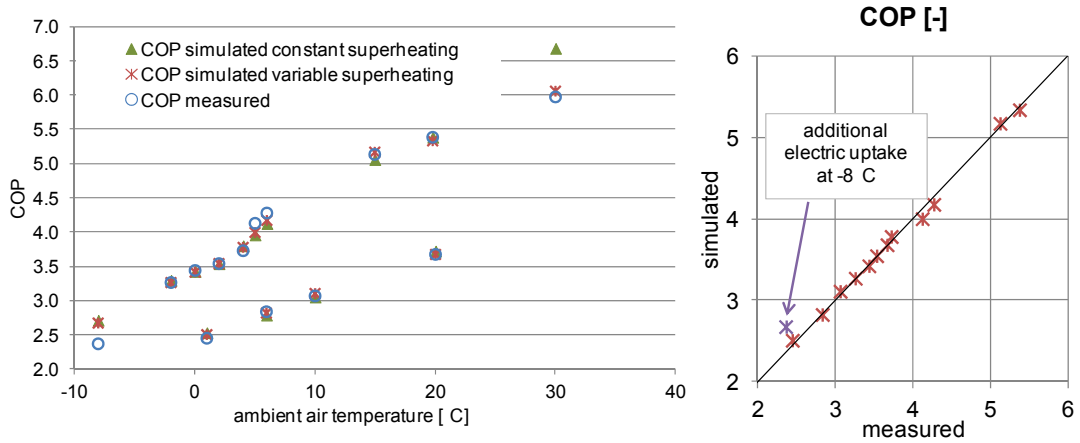

Figure 4.17: measured COP and COP simulated with constant superheating (green triangle) and with variable superheating (red cross).

4.5.2 Modelling of the air/water (split) heat pump II

This heat pump was a capacity controlled heat pump and the coefficients for the performance mapping of the compressor for different capacities were not available. Therefore, TRNSYS Type 877 was used in the mode where the isentropic and the volumetric efficiencies can be given as an input for the simulation.

In a first step, only steady state measurements were used in order to determine the parameters for steady state heat pump operation with GenOpt. These were:

- UA values for the evaporator and the condenser,
- isentropic efficiency and volumetric efficiency of the compressor, dependent on the speed of the compressor, and
- nominal capacity of the heat pump.

In a second step, also transients were included in order to determine the coefficients for the start and stop behaviour. Figure 4.18 shows measured and simulated values after the determination of the model parameters with GenOpt. Outlying values for electric uptake are due to two series of measurements with high ambient air temperatures (25 °C and 30 °C). Within the system simulations for parallel solar and heat pump systems that the model was used for, the heat pump was not operating under these conditions because these values correspond to sunny summer days with 100% solar thermal coverage.

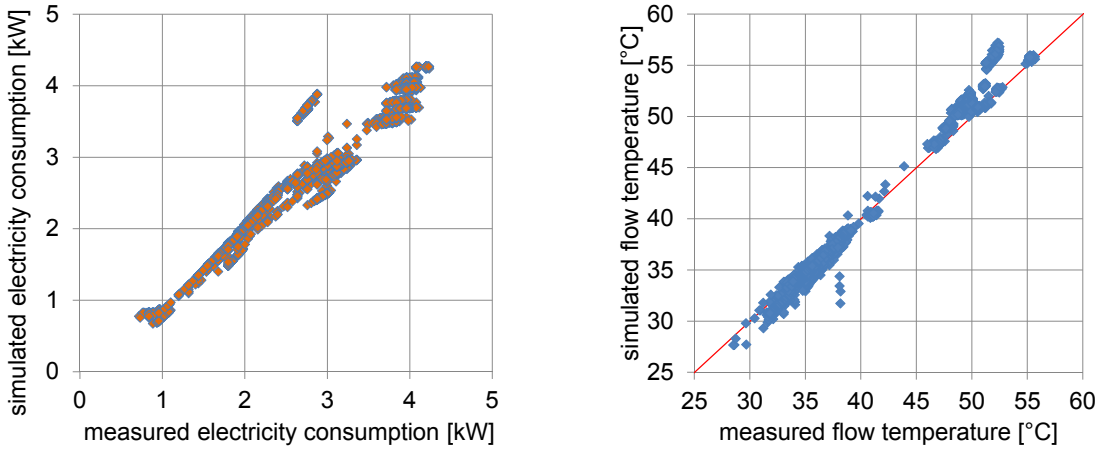

Figure 4.18: Measured vs. simulated electric uptake and measured vs. simulated condenser (water) outlet temperatures for the air/water heat pump II.

4.5.3 Modelling of a brine/water heat pump

A brine-to-water heat pump with a nominal heating capacity of 4 kW was measured during several charging processes of a storage tank (measurements not shown in detail in this report). In a first step, the UA-values of the heat exchangers, superheating and subcooling where fitted by comparison of measured and simulated temperatures in the working fluid cycle. Figure 4.19 shows simulated and measured COP during a charging process with condenser outlet temperatures between 35 °C and 45 °C and the brine source inlet temperature at about 1.5 °C. If the heat pump is assumed to be without heat losses, the simulated COP is considerably higher than the simulated one (left). After fitting the heat losses (a parameter of the model) the simulated and measured COP match quite closely with the exception of the start phase (middle). Figure 4.19, right, shows the result after fitting the start heat losses with the start time constant (another parameter of the model).

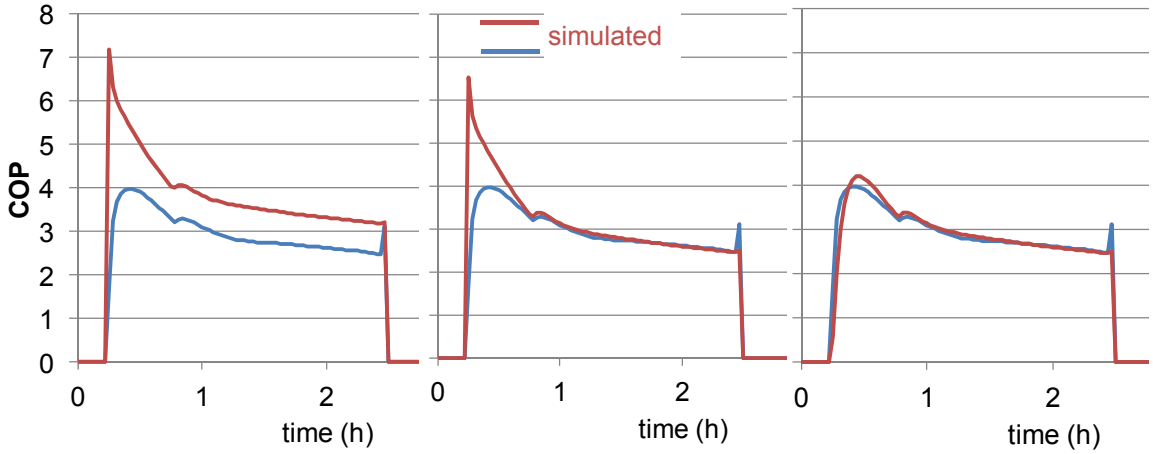

Figure 4.19: Simulated and measured COP over a boiler charging process with a brine-to-water heat pump without taking into account heat losses (left), only taking into account steady state heat losses (middle), taking into account steady state and start heat losses (right).

4.6 Parameter fit heat pump model

The YUM model described in Afjei & Wetter (1997) was adapted in the following way:

- Instead of fitting heating power and electricity consumption, the bi-quadratic curve fits were made for heating power and COP. Thus, the uncertainty of COP and seasonal performance factor calculation can be reduced slightly.
- In order to be compatible with the semi-physical heat pump model described in section 4.5, the simplified approach for the calculation of defrosting losses that is included in the semi-physical model was also introduced in this TRNSYS type.

The resulting TRNSYS Type 977 was parameterized with results from the semi-physical model and used in order to increase both speed and stability of the simulations for some of the simulation studies that are presented in this report (e.g. in section 6.3).

4.6.1 Modelling of a brine/water heat pump

The measured data of heat pump III (section 4.2.3) were used to parameterize TRNSYS Type 977 (Excel-Solver routines applied on sum of square differences between modelled and simulated COP and electric uptake). Figure 4.20 shows the comparison of modelled and measured COP with the mass flow rate that was also used during the system test (900 kg/h).

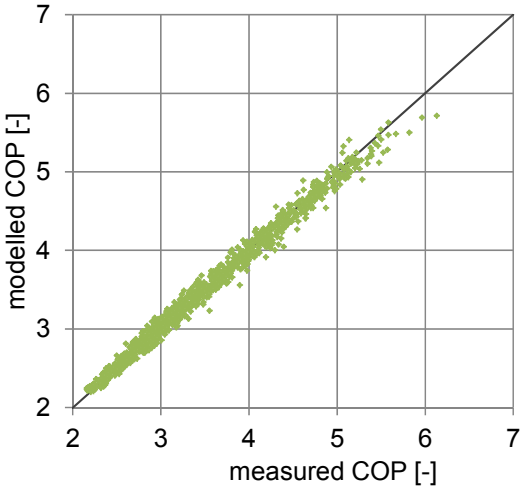

Figure 4.20: Modelled and measured COP for the brine/water heat pump III.

In a second step, the start and stop time constants were determined based on measurements from the heat pump in the twelve day concise cycle test period. Figure 4.21 shows the match of the dynamic heat pump operation.

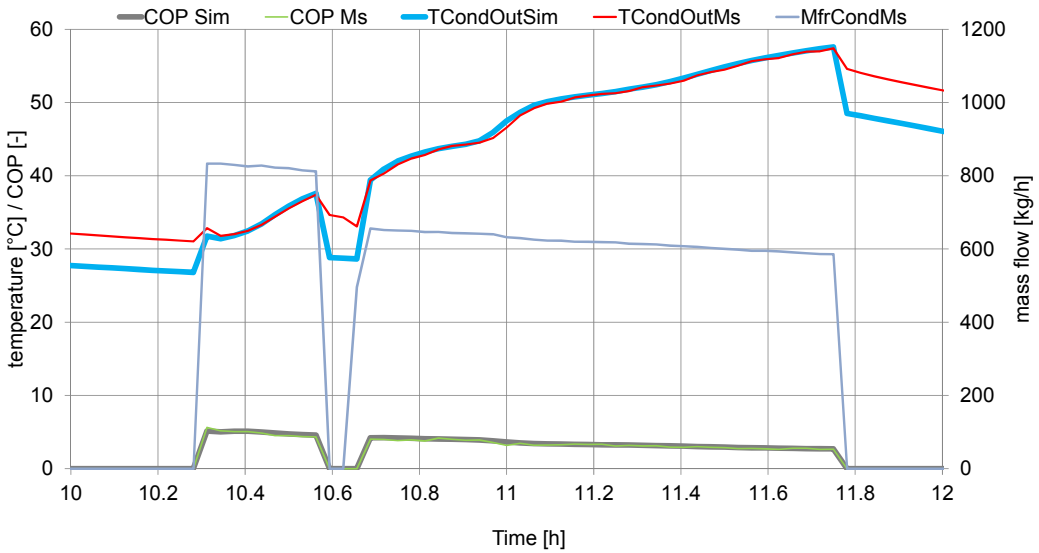

Figure 4.21: Match of COP in dynamic operation during a twelve day test.

5 Monitoring results for a parallel system

Within a project that was financially supported by Elektrizitätswerke Rapperswil-Jona (EWJR), detailed measurements have been performed between February 2010 and February 2012 on a parallel air source SHP system that provided space heat and domestic hot water. Results were presented in Haller & Frank (2012), and a summary of these results is given here. Both the heat pump and the solar thermal collectors provide heat for a solar tank-in-tank combistorage. The combistorage delivers space heat and DHW. Figure 5.1 shows the energy flow chart of the system.

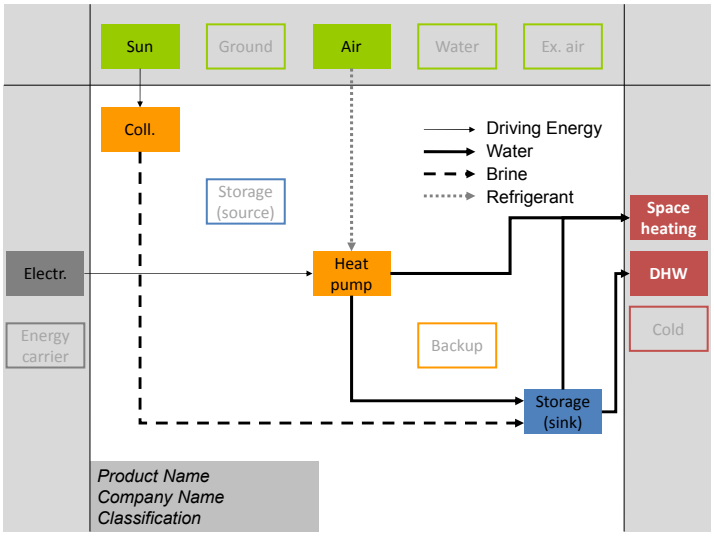

Figure 5.1: Energy flow chart of the monitored field SHP system.

Because of the present components and the connections shown in the energy flow chart, the system is classified as a parallel (P) system of type ${}^{Sol}_{skS}SHP^{Air}_{skS}$. The heat pump can charge the storage either in the upper part or in the lower part (two three way valves, one each in the supply and return line). Simultaneously to delivering heat into the space heating zone of the combistorage, part of the heat is directly taken from the supply line for the space heat distribution. Figure 5.2 shows the single family home with the roof-integrated solar collector field. An overview on the technical data and sizing of the components is given in Table 5.1. More details on the system and the measurement uncertainties can be found in Haller & Frank (2012).

Figure 5.2: Single family home with 15 m^2 solar thermal collectors.

Table 5.1: Technical data of the components of the system.

Air-water heat pump	
heating power (A2/W35)	19.7 kW / 11.4 kW
COP (A2/W35)	3.8 / 3.9
Collector field	
type	flat plate, glazed, selective
performance coefficients	η_0= 0.83, a_1= 3.7, a_2= 0.009 (reference: absorber area).
absorber area	15 m^2
orientation	slope 38 °, orientation 20 ° west (from south = 0 °)
Storage	
type	tank-in-tank
volume	1.8 m^3

Results of the field monitoring are summarized in Table 5.2. Figure 5.3 shows the performance factors of the system for single months as well as for the whole year. The performance of the single components is shown in Figure 5.4.

Table 5.2: Summary of the field monitoring results for the year 2011.

availability of data	>99.9% based on minutes.
irradiation on collector plane	1472 kWh/m^2
average outdoor temperature	12.0 °C
space heat supplied	18 700 ± 700 kWh
DHW supplied	1400 ± 400 kWh from storage
supply- and return temperatures	Mostly <35 °C supply from storage to supply mixer valve, and < 28 °C return
solar yield	501 kWh (±3.2%) per m^2 absorber surface
electricity used[a)]	4 563 ± 380 kWh
SPF_{bSt} (before storage)	5.1 ± 0.4
SPF_{SHP} (after storage)	4.4 ± 0.4
SPF heat pump	3.6 ± 0.3
SPF collector loop	80 ± 5

[a)] heat pump, collector loop, all controllers, pumps, and other components with the exception of the space heat distribution pump.

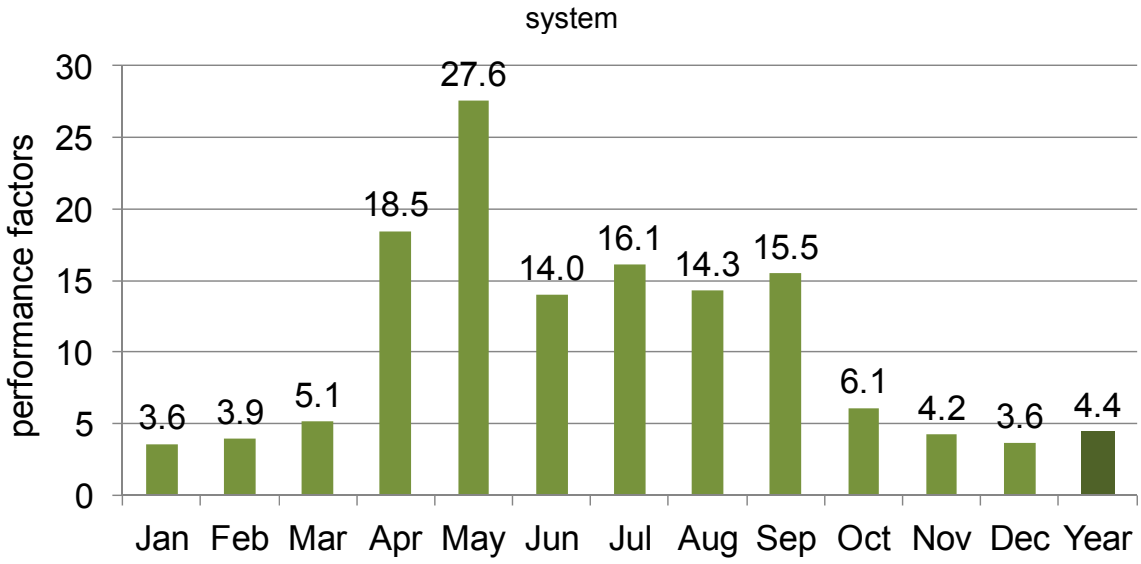

Figure 5.3: Monthly and annual performance factors for the system (SPF_{SHP}).

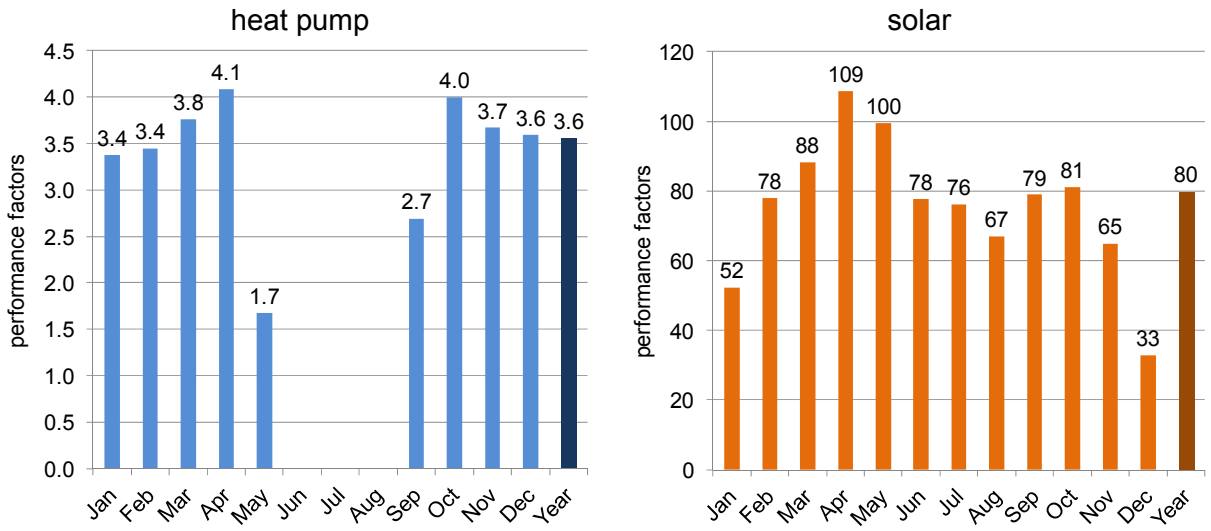

Figure 5.4: Monthly and annual performance factors for the heat pump and for the solar circuit.

The annual efficiency of the overall system with an SPF before storage of 5.1 and 4.4 after storage is quite high for an air-water heat pump combined with solar. In comparison with this, the average of air-water heat pumps in the field monitoring of Miara et al. (2011) was $SPF_{bSt} = 2.7$ (bSt = before storage). The high seasonal performance factor of this installation is interpreted to be a result of several factors:

- High solar coverage with high performance factors in summer and in spring and autumn (visible from the high system performance factors in the respective months.
- Larger than average collector area of 15 m^2 and water storage volume of 1.8 m^3.
- Low fraction of the total heat demand for DHW, and low temperatures for the space hat distribution.
- Good hydraulic integration and control of the heat pump with return to the heat pump during DHW charging above the space heating zone.

- Relatively mild temperatures in the winter months during the monitored year.

Despite of the good performance of this system it was noted that the heat pump delivered more heat in DHW mode to the storage than needed to cover the demand of DHW only. One reason for this are heat losses from the upper section of the storage combined with a low DHW demand in general. Another reason is that part of the heat that was delivered to the DHW zone of the storage is transferred to the space heating zone of the storage and subsequently mixed down to the supply temperature set point for space heating in the space heating mixer. Thus, even for this well performing system there seems to be room for improvements.

Including the electric heat tape that is installed along the DHW line between the storage and the DHW distribution reduces the SPF from 4.4 to 4.0. The use of electric heat tapes in combination with solar thermal systems may be seen as a waste of electric energy since solar heat is available in excess for more than 60% of the year. Short pipes between the storage and a DHW distributor can be kept warm by natural circulation within this pipe. In this case the heat trap that is usually installed at the storage connection to prevent natural circulation is installed for each DHW line connected to the distributor (see Nipkow et al. 2011). For multifamily houses, forced circulation loops profit from excess solar heat, whereas heat tapes do not.

6 Solar and heat pump system simulations

6.1 Comparison between solar DHW-systems and solar combisystems

Although solar DHW systems were not the main topic of the SOL-HEAP project, these systems are interesting because the benefit from adding solar collectors to a heat pump system is higher than for combisystems – as long as the applied collector areas remain low.

Simulations have been performed with Polysun for air and ground source heat pump systems in combination with solar thermal collectors for DHW only and in combination with solar thermal for DHW and space heating. The climate of Strasbourg was chosen with a similar DHW and space heat demand as in the SFH45 of T44A38 (DHW: 2085 kWh/a, space heating: 8080 kWh/a). A two storage solution (450 l DHW, 300 l space heat buffer) has been chosen for the DHW systems, and a buffer-tank with 750 l and external DHW heat exchanger for the combisystem. The results have been evaluated in terms of seasonal performance factors for the heat pump (SPF_{HP}) and for the whole system (SPF_{SHP+}), counting both DHW and space heat as useful heat in the SPF definition.

Results presented in Figure 6.1 show that the addition of solar collectors to the heat pump systems increases the seasonal performance factor of the systems by about 0.07 – 0.12 per m^2 collector area. The performance factor of the heat pump alone is increasing as well for the DHW systems, and decreasing slightly for combisystems, with increasing solar fractions. The reason for this is that in the case of a solar DHW system, the heat pump has to produce less heat at the higher temperature levels needed for DHW preparation. Thus, SPF_{HP} is approaching more the better COP in space heating mode.

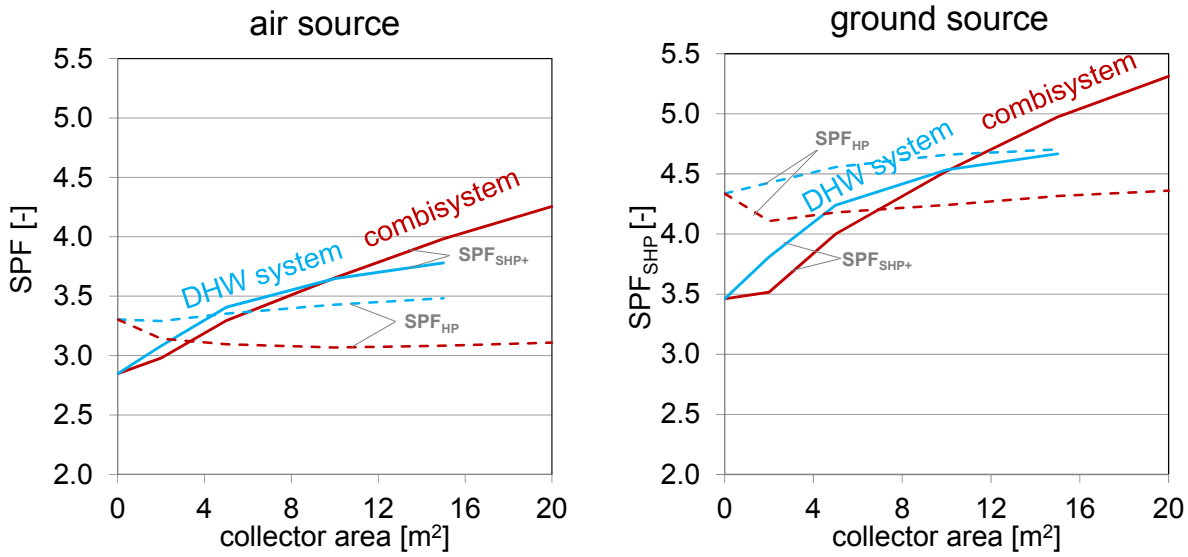

Figure 6.1: Simulation results (Polysun) for air-source (left) and a ground source (right) SHP system where solar heat has been used for DHW only (DHW system) or for DHW and space heating (combisystem).

6.2 The influence of additional Legionella safety measures on solar savings

Legionella (in general species of Legionella pneumophila) are pathogenic bacteria that may cause the illness Legionellosis. These species are present in many natural environments, and have been found to multiply excessively in anthropogenic wet environments in the temperature range between 32 °C and 42 °C. Although sanitary installations in single family homes are considered to be only a "low risk" for Legionella growth and infection[5], some recommend to preventively heat the stored domestic hot water to 60 °C at least once a day.

In order to investigate the effect of daily or weekly electric heating to 60 °C on the energetic performance and on solar electricity savings, an air source DHW system with a 450 l tank was simulated with Polysun[6]. One simulation was performed with 5 m^2 solar collectors heating the lower half of the DHW tank (HP-Sol). Another simulation was performed without solar heat use (HP). The heat pump was allowed to charge the DHW storage from 8 – 10 p.m., and from 48 – 52 °C. An electric heater was placed in the lower third of the DHW storage, and allowed to perform Legionella prevention heating up to 60 °C for one hour after the time-window of the heat pump heating. The following distinctions can be made between the simulations:

- *without*: no electric heating
- *Legio daily*: electric heating enabled daily from 11 – 12 p.m.
- *Legio weekly*: electric heating enabled only once a week from 11 – 12 p.m.
- *HP-Sol smart*: electric heater is disabled if the temperature of the storage tank was above 62 °C within the last 22 hours (Legio daily) or within the last week (Legio weekly).

Figure 6.2 shows the influence of electric heating on the system performance. Here the SPF_{SHP} only includes DHW as useful heat delivered (no space heating). Whereas the seasonal performance factor of the system is increased from 2.2 to 5 for the DHW system without electric heating. For daily electric heating, the heat pump contribution to DHW is reduced almost to zero, while the solar gain is only reduced by 7%. Only weekly instead of daily enabling of the electric heating reduces the negative effect on the heat pump substantially.

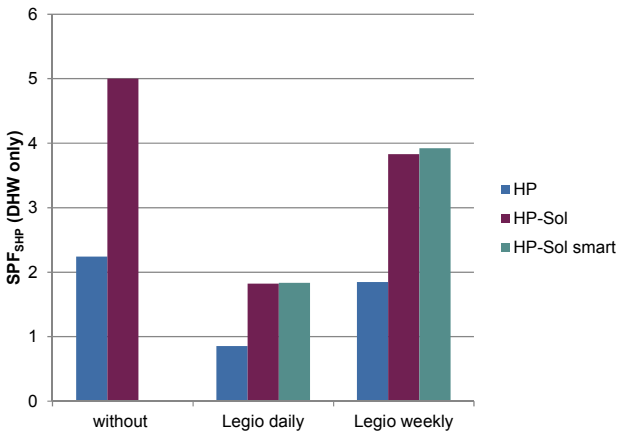

Figure 6.2: The influence of Legionella safety measures (electric heating to 60 °C) on the performance of solar DHW systems with heat pump backup heating.

[5] Bundesamt für Gesundheit BfG 2009.

[6] same DHW load and climate as in the previous section.

While electric savings through solar collectors are in the range of 100 to 120 kWh_{el}/m^2 for the systems without electric heating and with only weekly enabling of electric heating,

solar electric savings increase to 260 kWh_{el}/m^2 for the simulated system with daily enabling of electric heating for Legionella safety.

Today, heat pumps are on the market that can reach temperatures of up to 70 °C, which enables these heat pumps also to charge the DHW tank to 60 °C, even if the temperature difference across the internal heat exchanger is considered.

For systems with daily Legionella prevention by heating to 60 °C, only heat pumps that can reach these temperatures should be used.

6.3 The integration of solar combistorages

Combistorages are used frequently to store heat for SH & DHW within one unit instead of two separate units, especially in solar thermal applications in Central Europe. Field tests (Miara et al. 2011), as well as some of the laboratory results reported in chapter 7, show examples for disappointing performance results for systems that combine heat pumps with combistorages. The influence of the hydraulic integration and control of a heat pump into systems that include a solar combistorage was studied by means of annual simulations, and the differences in the energetic performance were evaluated and presented in Haller et al. 2013c; Haller et al. 2013b. The results of these simulations confirm conclusions that were also derived from the laboratory measurements presented in chapter 7. In this section, only a short summary and the final conclusions from these simulation studies are presented. Figure 6.3 shows the simplified hydraulic scheme of the simulated reference system.

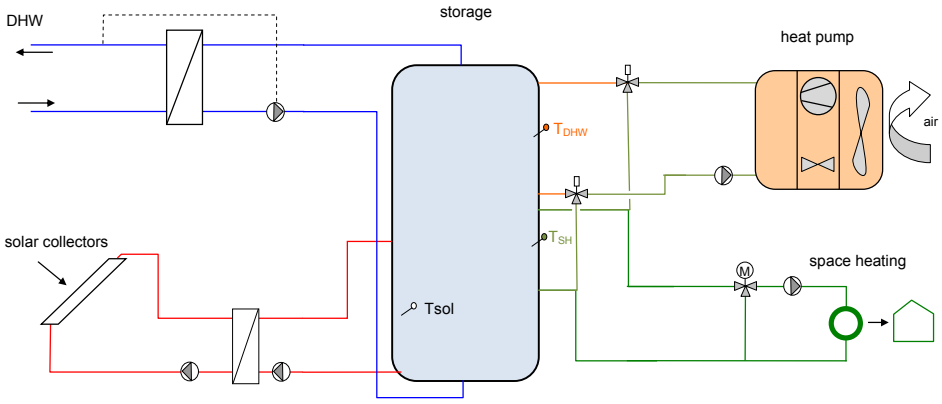

Figure 6.3: Simplified scheme for the system hydraulics of the base case.

The heat load (DHW and SH) corresponds to the heat loads defined for T44A38 for a single family home with 15, 45, and 100 kWh/(m^2a) space heating demand in the climate of Strasbourg and a DHW demand of 2100 kWh/a. The supply and return temperature of the heating system was 35/30 °C. The solar collector field was 15 m^2 (gross) and the stratifying thermal energy storage had a volume of 900 l. Mixing effects that may be caused by turbulences from inflowing fluid where not taken into account by the storage simulation model.

With the exception of matching the size and volume flow rates of the heat pump to the chosen buildings, the size and performance parameters of all components remained identical for all simulations. The only parameters that were changed in the different simulations were:

- The inlet and outlet heights of direct charging double ports from and to the heat pump in DHW and in space heat operation of the heat pump.
- The position of the temperature sensor in the DHW zone of the combistorage.
- The mass flow rate of water through the heat pump condenser in DHW charging mode.
- Interruption of space heat supply during DHW charging by the heat pump (DHW priority).
- The time-window during the day where the heat pump was allowed to charge the DHW zone of the combistorage.

The influence of storage stratification on the overall performance was studied by increasing the effective vertical thermal diffusivity parameter of the storage tank model until the simulated storage was close to an always fully mixed storage. The results were analysed with the method described in Haller et al. 2010 with the adaption of Logie et al. 2010 that computes the fully mixed storage tank reference with equal charging and discharging power and mass flows rather than with equal inlet temperatures and mass flows:

Eq. 6.1 $$\eta_{strat} = 1 - \frac{\Delta S_{St,sim}}{\Delta S_{St,mix}}$$

The influence of hydraulic concepts and control was evaluated in terms of the electric energy demand for the whole system (compressor and fan of the heat pump, pumps, controllers, etc.) over one simulated year.

Figure 6.4 shows results for different solutions of hydraulic integration and control of the heat pump in terms of additional electric energy demand compared to a good performing reference (Ref) in % (left axis) and in absolute values (right axis) for the SFH45 building of T44A38 in Strasbourg. In simulations with "time window", the heat pump was only allowed to charge the DHW zone of the combistorage from 6 p.m. to 8 p.m., and no DHW priority was set. The other simulations were performed without time-restrictions for DHW charging by the heat pump.

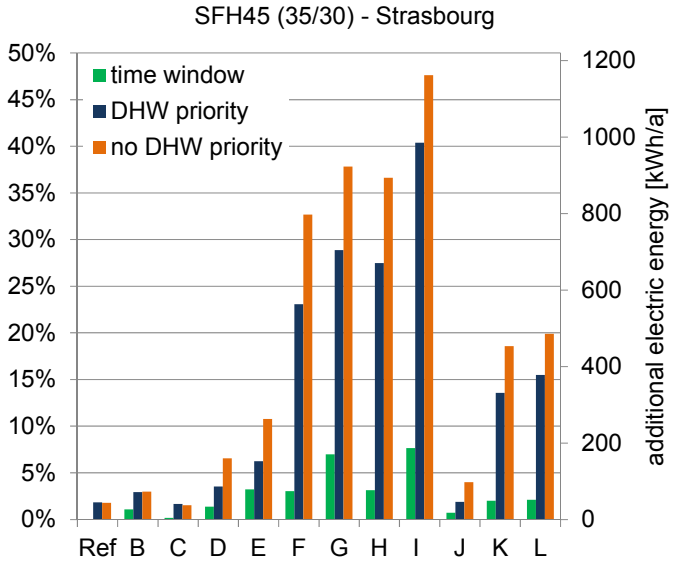

Figure 6.4: Additional electricity demand compared with the reference for SFH45 with a low temperature space heat distribution system of 35/30 °C for supply and return. Differences in hydraulics and control for the different systems Ref to L are explained in Haller et al. 2013b.

For system configuration F, simulations were performed setting a 2 h time window for charging the DHW zone of the combistorage for different times of the day. Figure 6.5 shows that choosing a time-window for DHW zone charging between 8 p.m. and 10 a.m. increases domestic hot water penalties, i.e. it reduces the comfort level for the user. The highest seasonal performance factors, together with low penalty values, are achieved if the 2 h time window is set between 2 p.m. and 8 p.m.

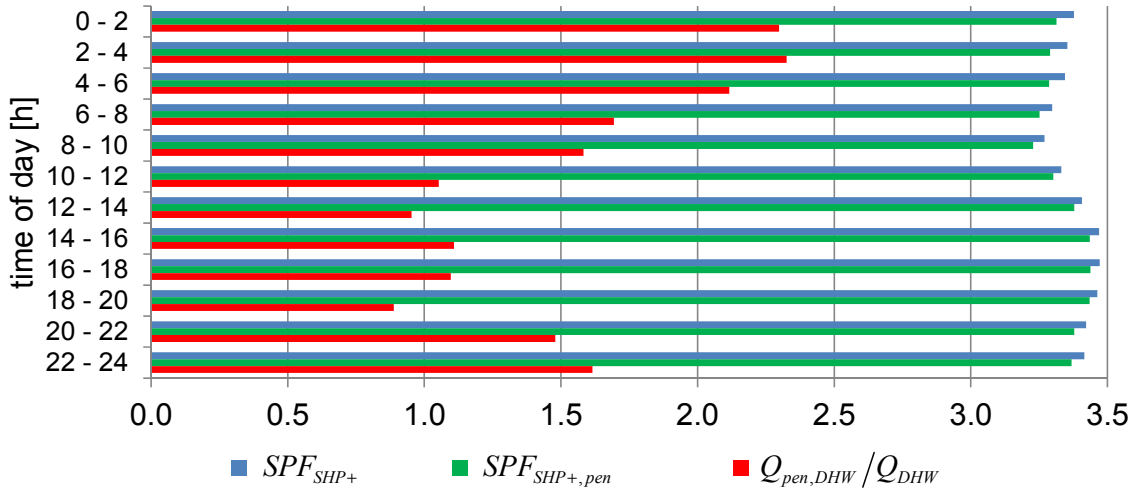

Figure 6.5: Effect of time of the day for the time-window for charging the DHW zone of the combistorage, based on system configuration F (Haller et al. 2013b).

The influence of storage stratification efficiency on the energetic performance is shown in Figure 6.6. It shows clearly that the influence of bad stratification (η_{strat} << 50%) on the electricity demand of the system is quite similar to the influence of bad hydraulics and control. In the figure shown, a stratification efficiency of 100% corresponds to an ideal (i.e. isentropic) storage process, whereas a stratification efficiency of 0% corresponds to an always fully mixed storage vessel. Naturally, real storage processes are expected to lie between these values.

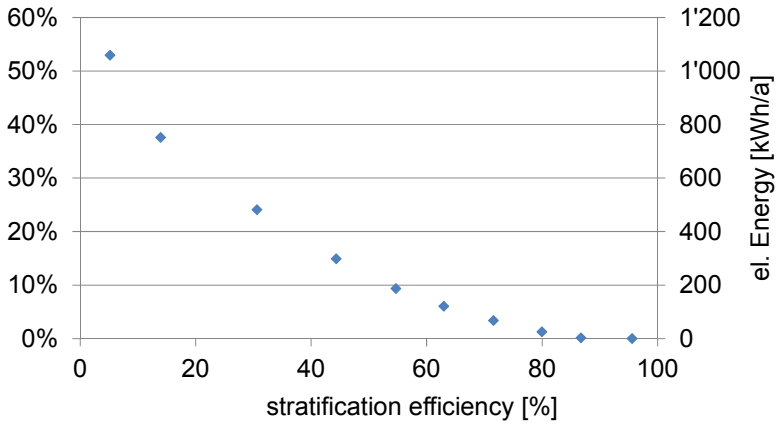

Figure 6.6: Additional electricity demand compared with the reference versus stratification efficiency.

The additional electricity demand compared with the reference can be interpreted as additional cost for energy purchase during the operational phase of the system. Depending on the variant of hydraulics and control, these additional costs compared with the reference amount up to 48 % (SFH45), or 1800 kWh_{el}/a (SFH100 35/30 °C, not shown).

The correlation of low seasonal performance factors with the amount of heat that the heat pump delivers in DHW mode is shown in Figure 6.7. For a system with good integration and control of the heat pump the ratio of $Q_{HP,DHW}/Q_{DHW}$ is 30%-40%. Such a low percentage is the result of solar coverage over a large part of the year on the one hand, and DHW pre-heating from 10 °C to 35 °C in the lower part of storage on the other hand. Thus, the heat pump only needs to provide the missing heat from 35 °C to 55 °C in DHW mode, and this only during part of the year. However, for systems with bad hydraulic integration and control, in particular for systems where the DHW sensor is too much influenced by the space heat operation of the storage, $Q_{HP,DHW}$ may increase by a factor of 10, with the corresponding negative effects on the seasonal performance factor of the system.

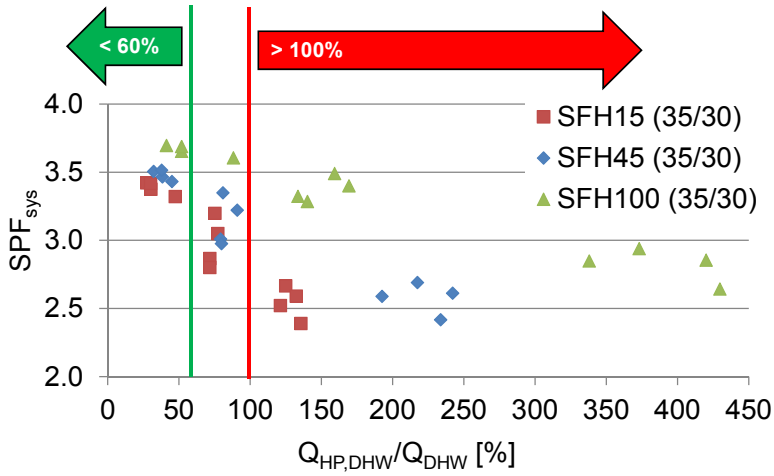

Figure 6.7: Dependency of the SPF on the amount of heat that the heat pump delivers in DHW-mode ($Q_{HP,DHW}$ variable, Q_{DHW} = 2100 kWh/a constant).

The electric energy demand of unfavourable hydraulic and/or control solutions can be about 50% higher than for a good solution with the same main components. The same is true for a badly stratifying storage. With current electricity prices (0.15..0.20 €/kWh for households in central Europe) this corresponds to additional operational costs for electricity of 120..360 €/a.

Based on these findings that are also backed up with whole system test results as presented by Haberl et al. (2013), simulations presented by Poppi & Bales (2013), as well as results from Polysun simulations by Zimmermann 2012, three recommendations for the integration of heat pumps into systems with solar combistorages can be given:

Recommendations for the integration of heat pumps into systems with combistorage

1. The position of the ***DHW sensor for boiler charging control*** must be placed at a safe distance from the space heating zone of the storage. This distance depends on the stratification efficiency of the storage and on the mass flows used for storage charging and discharging. It is thus system-specific. As a first approximation, a distance of ***20-30 cm*** may be seen as the absolute minimum for typical geometries of combistores with about 0.9 m^3 water volume. The ***storage stratification efficiency*** has to be tested with the volume flow rates that correspond to the volume flow rates that are later encountered in the field. Insufficient stratification may lead to a fast decrease in temperature at the position of the DHW sensor during space heat operation of the storage and/or the heat pump, and thus to excessive DHW charging by the heat pump.
2. The ***return from the storage to the heat pump in DHW mode*** must be placed above the space heating zone of the storage.
3. The heat pump should only be allowed to ***charge the DHW zone*** of the combistorage within a small ***time-window*** during the day. For a standard DHW load profile, the optimum time-window is ≤ 2 h between 6 p.m. and 8 p.m., or at the beginning of a reduced night-time electricity tariff.

For modulating heat pumps, in particular in combination with space heat distribution systems that can guarantee a minimum flow, bypassing the storage as much as possible in space heating mode should be considered. In this case, the storage is only used in space heating mode when there is either heat from the solar thermal system that can be used or when the heat pump needs to increase its running time (closing thermostatic valves).

The presented simulation results correspond well with results from whole system testing that are presented in chapter 7, showing that the amount of heat the heat pump delivers for DHW may on some days of the test-sequence be as high as 200% of the amount of DHW heat that the storage delivers on the same day. However, the simulation results presented here are to be interpreted with care. In particular, it has to be kept in mind that turbulences caused by the inflowing fluid streams (so called inlet jet mixing) and their negative impact on stratification were not included in the storage tank model that was used.

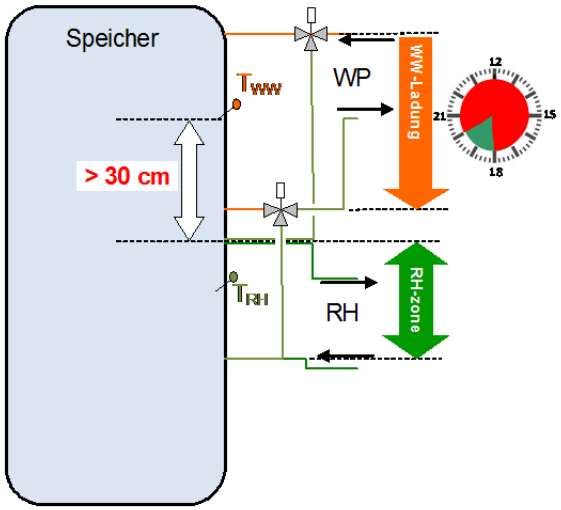

Figure 6.8: Recommendation for the integration of heat pumps into systems with solar combistorage.

6.4 Solar combisystems and the influence of space heat distribution control

In order to be able to limit effectively the space heat distributed to the minimum that is required to maintain the desired room temperatures, thermostatic valves are usually installed for each radiator or for each floor heating pipe loop in energy efficient buildings. However, for floor heating systems that have a high thermal capacity and are operated with low supply temperatures, it has sometimes been recommended to refrain from the general practice of using thermostatic valves in combination with heat pumps. Thus, a minimum mass flow rate across the condenser of the heat pump can be guaranteed and frequent on/off cycling of the heat pump can be avoided even without the use of a technical storage in the space heat distribution.

In order to study the effect of refraining from the use of thermostatic valves within the space heat distribution, three simulations have been performed with TRNSYS using the same SHP system as in the previous section. In all simulations the space heat supply temperature was controlled dependent on the 24 h outdoor air temperature and the design temperatures for supply and return (35 / 30 °C). The three simulations differed in the following way:

1. *With thermostatic valves (TV):* The mass flow rate in the space heat distribution was reduced by a PI-control algorithm. The process variable was the air temperature of the one-zone building, and the set-point was 20 °C.
2. *Without TV*: The mass flow rate was constant (design volume flow rate of the space heat distribution).
3. *Without TV and supply temperature reduced*: Same as 2, but the design supply and return temperatures were reduced as much as was possible without reducing the comfort significantly (see section x for comfort criteria). The assumption here was that without thermostatic valves the user will notice excessive heating and try to reduce it as much as possible.

The simulation results presented in Figure 6.9 show that refraining from using thermostatic valves in solar and heat pump systems may lead to a higher seasonal performance factor. However, the electric energy use increases at the same time. The reason for this is that the building is overheated on days with passive solar gains, and in these periods more heat is supplied to the space heat distribution than actually required. Since the heat demand increases more than the SPF, the total electricity consumption increases too.

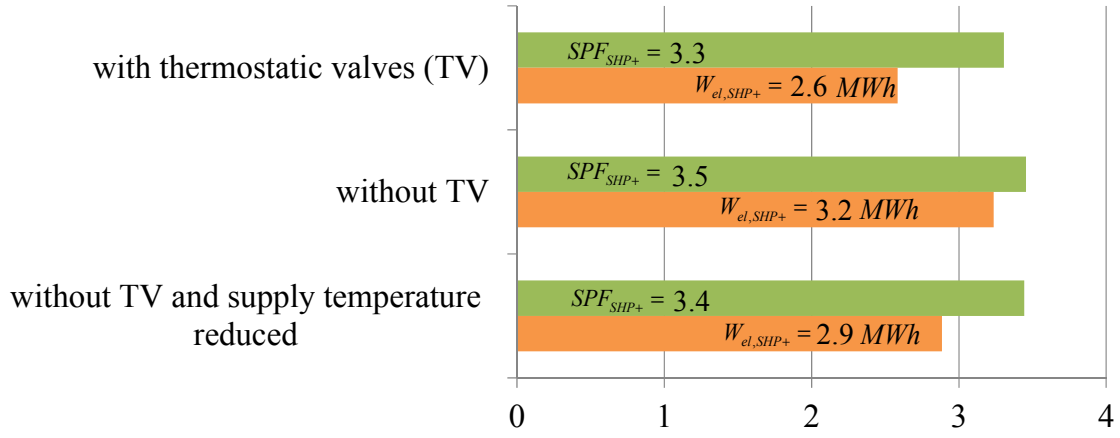

Figure 6.9: Performance of a solar and heat pump heating system with different control of space heat distribution.

6.5 Parallel systems for DHW and space heating

6.5.1 Simulation with T44A38 boundary conditions

In this section the analysis of parallel SHP systems with air source and with ground source heat pumps is presented. The simulations have been carried out with the reference boundary conditions of T44A38 on the platform TRNSYS-17. A platform intercomparison check has been performed and the results match very well the reference values.

Results for 15 m^2 of collector area and a storage volume of 60 l/m^2 are presented in Table 6.1 for the three buildings SFH15, SFH45 and SFH100. The lowest SPF_{SHP+} is obtained for SFH100, due to the higher supply temperature to the building.

Table 6.1: Overall system performance table for different buildings and the same collector area of 15 m^2 and storage volume of 60 l/m^2.

		SFH15		SFH45		SFH100	
		air source	ground source	air source	ground source	air source	ground source
$SPF_{SHP+,pen}$		**3.72**	**5.77**	**3.63**	**5.72**	**2.68**	**4.27**
SPF_{SHP+} without penalties		3.74	5.85	3.69	5.78	2.69	4.30
SPF_{HP}		2.68	4.73	3.64	5.23	2.40	4.13
Useful heat							
DHW	kWh/a	2074	2075	2075	2075	2075	2075
space heat	kWh/a	2471	2471	6474	6474	14042	14042
Total	**kWh/a**	**4546**	**4545**	**8549**	**8549**	**16117**	**16117**
Used Electricity							
System	kWh/a	1215	776.6	2348	1478	5998	3748
Penalty DHW	kWh/a	10.3	13	10.9	18	13.3	17.1
Penalty SH	kWh/a	1.3	1.6	0.7	0.8	13.8	13.9
Total	**kWh/a**	**1226**	**789.5**	**2359**	**1497**	**6025**	**3779**

The SPF of the system (SHP+) and of the heat pump (HP) are presented in Figure 6.10 as a function of collector area for ground source (left) and air source (right) SHP systems. One can clearly see that the increase in SPF_{SHP+} with increasing collector area is significant in both systems. Comparing one against each other it can be observed that the increase in SPF_{SHP+} as function of collector area is higher for ground source (higher slope) compared to air source systems. The SPF_{SHP+} range from 3.8 to 7 for ground source SHP and lower values ranging from 3 to 4.6 are found in air source SHP systems. The performance of the heat pump alone is not significantly affected by the collector area in these simulations.

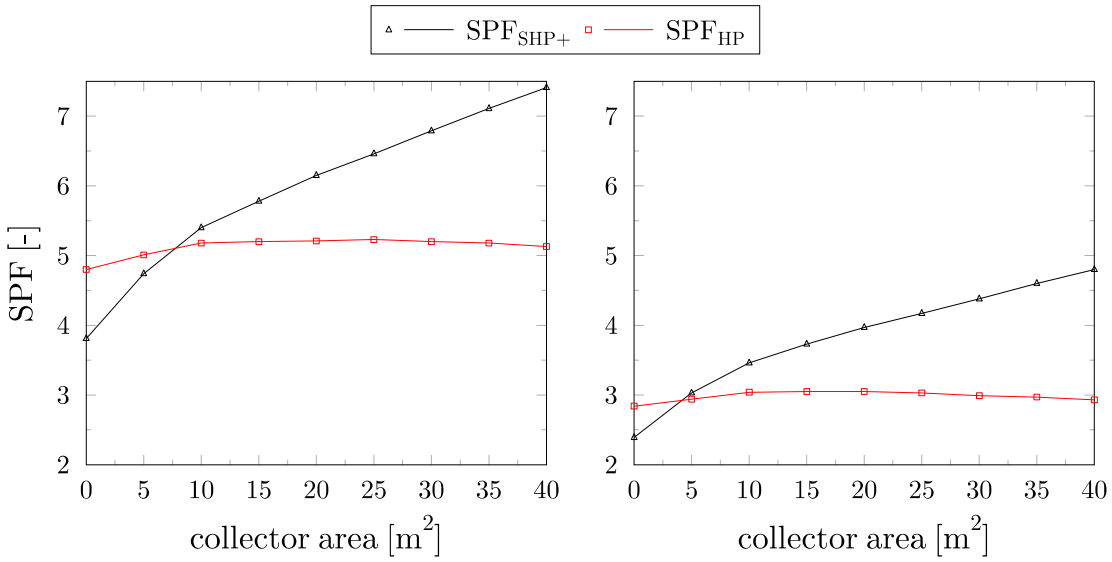

Figure 6.10: Heat pump and system seasonal performance factor as function of collector area for ground source (left) and air source (right) SHP systems.

6.5.2 Benefit from adding solar collectors to a heat pump system

The objective of this section is to systematically assess the potential benefit of adding solar thermal systems to a heat pump in different climates around Europe. Only system concepts (hydraulic solutions) that proved to show a good performance in section 6.3 have been considered (see Haller et al. 2013b for more details).

A pre-validation of Polysun-6® simulations (http://www.polysun.ch) was carried out by comparing the results with results achieved by TRNSYS simulations (http://www.trnsys.com) for parallel air source and ground source SHP systems. Polysun simulations were compared with results presented in section 6.5.1 for buildings SFH15, SFH45 and SFH100 of T44A38 in Strasbourg.

For the mentioned pre-validation, the space heating (SH) loads were introduced as a heat sink element in Polysun. The heating loads were previously calculated with TRNSYS building model Type56. Once these comparisons were showing little deviations, the same system template was used in Polysun including its own building model to avoid the necessity of creating different sink files for each climate and heat load. The building model of Polysun is not as detailed as the one used in Type 56, but since the interest of the present study is in relative values, the simplified model of Polysun was considered to be accurate enough. Values were selected in the Polysun building model to obtain a similar yearly heating demand as in the case of TRNSYS for Strasbourg. Afterwards, the same building was moved around Europe without any modification of the building definition. In this case, the buildings are labelled as SFH15*, SFH45* and SFH100* to differentiate from those exact T44A38 conditions.

The domestic hot water (DHW) tapping profile is obtained from T44A38, and the cold water temperature is set to 10 °C. Thereby DHW energy load is considered to be constant for all locations.

The combined systems consist of a parallel system with a combistorage as a connecting component between the heat delivered from the heat pump, the solar thermal heat input, and the useful energy delivered to DHW or SH. In order to show the possible energy flows within the system the chart proposed by Frank et al. (2010) is used in Figure 6.11a to present the scheme of the parallel SGSHP system simulated in Polysun that is shown in Figure 6.11b.

The combistorage has separate connections for charging the storage DHW and SH zones by the heat pump. As recommended in section 6.3, the return line from the storage to the heat pump in DHW charging mode is above the zone affected by SH operation, and the position of the sensor used for DHW charging control is well above the space heating zone of the combistorage.

When the heating systems are to be simulated at different locations the heating loads for each building change and therefore the systems need to be redesigned. The peak load for SH is calculated and the heat pump size is selected from the catalogue of Polysun from this peak value adding a safety factor of 1.5 to account for DHW loads. The idea is to obtain a system that does not need any auxiliary energy from another source apart from the heat pump and the solar thermal system. Each heat pump selected has a different COP at nominal conditions; the range is between 4.3 and 4.7 at B0/W35 for brine source and between 3.2 and 3.7 at A2/W35 for air source heat pumps. With the nominal conditions of the heat pump the length of the borehole is obtained using the rule of thumb of 50 W of nominal heat extraction per meter of borehole. Only single boreholes are used.

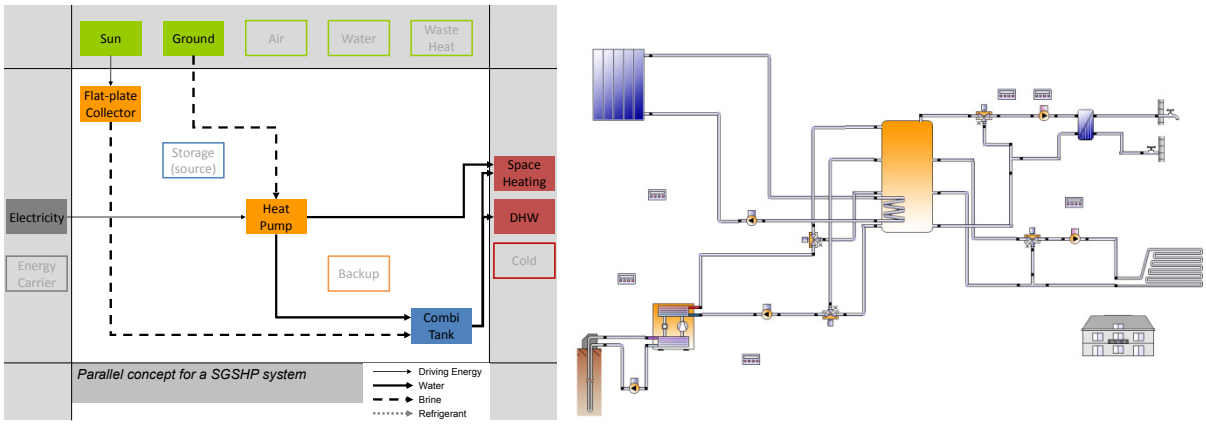

Figure 6.11: (a) Energy flow chart visualization scheme and (b) Polysun-6® scheme for the parallel ground source SHP system simulated.

Eight different cities have been chosen to analyse the influence of the climate on the performance of the combined solar and heat pump system. These cities represent a great part of the European climate. The Continental climate, typical in Central and Eastern Europe, is represented by Strasbourg, Wurzburg and Warsaw. The Atlantic climate particularities are included by simulations for Nantes. Madrid and Barcelona represent the Southern European climates. Barcelona has a Mediterranean climate and Madrid a Mediterranean-Continental climate. The colder climates are represented by Helsinki from Northern Europe and Davos, a typical alpine location.

6.5.3 Simulation results

The heat pump seasonal performance factor for SFH45* is shown in Figure 6.12.

For the ground source system, the performance of the heat pump alone (SPF_{HP}) may increase when the solar system is added because the solar thermal collectors cover some of the DHW loads at high temperature and therefore the heat pump works less time at high sink temperatures.

Nevertheless, for the case of SFH45* presented in Figure 6.12 the performance of the heat pump is quite stable, not much depending on the collector size except when the share of collector energy in the total demand is large (large collector areas in sunny locations).

For the air source SHP system, the heat pump performance (SPF_{HP}) decreases when the solar thermal system is added. This decrease of performance can be observed in almost all simulations and it is more significant for low energy buildings (not shown here). Despite of this, the SPF_{SHP} increases because the solar thermal system has a much higher ratio of heat delivered to electricity consumed compared to the heat pump. The reason why the SPF_{HP} decreases for air source heat pumps is that the solar thermal system covers part or all of the loads at times when the ambient temperature is moderately high, i.e. spring and summer periods, where also the performance of the air source heat pump is best. However, care has to be taken with the interpretation of these results since the air source temperatures in summer are outside of the temperature range that is used for standard heat pump testing and model parameterization which was the base for the Polysun heat pump models.

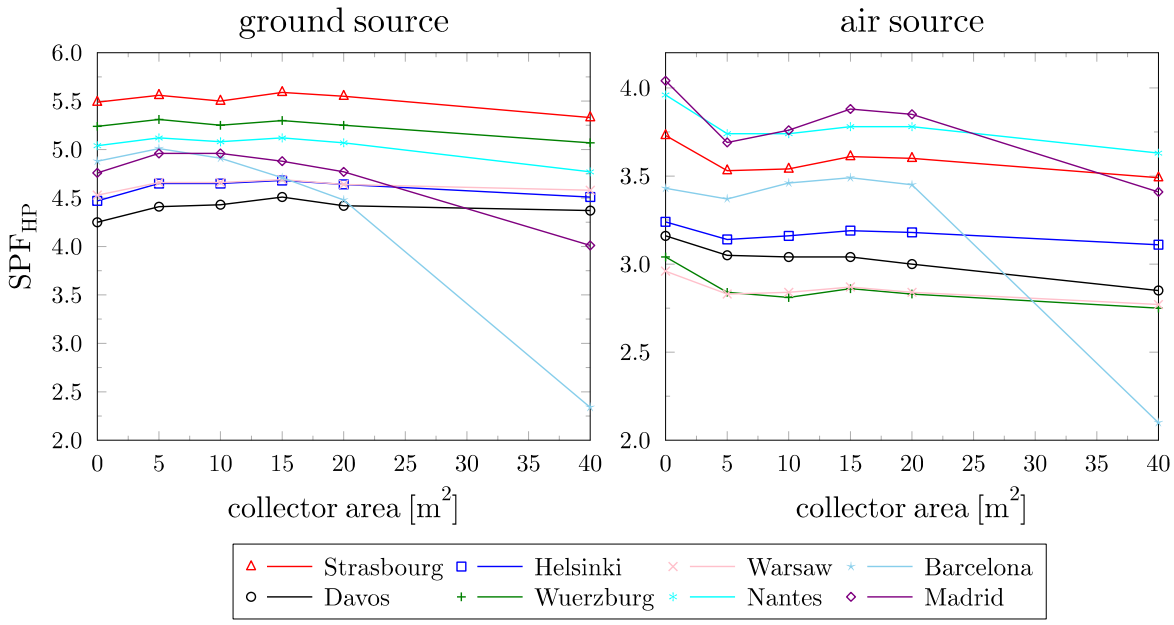

Figure 6.12: Heat pump seasonal performance factor for SFH45 as a function of collector area for a) ground source; and b) air source SHP simulations.*

Results of fractional electricity savings ($f_{save,el}$) are presented in Figure 6.13 for SFH45*. In almost all cases $f_{save,el}$ is higher for the ground source system than for the air source system. An exception to this tendency can be observed in the results for Barcelona. In this case, the heating demand for SFH45 is lower than that of the DHW which leads to quite different results.

Having a more constant source temperature for a ground source system compared to an air source system is beneficial when the solar thermal system is included. Additionally, the solar thermal system leads to lower heat extraction in the ground and thus less decrease in ground source temperature both on the short and, assumingly, on the long term. However, the long term effect cannot be seen in the presented results because only one year has been simulated.

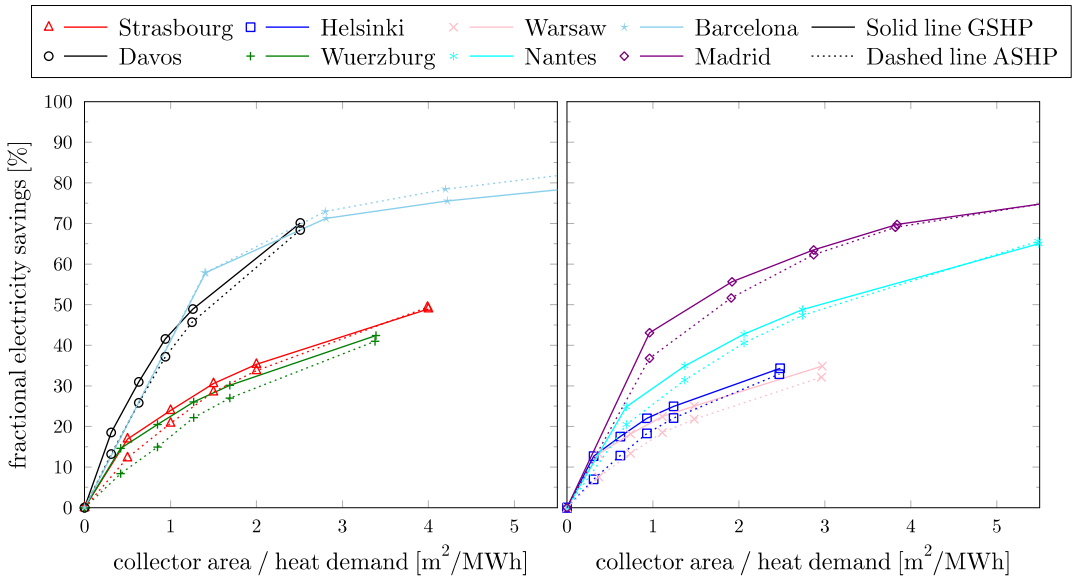

Figure 6.13: Fractional electric savings as a function of collector area for ground source (solid lines) and air source (dashed lines) SHP simulations and SFH45.*

In order to assess the long term effects, a comparison with simulations for seven years has been performed for some cases but these showed only minor differences to the one year results (notice that only single boreholes are used).

Although the potential benefit in terms of $f_{save,el}$ is higher for ground source compared to air source SHP systems, it does not imply a higher absolute decrease of electricity consumption. In Figure 6.14 to Figure 6.16 the absolute electricity savings have been plotted for SFH15*, SFH45* and SFH100* respectively. Even though the $f_{save,el}$ of ground source SHP is higher compared to air source SHP, the absolute electricity savings are usually lower for the same collector area. Absolute electricity savings are not only functions of the electricity consumption of the reference system but also to the relative improvements for the combined system. Basically, the combination of $f_{save,el}$ and the performance of the reference system determines the potential benefit from adding the solar thermal system.

The reason why $f_{save,el}$ increases with the solar radiation of a specific location is clear. However, it should be taken into consideration that in most cases, except in Davos, higher irradiation means lower energy demand, and therefore it can happen that even though the $f_{save,el}$ can be very high, the absolute savings may not be as important as one might expect. For the same reason absolute electric savings can be higher for SFH100 compared to the SFH45 building even with lower $f_{save,el}$. The absolute electric savings of Davos are in most of cases the highest because this climate has a very high space heating demand while at the same time having high values for irradiation in winter.

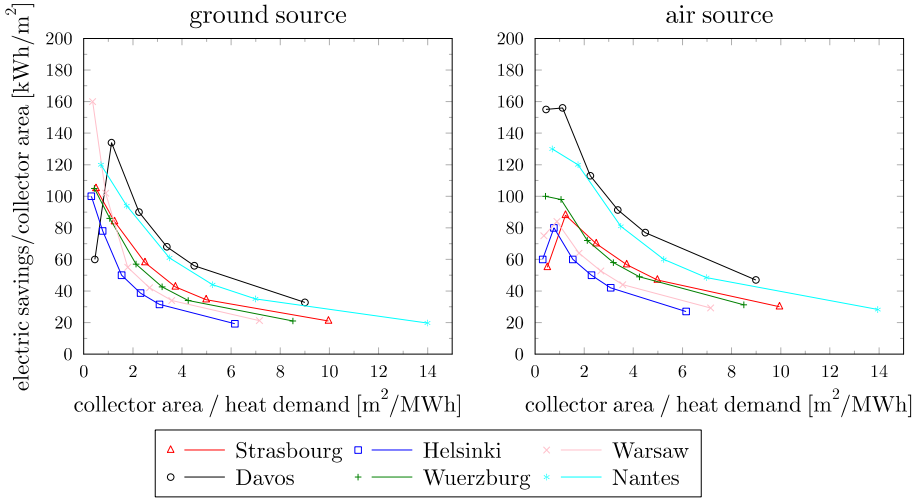

Figure 6.14: Absolute electric savings as a function of collector area for ground source (solid lines) and air source (dashed lines) SHP simulations and SFH15.*

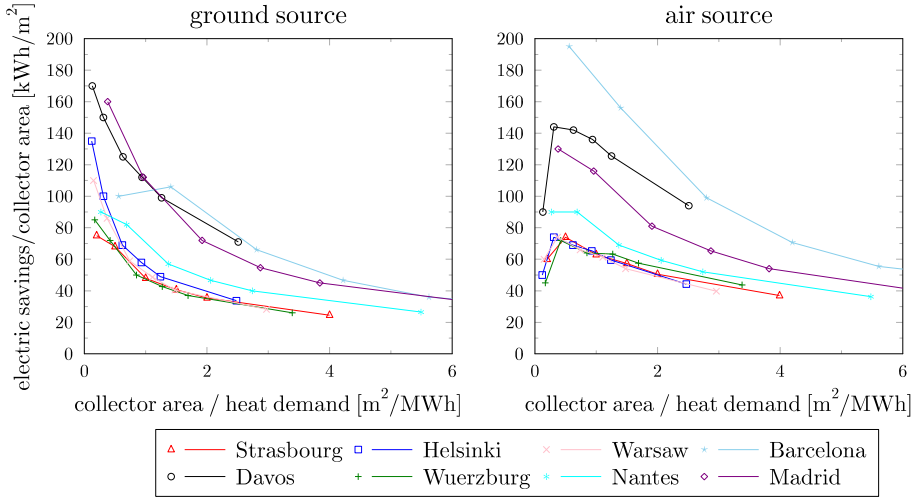

Figure 6.15: Absolute electric savings as a function of collector area for ground source (solid lines) and air source (dashed lines) SHP simulations and SFH45.*

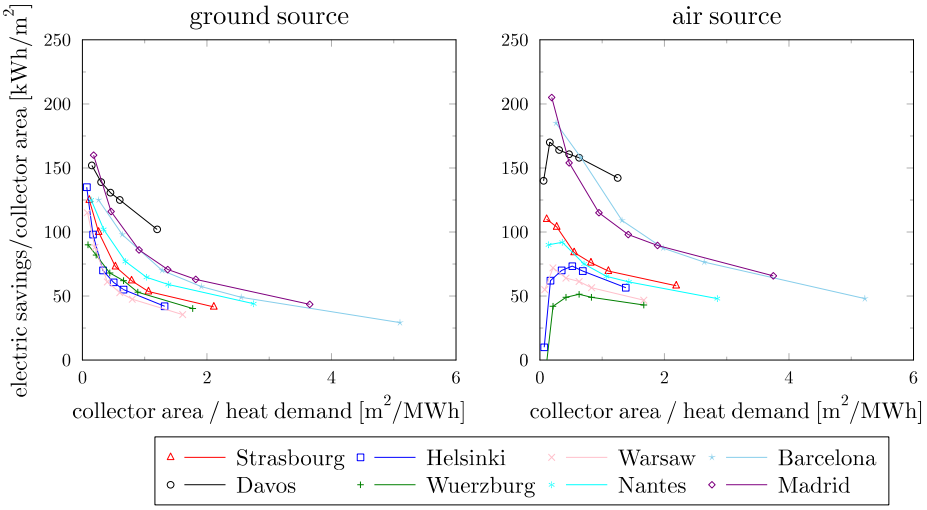

Figure 6.16: Absolute electric savings as a function of collector area for ground source (solid lines) and air source (dashed lines) SHP simulations and SFH100.*

6.5.4 Conclusion

Performed simulations show that the seasonal performance factor of the overall heating system increases when a solar thermal system is added for both air source and ground source heat pumps. The performance of the ground source heat pump alone usually is not significantly affected when it is combined with a solar thermal system (except for a very high share of solar energy in the total energy demand). On the other hand, the performance of the air source heat pump alone decreases when it is combined with a solar thermal system. For this reason, in terms of fractional electricity savings, the potential benefit of ground source based systems is higher than that of an air source heat pump. Obviously the energetic benefit also increases with collector area and solar radiation.

In terms of absolute electricity savings, the benefit of adding solar thermal to a heat pump system increases with the electric energy consumption of the reference system without the solar thermal part. Therefore air source systems have usually higher potential compared to ground source based systems despite of the lower fractional electricity savings. For the same reason, systems with high energy demand, e.g. systems in colder climates or with lower building insulation standard, will also benefit more than those of low energy demand. The optimum climate in terms of absolute electricity savings is found in a typical alpine location with cold climate but at the same time high irradiation in winter.

6.6 Potential of parallel/series systems with dual source heat pumps

According to the classification scheme that was introduced in section 2.1.3, a P/S system with dual source heat pump is a system that can use solar heat either directly at the temperature level that is required to serve the demand or at lower temperature levels for the evaporator of the heat pump. Furthermore, the dual source concept implies that the heat pump can use either solar heat or another heat source (e.g. ambient air).

The control of these systems has a large influence on their performance. For the case of available solar irradiation on the collector field, it has to be decided if solar heat shall be used directly at the temperature level of the demand, or as a source for the heat pump. It has been shown in section 3 that from a thermodynamic point of view using solar heat in series is disadvantageous if the irradiation on the collector field is high enough and the collector efficiency in parallel operation would not be extremely poor (or even negative). The annual potential to use solar heat for the evaporator of the heat pump without decreasing the system performance can be split into two kinds of potentials:

- ***Additional runtime potential*** indicates the potential to use solar heat in series at times where it would not be possible at all to use it directly because the temperature level of the heat demand or of the heat storage device cannot be reached (negative collector efficiency at this temperature).
- ***Switching potential*** indicates the potential to use solar heat in series at times when it would also be possible to use it in parallel, but the efficiency in a parallel operation mode would be so poor that the overall system performance increases in the series operation mode (compared to the parallel delivery of heat from solar collectors and the heat pump using another source).

The additional runtime potential was analysed based on the simulation of a parallel (P) solar combisystem with 16 m2 collector field and a heat demand for space heating and DHW of 17'000 kWh in the climate of Zürich (results presented in Haller & Frank 2010). The analysis was based on cumulative daily energies for:

- Solar irradiation at times when the collector pump was operated (H_{ON})
- Solar irradiation at times when the collector pump was not in operation (H_{OFF})
- Heat used (from ambient air) for the evaporator of the heat pump (Q_{evap})

From these daily values, the maximum possible additional runtime potential – assuming not more than a daily storage on the low temperature side of the heat pump – was calculated based on the daily values as $H_{OFF,match} = \min\left(H_{OFF,} Q_{evap}\right)$. Then, all values where grouped according to the average ambient air temperature of the respective days.

Figure 6.17 shows that unused irradiation on the collector field is frequent on days with relatively high ambient air temperatures of 10 – 25 °C and matches poorly with the days where most heat is needed for the evaporator of the heat pump (ambient temperatures -5 to +8 °C). The irradiation that is available for additional runtimes with not more than a daily storage ($H_{OFF,match}$) is only 14% of the heat needed for the evaporator of the heat pump (Q_{evap}). With the – in the eyes of the author optimistic – assumption, that the COP of the system could be increased by 20% during these times, using the additional runtime potential is increasing the seasonal performance factor of this system by a maximum of 3%. This is, however, assuming, that operating the collector as a source for the heat pump does not affect the amount of heat collected and the temperatures provided in the parallel operation mode. Taking into account the colder temperatures of the collector circuit after switching from series to direct operation mode may however further decrease the potential for improving the overall system efficiency, and even lead to negative results at worst.

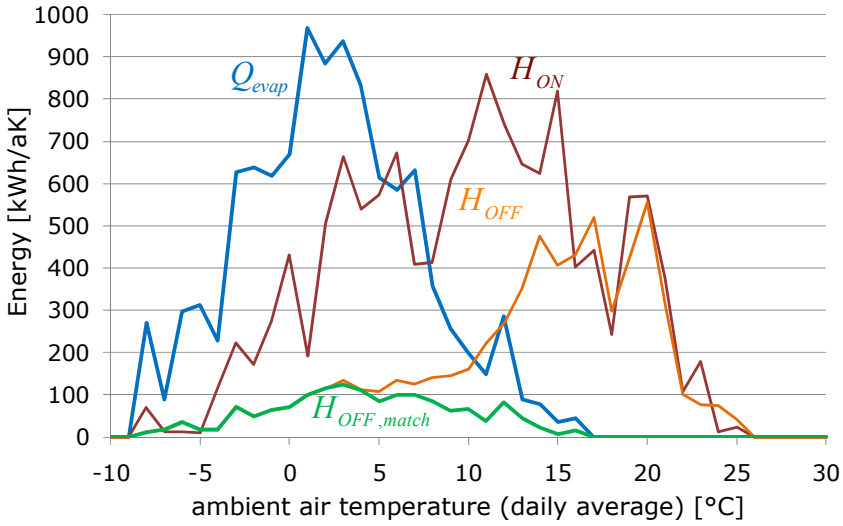

Figure 6.17: Cumulative annual energies for the evaporator of the heat pump and available used and unused irradiation on the collector field for a parallel system with 16 m² collector field area.

Additional system simulations were performed in TRNSYS in order to determine also the potential for switching from parallel collector heat use to series heat use at times when parallel heat use would have been possible. The evaluation was based on Eq. 3.4 (p. 18), details on the simulation models and sizing of the system were presented in Haller & Frank 2011a.

Figure 6.18 shows that for both covered collectors as well as unglazed absorbers the switching potential is considerably lower than the additional runtime potential. At the same time it is clearly visible that the potential for series heat use is – as expected – significantly higher for unglazed absorbers than for covered collectors. In this case, the possibility to use uncovered absorbers also as ambient air heat exchangers was not considered since the other heat source of the heat pump is already an ambient air heat exchanger.

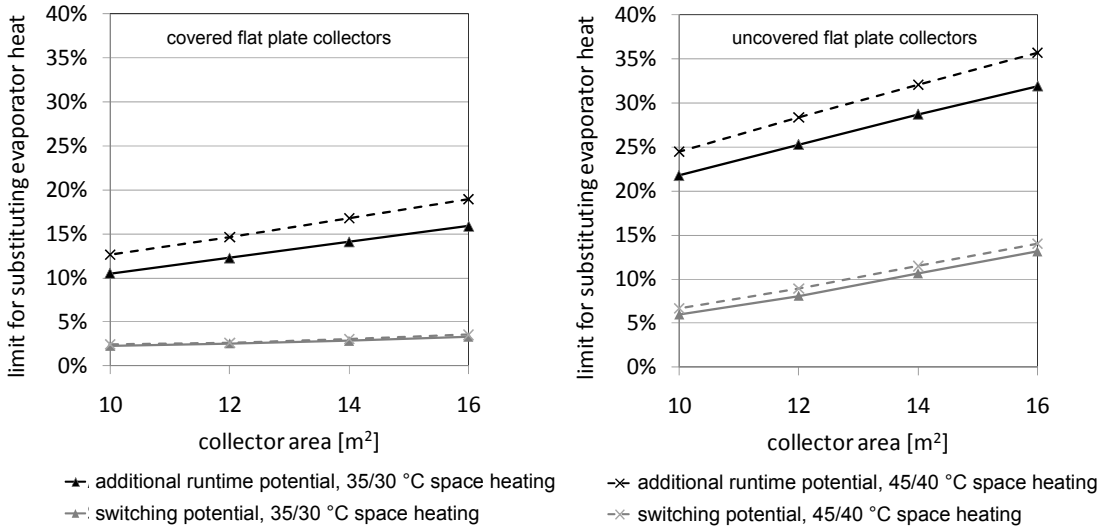

Figure 6.18: Theoretical limit of using heat from the solar collectors for the evaporator of the heat pump with benefit for the system's performance factor, given in % of the heat needed for the evaporator of the heat pump, for the climate of Zurich (Source: Haller & Frank 2011a).

6.7 Parallel/series systems with single source heat pump and ice storage

In this section, an ice storage system based on immersed flat plate heat exchangers that can be de-iced is presented and simulated. The system concept has been explained by Philippen et al. (2012a) and the ice storage model description and validation has been provided by Philippen et al. (2012b) and Carbonell et al. (2014). The scheme of the system is presented in Figure 6.19 along with the temperature sensors used for the control.

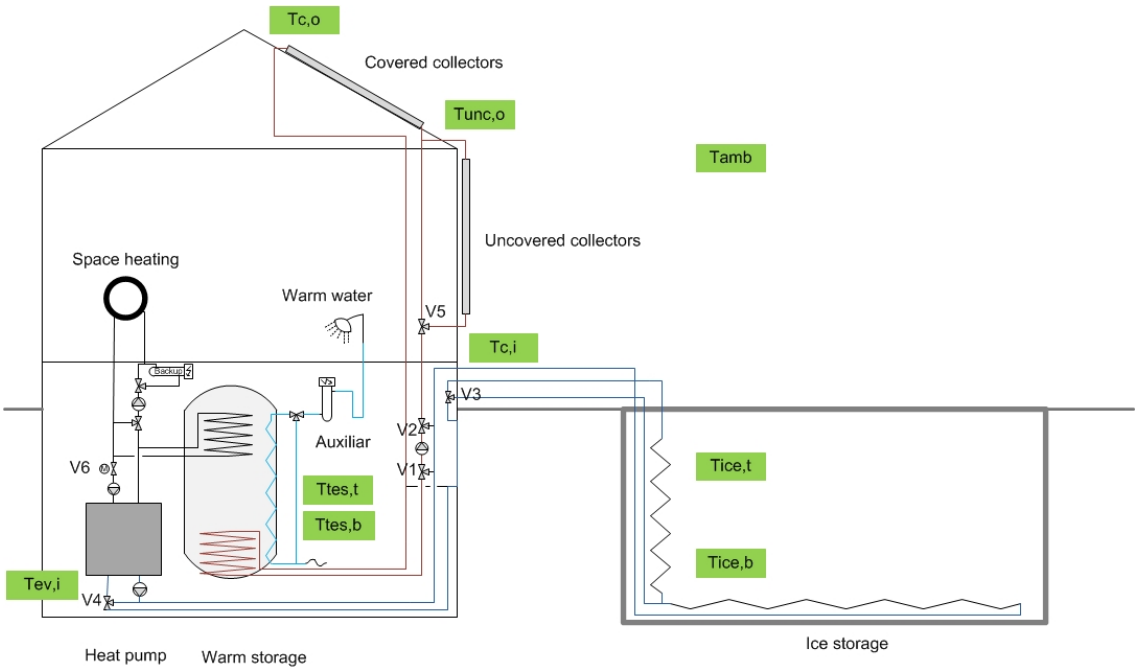

Figure 6.19: System simulated with a large ice storage buried in the ground. Green values are temperature sensors used for the control strategy explained in the next section.

A short explanation of the ice storage system concept is provided hereafter. When the heat pump extracts heat from the ice storage the growing ice layers on the heat exchanger decrease the overall heat transfer coefficient from the water in the storage to the brine in the heat exchanger. As a result lower brine temperatures and heat pump performance are obtained. A strategy to prevent the effect of a decreasing overall heat transfer coefficient is to remove the ice layers periodically. The heat exchanger is de-iced before reaching too low brine temperatures by melting the contact layer between the ice and the heat exchanger when the heat pump is switched off. When the melted ice thickness is large enough, the ice layers separate from the heat exchangers and due to buoyancy forces they are accumulated at the water surface of the ice storage. The ice storage is only insulated against the surrounding ground for the upper half of its volume, thereby allowing high heat losses (summer) or heat gains (winter) through the lower half of the storage.

Since ice storages can be considered as an alternative to ground source heat pump systems the ground source system is used here as a reference. Systems based on large ice storages, as the ones proposed here, may not make sense for low energy buildings due to their high costs. Therefore only SFH45 and SFH100 are simulated.

As an illustrative example of the behaviour of the ice storage tank, a monthly energy balance plot (left axis) has been presented in Figure 6.20 for a system with 20 m^3 ice storage and 20 m^2 collector area (Ice20A20) and building SFH45. The terms presented in the legend from top to bottom are (inputs positive, outputs negative):

Q_{heat}	heat input from the collector field
$Q_{gain,loss}$	gains (positive) and losses (negative) due to heat exchange with the ground
$Q_{release,acum}$	change of sensible heat contained: heat used for decreasing (positive) or increasing (negative) water temperature
$Q_{ice,form}$	energy released by ice formation
Q_{cool}	energy extracted by the heat pump
$Q_{melt,hx}$	energy used to melt the ice on the heat exchangers for de-icing
$Q_{melt,floating}$	energy used to melt the floating ice at the surface of the ice storage

Ice is formed from December to February ($Q_{ice,form}$) when the solar energy and sensible heat in the storage are not able to compensate the heat extraction of the heat pump. Notice for example that in October and November, no ice is formed because there is still enough sensible heat in the ice storage and therefore the sensible heat that is removed from the ice storage is very high ($Q_{release,acum}$ on the positive y-axis of Figure 6.20).

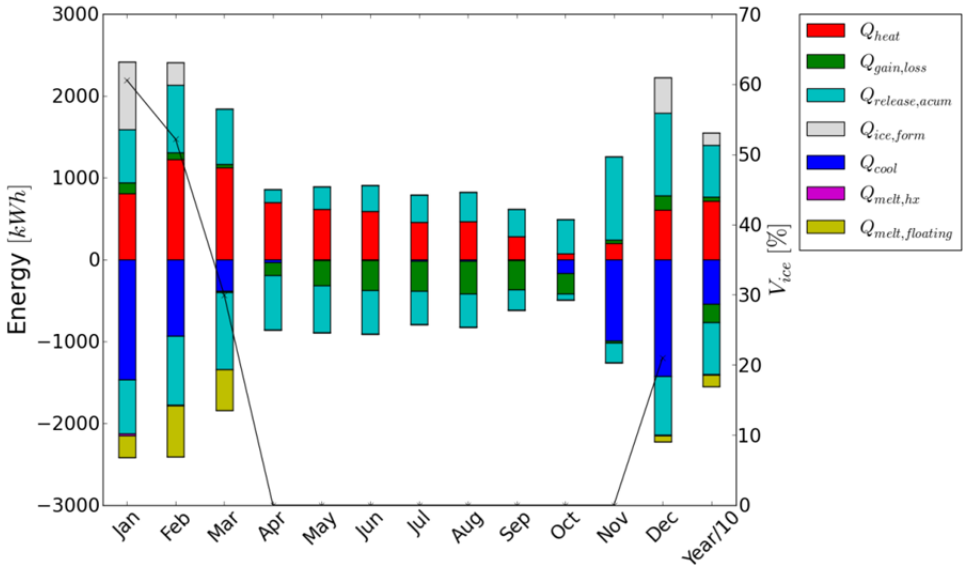

Figure 6.20: Monthly and yearly energy balances of and ice storage for the Ice20A25 and building SFH45.V_{ice} is the maximum monthly percentage of the iceable storage volume that is occupied with ice – represented by the thin black line.

The solar collector input (Q_{heat}) increase from November to February, where the maximum solar energy is used by the ice storage, and afterwards the solar energy decreases until October where the minimum solar energy input is found. The time of maximum usage of solar energy correspond the month of maximum ice melted. From January to March the solar input increases with the melting of the floating ice. In summer the ice storage is almost charged of sensible heat (average temperature in August is around 65°C), and during these months most of the solar energy is used for balancing the losses to the ground. From November to March the storage gains energy from the ground, and from April to October the storage loses energy to the ground. However at yearly level, the storage losses to the ground are higher than the gains from the ground due to the size of the storage and the high temperature achieved in summer.

The ratio between the maximum volume of ice and the volume of the ice storage is shown as solid line in the right axis of Figure 6.20 for each month. It can be observed that there is no

ice in the storage from April to November. The maximum value of 60% is found in January. As a design criterion it is not allowed to have more that 70% of ice because, in this case, the ice layers may not be detached from the heat exchanger surface anymore and the evaporator temperature of the heat pump may be too low to run.

Table 6.2: Results of several ice storage SHP systems compared against ground source SHP reference system for different building loads.

System	Building	V_{ice}	A_{coll}	A_{uc}	Q_{dem}	$P_{el,SHP+}$	SPF_{HP}	SPF_{SHP+}	ΔSPF_{HP}	ΔSPF_{SHP+}
	SFH	[m³]	[m²]	[m²]	[MWh]	[MWh]	[−]	[−]	[%]	[%]
ground source SHP	45	-	15	0	8.55	1.41	5.39	5.83	-	-
Ice25A15	45	25	15	5	8.52	1.52	5.35	5.01	-0.82	-14.17
Ice20A20	45	20	20	5	8.52	1.41	5.42	5.53	0.64	-8.31
Ice20A30	45	20	30	5	8.52	1.26	5.61	5.90	4.12	1.13
ground source SHP	100	-	15	0	16.12	3.60	4.26	4.40	-	-
Ice40A30	100	40	30	5	16.05	3.19	4.53	4.78	6.47	8.76
Ice30A45	100	30	45	5	16.06	2.98	4.57	5.10	7.40	15.93

Results for different ice storage based systems and a ground source SHP system used as reference here are presented in Table 6.2. The ice storage systems include 5 m² of uncovered collectors, mostly for de-icing in periods where the sun is not shining. For SFH45 (upper part of Table 6.2) the system performance of the ground source SHP system is very high, with a SPF_{SHP+} of 5.8. Using an ice storage of 25 m³ with the same collector area as the ground source system, a lower SPF_{SHP+} of 5.01 is obtained. Increasing the collector area, from 15 to 30 m² (Ice20A30) the system performance increases to 5.9, while the volume of the storage was reduced to 20 m³ without ever having the storage at 70% of the ice capacity. With 20 m³ of ice storage volume and a collector area of 20 m² a SPF_{SHP+} of 5.53 is achieved.

Results for SFH100 are shown in the bottom part of Table 6.2. Both ice storage simulations perform energetically better compared to a ground source SHP system under these specific conditions because the collector area is much higher for the ice storage systems. In this case reducing the storage volume from 40 to 30 m³ and increasing the collector area from 30 to 45 m² improves system efficiency reaching a SPF_{SHP+} of 5.1.

6.8 Weather forecast for systems with large ice storages

A predictive control based on weather forecast is thought to be useful especially in systems where two or more large storages are present. Otherwise it is expected that only minor improvements can be achieved. Therefore the predictive control strategy has been used for systems that use large ice storages as source for the heat pump as the ones described in chapter 6.7. In order to understand what can be improved with weather forecast, the control strategy of the system will be described and afterwards the strategy for predictive control will be explained. In the present simulation it is assumed that the weather forecast is perfect.

6.8.1 Control strategy

The global control strategy priorities are defined in Figure 6.21. The first priority is switching on the heat pump to avoid having low comfort for not delivering the heat demand needed. When the heat pump is switched off, then the other programs can be activated. Among them the de-icing programs are of higher priority since too thick ice-layers on the heat exchanger may lead to a too low brine temperature in the heat pump evaporator circuit, which may cause failure of the heat pump. After the de-icing program the loading of the warm storage (Ws) from solar collectors is used, since several studies show that direct use of solar energy leads to maximum electricity savings in most of cases (see for example section 3). Afterwards the control checks if it is possible to load the warm storage from the cold (ice) storage. This program can usually run in early autumn if the ice storage is loaded with solar energy from the summer with high temperatures that can be used directly in the building (without using the heat pump). The last programs are those related with loading the cold (ice) storage (Cs) from solar collectors. The option of cold storage load priority switches the order of priority giving higher importance of loading the cold storage instead of the warm storage with solar energy. It will be shown afterwards that this control improves the system when the ice storage is undersized and the electrical backup is needed during several hours in winter.

Each program block has its own programs inside with their own priorities.

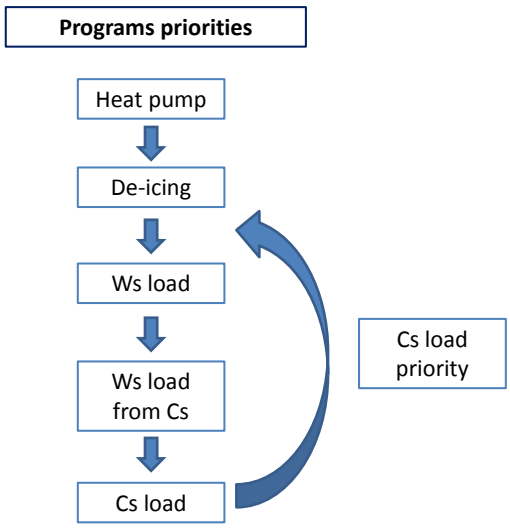

Figure 6.21: Global priority control strategy. Priority from up to down.

6.8.2 Weather forecast strategy

The idea to use weather forecast for improving system performance is mainly using the Cs load priority when the solar irradiation during one day is below a certain limit. The typical control tries always to use solar energy directly. Nevertheless the system with large collector areas have a large inertia and it is usual the case where the control tries to load the warm storage for some time (half an hour), and then the pump of the solar circle stops because there is not enough solar radiation. After a while the control tries to load again the warm storage switching off again after some minutes. This situation means that for several hours the control tries to load the warm storage with little effect. A better strategy would be to predict the solar radiation during the following hours to check if it makes sense to load the warm storage at all. Loading the cold storage instead could be in this case much more beneficial.

The collectors work at better efficiency for lower temperatures and the collector usage increases. Moreover in this way it can be avoided that the ice storage is filled up with ice. This effect is of special interest in undersized systems.

The predictive control is based on a weather forecast. Nevertheless, in the present simulation it is assumed that the weather forecast is perfect, so the meteorological data loaded in the simulation is used for the predictive control. A new TRNSYS type has been developed that is able to read meteorological data with the Meteonorm format and process it in order to calculate the total irradiation on the collector surface for one day, several morning hours or even a week. However, in the simulations presented here only the daily irradiation has been used.

6.8.3 Results

The strategy to use a predictive control is based on switching to Cs priority. The first approach is using the Cs priority always during the whole winter (CsWinter) without any predictive control at all. Usually problems of too much ice in the storage start at January, therefore CsWinter program sets Cs priority in January and February.

Results are presented in Figure 6.22 for SFH45, several ice storages volumes and collector areas. The CsWinter strategy tends to improve the SPF_{SHP+}, especially for lower collector areas. In this case it is more important to have the ice storage as warm as possible to avoid using the electrical backup heater. Basically when the ice storage is full of ice or de-icing is not possible, the temperature in the heat pump evaporator drops fast and when it is below the minimum accepted value, the heat pump switches off and then the electrical heater is activated. If the Cs is loaded always, the heat pump stops less often and the auxiliary heater is used less. Nevertheless for higher collector areas the CsWinter does not always improve the results because less solar heat is used directly. Improvement in the rage of 5% can be achieved for low storage volumes and collector areas.

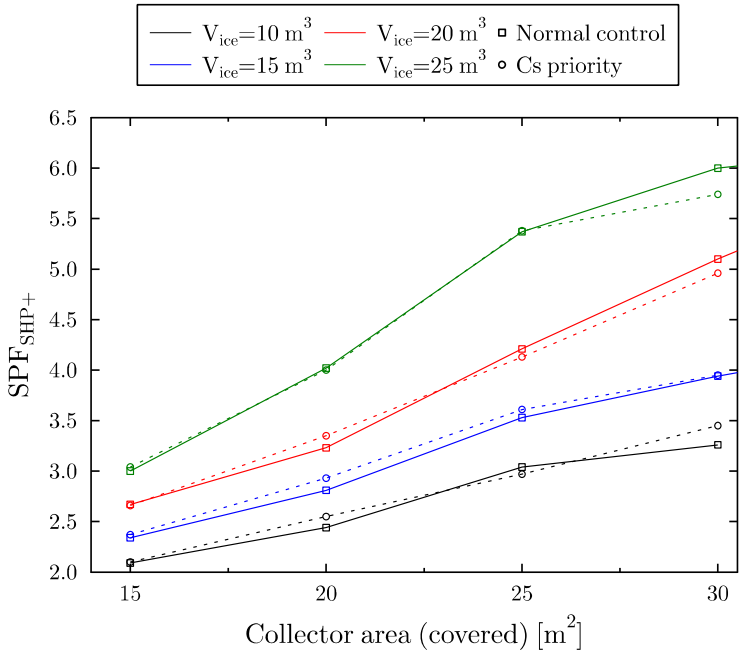

Figure 6.22: Comparison of system performance versus collector area between cold storage priority in winter (dashed line) and normal control (solid line).

It should also be noted that CsWinter priority is not only of benefit to increase the system performance but to avoid freezing the ice storage totally. This can be especially important if the electrical back up system is not able to provide the full heating demand.

A solution to improve results shown before consists in using a predictive control based on weather forecast. In this case the Cs is loaded only when Ws loading is not worth because not enough irradiation will be present. The first studies are focussed on the daily irradiation specific value (HT_{lim}) used to decide whether we use the cold storage load priority or not. Several values have been used and two are presented here: 0.5 and 1.5 kWh/day m^2.

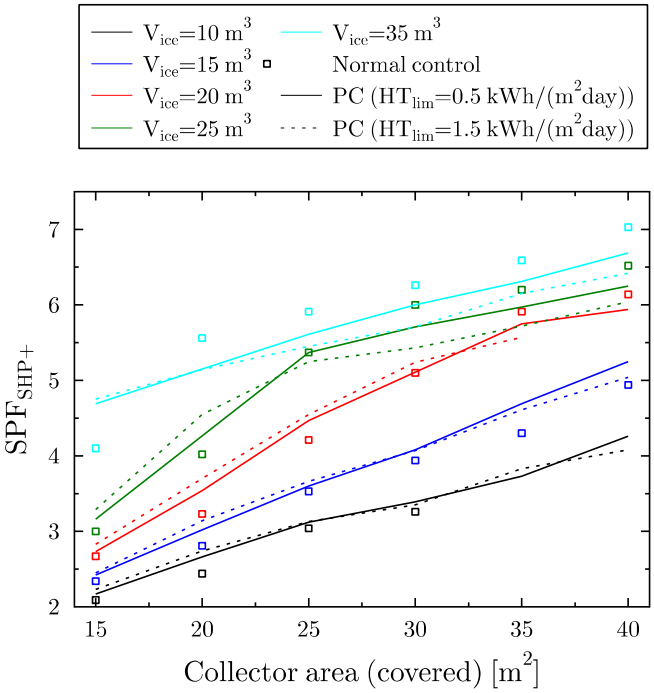

*Figure 6.23: System performance for SFH45 as function of collector area, volume of ice storage for three different controls i) normal control (squares), using predictive control (PC) with weather forecast for ii) HT_{lim}=0.5 kWh/(m^2*day) (solid line) and iii) HT_{lim}=1.5 kWh/(m^2*day) (dashed line).*

The system performance using normal control strategy and predictive control with different HT_{lim} values have been compared for several collector areas and storage volumes for SFH45 in Figure 6.23. Comparing the simulation results using different HT_{lim} values one can see that usually the value of 1.5 is slightly better for lower sizing of the components. For an ice storage of 35 m^3 the value of 0.5 works better because the system is sized in a way that no auxiliary heating is needed and then the use of solar energy directly is more beneficial. For all the cases shown here the predictive control clearly improves the system performance except when the system has both a large collector field and a large ice storage, and thus the need for auxiliary heating is low or even negligible. For example using an ice storage of 35 m^3 and collector areas above 20 m^2 there is no need for the present predictive control. As an order of magnitude, one can see that when the system performance is above 5 the predictive control implemented here may be worst that the normal control. For the other cases the improvements are promising. For example for an ice storage of 20 m^3 and collector areas of 20 m^2 the improvements due to predictive control are in the order of 16% and with 25 m^2 of collector area the improvements are around 9%.

6.8.4 Conclusions

From the simulations shown above it seems clear that a predictive control can be very beneficial for the system performance when the system performance is approximately below 5. Moreover, the predictive control presented here is very simple and only based on one day weather forecast, which is much easier to predict correctly than one week weather forecast. Nevertheless, studies that also include a randomly prediction error should be considered. Future studies should also focus on special weather conditions. For example it can be of interest knowing what can a predictive control provide when for a long time fog or very cold weather will be present. Meteorological data can be modified to force extreme conditions to happen and check the potentials of the control under these conditions. In the case of ice storage this long term predictions can be used to avoid freezing completely the ice storage. These measures should be studied not only for system performance but also for reliability and safety reasons (the backup may not be sized to provide heating for a full week in extreme cold conditions).

For future research it may be possible to develop a smarter predictive control that is able to increase the performance always, or at least performs equally well as the normal control for systems with large collector area and ice storage volumes. It is not a robust solution to implement a control that depends on the sizing of the components but it should be able to react with the dynamic performance of the system.

7 Whole system testing of solar and heat pump systems

The energetic efficiency of a heating system is the result of dynamic interactions between hydraulically connected components under the boundary conditions encountered in the given application. Thus, not only the characteristics of the single components play an important role, but also the hydraulic connections and control, the sizing of components, as well as the characteristics of the dynamic heat loads. Because of these complex relationships the energetic efficiency of the whole system is often quite different from what was expected based on the single component performance that was measured in quasi steady state operation. For this reason, since more than 15 years the Institut für Solartechnik SPF has followed the approach of testing complex systems as a whole in the laboratory based on a "hardware in the loop" approach.

The Concise Cylce Test (CCT) is a whole system hardware in the loop test method that was described by Vogelsanger (2002) as a contribution to the IEA-SHC Tasks 26 and 32. In the following years, the method was applied successfully for the testing of solar combisystems with oil and gas backup heating (Haller & Vogelsanger 2005a; Haller & Vogelsanger 2005b), and pellet backup heating (Konersmann et al. 2007; Haberl et al. 2009; Haberl et al. 2011). The test duration is twelve days and includes an additional pre-conditioning phase at the beginning. Each test day is based on the climatic profile and heat load of a real day of the year, and each season of the year is represented within these twelve days. The advantages of this test method in comparison to single component testing are the inclusion of the following effects and influences on the system performance:

- Complex dynamic interactions between different components of the systems. This includes components like controllers, hydraulics, solar circuit, heat pump, etc.
- Start and stop behaviour including the realistic frequencies of starts and stops.
- The influence of storage stratification efficiency during realistic dynamic operation.
- Heat losses of all components that are installed in the technical room (storage, hydraulic connections, heat pump, etc.) as they occur in a real installation.

Within the SOL-HEAP project, the CCT method was further developed for the testing of solar combisystems with air source and brine source heat pumps. Further information on this test method and a comparison with other whole system test method developments has been published in Haller et al. 2013d.

7.1 Methods

Figure 7.1 shows the general approach of the dynamic whole system "hardware in the loop" test method. Based on the results of the twelve day CCT, annual performance results are obtained by modelling the tested system and calibrating the model with the test results, followed by annual system simulations. Another whole system testing approach is to extrapolate directly from the test sequence results to the annual values. Figure 7.2 shows which components are installed in the technical room of the test bench and thus part of the tested system (hardware…), and which components are simulated and emulated by the test bench (…in the loop).

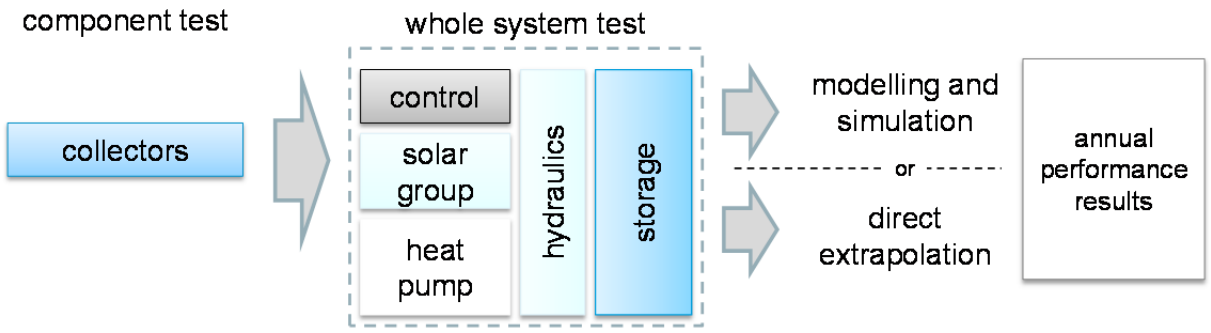

Figure 7.1: Scheme of the dynamic whole system "hardware in the loop" test method.

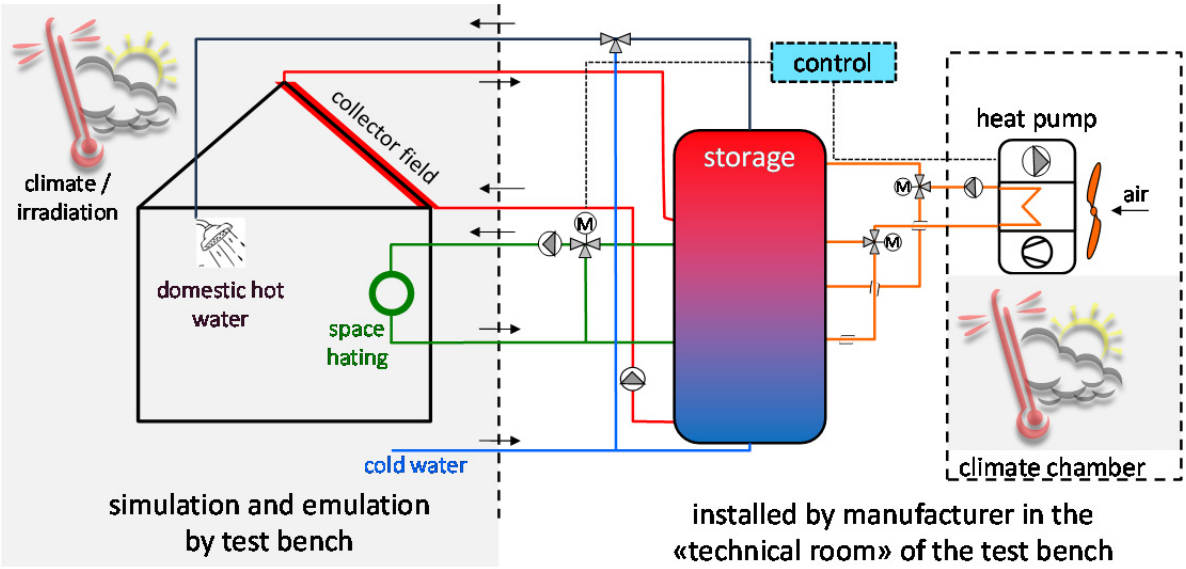

Figure 7.2: Parts of the system that are installed in the test bench and part of the tested system (right, white background) and that are simulated and emulated by the test bench (left, grey background) for a CCT.

The system to be tested is installed and insulated by the manufacturer or an installer sent by the manufacturer. The installer is only allowed to insulate on site up to a defined limit defined by the test institute that is based on the usual practice in the field. The staff of the testing institute does not insulate or improve anything inside the technical room. During the twelve day[7] CCT the tested system provides space heating and DHW for the simulated and emulated building without human interference of any kind. The response of the simulated components is simulated in times steps of 1/32 h[8], taking into account the behaviour of the system within the precedent time step. The temperature of the technical room was conditioned to 20 °C.

[7] plus 18 h pre-conditioning.

[8] in some cases of extremely dynamic system behaviour (parallel/series systems) 1/64 hours were used.

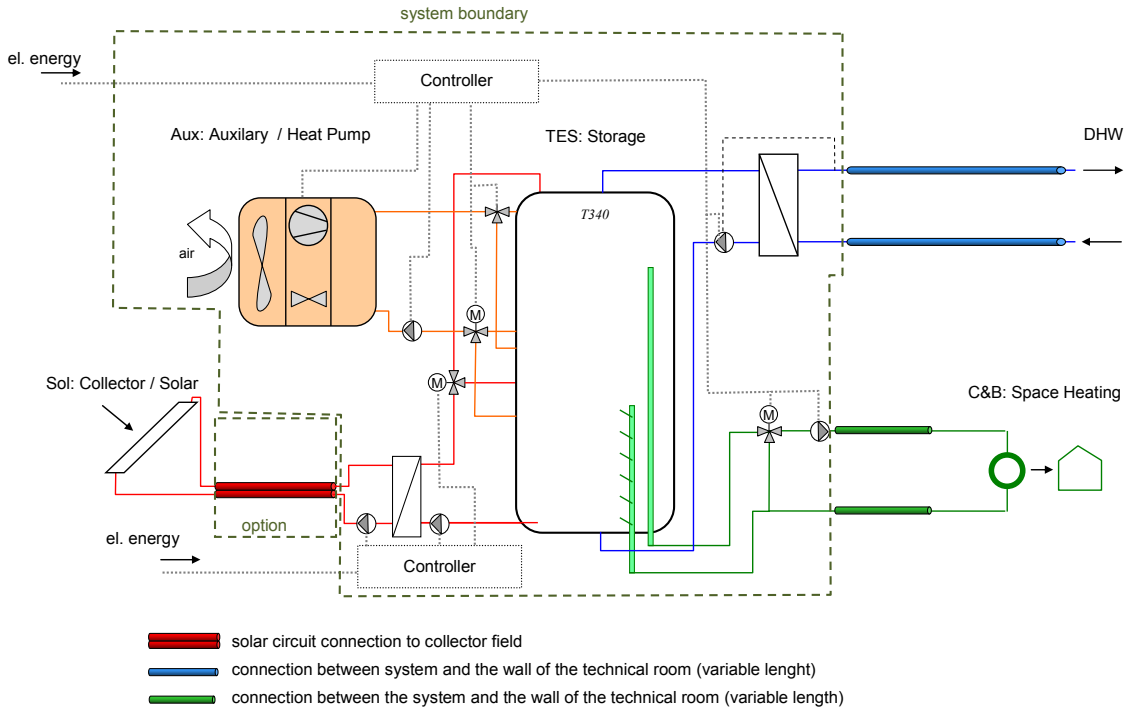

Figure 7.3: Boundaries of the whole system "hardware in the loop" test method. All components within these boundaries are installed and tested.

7.1.1 Twelve day weather profile for the CCT based on annual TRY data

A test reference year (CCT TRY) was assembled by selecting months from 5 years (1994-1998) of measured data from the weather station SMA Zurich-Fluntern that was obtained by MeteoSchweiz (1999). For each month of the year, a representative month[9] was chosen from the five years period in order to obtain the weather data for the reference year. From the test reference year (TRY) representative months were used for the creation of the twelve days Concise Cycle Test weather data (Table 7.1). Figure 7.4 shows the profiles of climate and DHW tapping energy over the twelve test days.

Table 7.1: Climatic boundary conditions of the chosen test reference year.

Method	***CCT***
Annual temperature average (°C)	9.0
Annual irradiation total on the horizontal (kWh/m^2)	1111
Annual wind speed average (m/s)	1.2
Annual relative humidity average (% rH)	76.4

[99] The selection of data for weather and irradiation was performed by Peter Vogelsanger between 1999 and 2003 for whole system testing of solar combisystems with oil and gas backup heating. As far as can be reconstructed, only the horizontal total irradiation and the ambient temperature were used as criteria to evaluate the representativeness of the months.

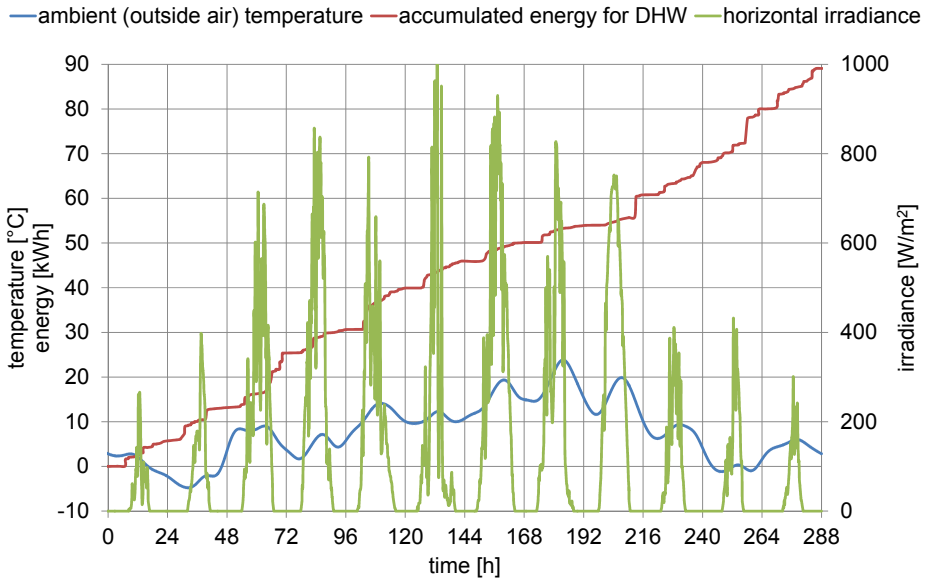

Figure 7.4: DHW draw-off energies and weather profile for the twelve CCT days.

7.1.2 Emulation of space heating and DHW tappings

A single-family house was defined to provide the building heat load. The building has an annual heat demand of 12500 kWh/a if it is heated to 20 °C by an ideal heater. However, during the test phase and the annual simulation it is heated via the floor (slab) dividing the two stories. With good settings of the controller to assure 20 °C indoor air temperature, it consumes about 15500 kWh/a which means a standard heating load of 100 kWh/(m^2a). The building is modelled with TRNSYS type 56, the floor or slab heating is modelled as active layer. The design supply temperature to the slab heating is about 39 °C at a design ambient temperature of -10 °C and a flow rate of 550 litres per hour. With both, its mass and its window areas being moderate, the house benefits moderately from passive solar gains (Vogelsanger 2002). Thermostatic valves were simulated that close the space heat distribution loop. If required, a minimum mass flow rate was guaranteed to the system. This building load is referred to as SFH100.

A second single-family house was defined with a lower heat demand that represents a contemporary building with an heat demand of 60 kWh/(m^2a) for the climate of Zurich. The parameters of the building are taken from the SFH45. The emulation is based on simulations with a model based on ISO 13790-2008 (simplified version for heating including dynamic effects). This building load is referred to as SFH60.

As a third single-family house to provide the building heat load was the SFH15 used in case of systems that were designed specifically for a passive house system.

Statistical distributions based on Jordan & Vajen (2000) have been used for the creation of different types of DHW draw off for the CCT method. Draw off events are handled directly by the test bench control software and thus draw offs may be quite smaller than the simulation time steps that are used for the simulation and emulation of the space heat distribution or the solar collector field. Different types of draw offs and different volume flow rates were used. Variable set-temperatures that had to be reached (useful temperature) and time limits for reaching the set temperature have been defined depending on the type of draw off.

Table 7.2: Different types of DHW tappings of the CCT method.

Type	***short name***	***description***
0	volume draw off	This type of hot water draw off is characterized by a small fixed volume of hot water that is taken independently of its temperature. In reality this occurs when a user is opening a “modern” tapping device that will always mix some hot water into the tapping if the handle is not all the way moved to the cold endpoint. The average frequency is 11 per day, the average volume is 0.98 liters per tapping.
1	energy draw off	Energy draw offs are characterized by the fact that not a fixed volume is taken, but a fixed amount of energy. Energy draw offs are of different flow rates from 300 l/h to 1080 l/h with cold inlet temperature defined for each tapping. The energy is only counted from the time the drawn water temperature is above the useful temperature which is 40 °C for most tappings, but 38 °C or 30 °C for some of the tappings. The time allowed for reaching the useful temperature is 40 sec, the time allowed for reaching the energy set point is different for each tapping. The average frequency is 22.5 per day, the average daily energy tapped is 7.05 kWh.

The stop time of energy draw offs may thus not be at a fixed time of the test-procedure, but after the energy target has been reached.

7.1.3 Measurement devices and measurement uncertainty

The interface of the test rig with the tested system is defined by the points of measurement of the energy balance between the test rig and the tested system. The measured quantities allow for the calculation of all relevant energies that cross the system boundary.

Inlet and outlet temperatures of fluid circulating between the tested systems and the test-rig were measured with in-house calibrated 4-wire Pt100 sensors (uncertainty < 0.05 K), and mass flow rates were measured either with in-house calibrated magnetic inductive or coriolis flow sensors (accuracy better than 0.5 %). The main electric energy consumption of the heat pump has been measured with a polyphase power measurement device with auto scaling measuring range that analyzes the effective values in each quadrant of the alternating current (accuracy better than 0.3 %). If the system allowed, the electricity of independent subsystems like space heat pumps, space heat mixing valves, solar pumps or the solar system controlling units have been measured by a separate universal single phase power measuring device with fixed measuring range (accuracy better than 5.5 W).

If possible the temperature and flow rate of the water circulating between the combistorage and the auxiliary heater were measured in order to get more detailed information about the behaviour of the tested system.

Table 7.3 gives an overview on the measurement uncertainties. Data acquisition cycle was 1 sec for all values. Mass flow rates and thermal power were calculated online based on the physical properties of the fluid, the temperature readings of the inlet and outlet temperature sensors, and the volume flow rate. Calculated thermal power and measured electrical power consumption were integrated over time to cumulated energies based on one second time steps.

Table 7.3: Accuracy of measurement equipment.

Flow rate: magnetic inductive	[%]	0.5
Flow rate: coriolis	[%]	0.15
Temperature: absolute temperature with 4-wire Pt100	[K]	0.05
Temperature: difference with two 4-wire Pt100	[K]	0.035
Electric power consumption of subsystem measured by Socket A: ≤ 500 W (sampling of voltage and current, based on measured basefrequency)	[W]	±2.5
Electric power consumption of subsystem measured by Socket B: ≤ 230 W (sampling of voltage and current, based on measured basefrequency)	[W]	±1.15
Electric power consumption of subsystem measured by Socket C: ≤ 1100 W (sampling of voltage and current, based on measured basefrequency)	[W]	±5.5W
Electric power consumption of Heat Pump of each phase: ≤ 4500 W (sampling of voltage and current, based on measured base frequency)	[W]	±45W[10]

7.1.4 Emulation of collector field, ground heat exchanger, and air source

Solar collector field

The slope and orientation of the simulated and emulated collector field was 45° south. Collector Type 301 (Isakson & Eriksson 1994) was used for the simulation of covered flat plate collectors, Type 832 (section 4.4) was used for uncovered absorbers. The collector parameters were set according to a collector test certificate according to EN12975. The maximum collector field area allowed was 15 m^2 gross in general. The manufacturers temperature sensor was installed in a temperature controlled conditioning block. The collector pipes (2 x 15 m) were installed by the manufacturer in the test rig (ambient temperature of the technical room). They were thus part of the tested system.

Air source for heat pumps

A climatic chamber was used to condition the ambient air temperature and humidity according to the climatic data of the twelve day CCT. The outdoor units of air source systems were installed in this climatic chamber that was close (6 m pipe length) to the technical room where the indoor equipment of the tested system was installed.

[10] The accuracy of the determination of the electric power consumption of the heat pump was improved during this project, due to a new measuring device with an autosacale function (≤1% of current measuring power value).


Figure 7.5: Climatic chamber for the outdoor unit of air source heat pumps (left) and emulation module for the ground heat source (right).

Ground source for heat pumps

TRNSYS Type 451 (EWS model) for the simulation of vertical borehole heat exchangers (double-U-pipes, Huber & Schuler 1997; Wetter & Huber 1997) is used for the simulation and emulation of the ground source. The IEA SHC Task 44 / HPP Annex 38 parameters for the ground properties were used (Table 7.4), and a borehole length was 2 x 115 m for the SFH100 in the climate of Zürich.

Table 7.4: Properties of the earth according to the "base case" of T44A38.

conductivity of the ground, average ground (base case)	λ_{grd}	2	W/(mK)
density of the ground	ρ_{grd}	2500	kg/m^3
specific heat capacity of the ground	cp_{grd}	800	J/(kgK)
geothermal gradient	G_t	0.025	K/m

The parameters for the emulation of the ground source heat exchanger are described in Table 7.5. In these calculations, the volume flow of 2000 l/h was divided between two separate lines. A surcharge of 100 % was made for the pressure drop according to Huber (1999) in order to account for header losses, connections, angle pieces, etc.

Table 7.5: Parameters for the emulation of the ground source heat exchanger.

Number of tubes	2	[-]
Length of each line	115	[m]
Inner diameter	0.026	[m]
Density of the fluid	983	[kg/m3]
Volume flow rate	2000	[l/h]
Pressure drop (@ 2000 l/h)	0.38	[bar]

7.1.5 Emulation of temperatures for the controller of the tested system

The controller that is part of the tested system uses two temperature sensors that are not installed in the technical room:

- The ambient air temperature sensor is placed in a conditioned box for the outdoor temperature according to the twelve day CCT weather data
- The collector field sensor is placed in a calibration block that is conditioned to the simulated collector field outlet temperature during the test.

The temperature of the heated room was not available to the controller. The outdoor temperature averaging for the determination of the heating season or the supply temperature set point for space heating was disabled. The set point for the room temperature was constant 20 °C.

7.1.6 Additional tests for model fitting

The determination of the thermal capacitance [J/K] and the heat loss rate [W/h] of the storage tanks were based on a procedure that is similar to prEN-12977-3.

Measurements for the determination of parameters that are necessary for the subsequent simulation of auxiliary heaters were performed taking into account the type and the control of the auxiliary heater in the twelve day CCT.

7.1.7 Requirements for passing the test

The systems that were tested had to fulfil the defined comfort requirements for DHW supply and space heating:

- The simulated room temperature must be kept above 19.5 °C at all times during the CCT (no night-time set point reduction).
- The tested system must be able to deliver a DHW temperature of 45 °C at the outlet of the system at any time.

7.1.8 Processing of test results

From the test results, a number of parameters were computed directly (results of the CCT), and upon request by the manufacturer also a simulation model of the system was created and calibrated with the test results in order to obtain annual performance factors.

A load file was used for domestic hot water and space heating energy in the annual simulation in order to obtain identical amounts of heat delivered for all tested systems. The load file was generated with the same building simulation model and climate that was used for the CCT.

The standard DHW load is multiplied with a factor > 1 to account for energy measured during the 12-day test that was drawn with temperatures below the defined minimum for useful temperature at the beginning of the draw-off. This penalizes systems that need longer time to provide a sufficient high temperature for the customer (e.g. inertia due to external heat exchangers or long pipe runs).

7.2 Tested systems and their results

7.2.1 Description of tested systems

A total of eleven system tests were performed on systems from six different manufacturers, including parallel ground source and air source heat pump systems as well as series & parallel combinations, and one "series only" system that used solar thermal collectors as the only heat source. The energy flow charts and letter codes for the system hydraulic concepts are shown in Figure 7.6. Technical data for the components of the systems can be found in Table 7.6 to Table 7.8.

Systems **I & II** were parallel air source and ground source solar and heat pump systems available on the market from the same company, i.e. the same storage tank was used with different heat pumps. The air source heat pump was capacity controlled.

System tests **III & IV** were performed with a parallel/series concept with dual source heat pump that was available on the market. The system was once tested with 15 m^2 covered flat plate collectors (III) and once with 20 m^2 selective uncovered collectors (IV).

System **V** was a parallel air source solar and heat pump system available on the market, with a capacity controlled heat pump.

System tests **VI, VII & VIII** were performed with a parallel ground source solar and heat pump system that was tested three times with different hydraulics and/or control configurations.

System **IX** is a parallel ground source solar and heat pump system with the condenser of the heat pump integrated into a solar combistorage. The system contains other innovative features and is a prototype to be released into the market soon.

Systems **X & XI** were "series only" solar and heat pump systems that used 30 m^2 façade integrated flat plate collectors as the only heat source for the heat pump. The two systems were from the same prototype development of one manufacturer, once measured at the beginning of the development phase and once at the end, after improving the concept based on the feedback from the first system test. This system is intended for passive house applications only and has therefore been tested with a lower space heating demand of 15 kWh/(m^2a).

More details on the hydraulic concepts and concepts for the control of these systems are not given in order to maintain the anonymity and protect the intellectual property rights of the involved manufacturers.

All systems have been installed completely (i.e. with all pumps, controllers and hydraulic connections) in the technical room of the test bench.

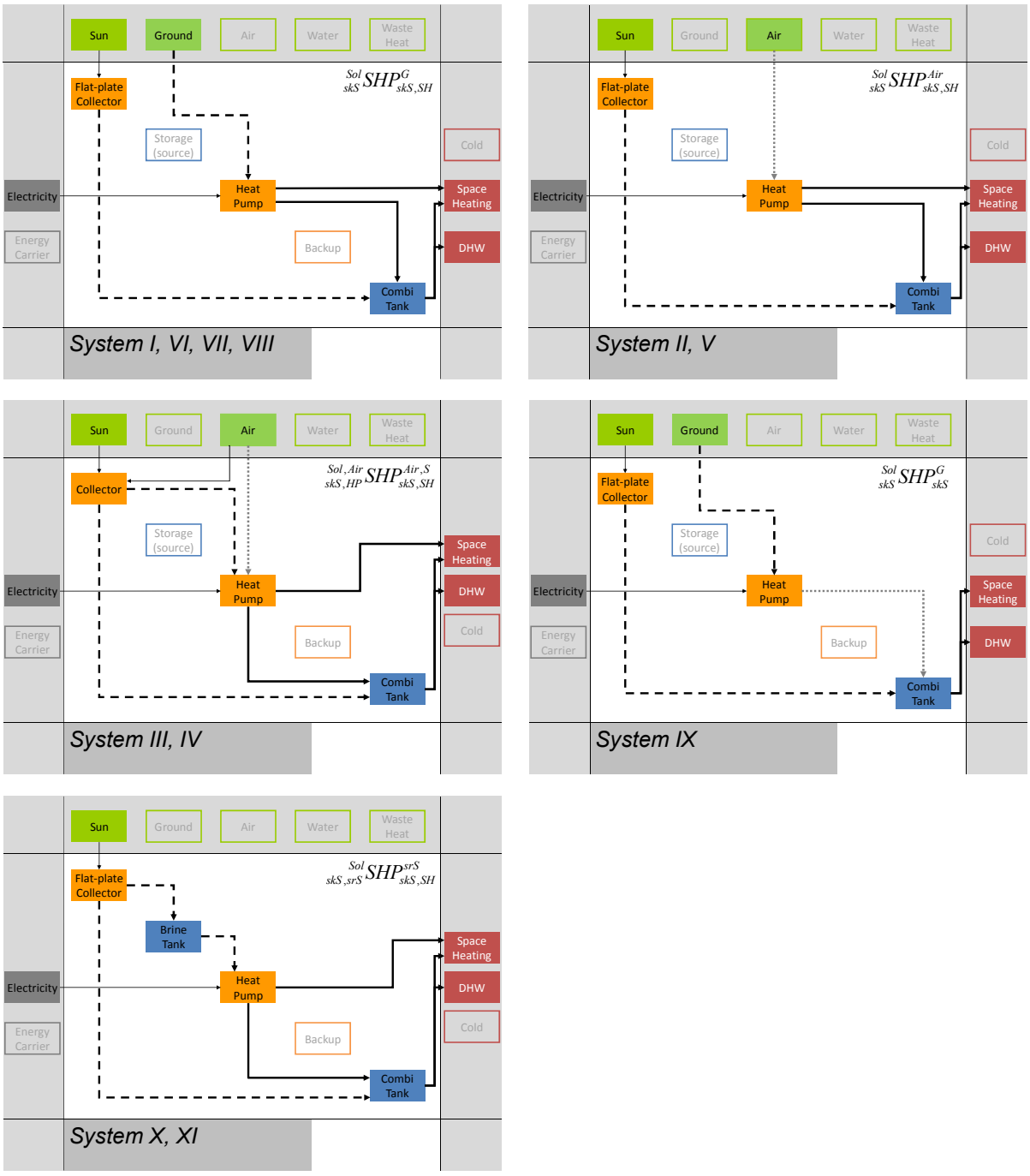

Figure 7.6: Energy flow charts for the eleven tested systems.

Table 7.6: System classification and heat pump properties of the tested systems (based on manufacturer's data).

	Classification	Heat source	Min. / Max. thermal power	Max. el. power	COP[a)]
I	P	brine (GHX)	8.2 [a)]	1.7	4.9
II	P	air	3.1 / 8.3 [b)]	2.4	3.7
III + IV	P/S dual source	brine (air and solar)[b)]	n/a	n/a	n/a
V	P	air	1.3 / 5.6 [b)]	1.7	3.2
VI - VIII	P	ground (GHX)	8.3 [a)]	1.8	4.6
IX	P	ground (GHX)	n/a	2.4	n/a
X + XI	P/S single source	brine (solar only)	n/a	n/a	n/a

a) @ B0W35 for brine source; @ A2W35 for air source.

b) dual source heat pump, air source heat exchanger accessible via brine circuit.

Table 7.7: Properties of the storage tanks of the tested systems.

	V [m^3]	d_{tank} [m]	$d_{tank+insulation}$ [m]	h [m]	IHX solar	DHW preparation
I + II	0.9	1.0	0.8	2.1	Yes	TiT
III + IV	1.0	1.1	0.8	2.0	No	Ext.
V	1.0	1.0	0.8	2.2	Yes	IHX
VI - VIII	0.9	1.0	0.8	2.1	No	Ext.
IX	0.8	0.9	0.8	2.0	Yes	IHX
X + XI	1.0 [a)]	1.0	0.8	2.2	Yes	TiT

a) an additional 0.080 m^3 glycol storage tank has been used on the cold side of the heat pump.

TiT = Tank In Tank; Ext. = External heat exchanger; IHX = Immersed heat exchanger

Table 7.8: Collector field of the tested systems (orientation: south).

	A_{coll}[a)] [m^2]	Eta_0[a)] [-]	A_1[a)] [W/(m^2K)]	A_2[a)] [W/(m^2K^2)]	Type	Slope
I + II	12	0.73	3.5	0.01	Flat plate	45°
III	15	0.75	3.4	0.01	Flat plate	45°
IV	20	0.84	7.9	0.01	Sel. unglazed	45°
V	10	0.73	3.7	0.01	Flat plate	45°
VI - VIII	13	0.79	3.1	0.02	Flat plate	45°
IX	10	0.72	3.3	0.02	Flat plate	45°
X + XI	30	0.79	3.4	0.01	Flat plate	90°

a) based on the collector gross area. Sel. = selective coated. A_{coll} = area of collector field.

7.2.2 Results of the Concise Cycle Tests (CCTs)

Results of the twelve days test sequence are summarized in Table 7.9. However, a direct comparison of the results from different system tests is difficult for several reasons:

- The design space heat demand of the simulated (and emulated) building ranged from 100 kWh/(m2a) for the first tests performed over 60 kWh/(m^2a) for the new test profiles that were adopted in 2011, down to 15 kWh/(m^2a) for the special case of a system that is specifically intended for the use in a passive house. These different design space heat demands are indicated by "SFH100", "SFH60" and "SFH15" in the following.
- The simulated space heat supplied deviates substantially from the design space heat demand for some of the systems tested. This is because the systems were let to deliver space heat according to their own control. Although thermostatic valves in the space heat distribution were simulated and emulated[11], many systems delivered up to 50 % more space heat than required for the most efficient space heat distribution control, and system VII with particularly unfavourable control settings delivered twice as much space heat as required.
- Different collector areas were applied from 10 – 15 m^2 for the "normal" cases, with the exceptions of 20 m^2 for the case of uncovered selective absorbers in system IV and 30 m^2 for façade integrated flat plate collectors used as the only heat source for the heat pump in systems X and XI.

Table 7.9: Results of twelve-day CCTs.

standard space heat load (Q_{SH}) 100 kWh/(m^2a)					
	PF_{SHP+} [-]	**$W_{el,tot}$ [kWh]**	**Q_{SH} [kWh]**	**Q_{DHW} [kWh]**	**$Q_{HP,DHW/QDHW}$ [%]**
I	4.8	128.0	519.7	99.9	100
II	3.5	184.2	566.8	72.0 a)	114 a)
standard space heat load (Q_{SH}) 60 kWh/(m^2a)					
	PF_{SHP+} [-]	**$W_{el,tot}$ [kWh]**	**Q_{SH} [kWh]**	**Q_{DHW} [kWh]**	**$Q_{HP,DHW/QDHW}$ [%]**
III	3.2	95.1	203.7	99.8	-
IV	3.0	106.6	223.7	100.1	-
V	2.7	139.7	280.5	96.3	165
VI	4.0	105.2	315.6	102.1	112
VII	4.8	111.5	430.6	101.6	86
VIII	4.0	104.3	312.3	100.5	158
IX	4.5	95.3	334.7	91.6	-
standard space heat load (Q_{SH}) 15 kWh/(m^2a)					
	PF_{SHP+} [-]	**$W_{el,tot}$ [kWh]**	**Q_{SH} [kWh]**	**Q_{DHW} [kWh]**	**$Q_{HP,DHW/QDHW}$ [%]**
X	3.1	41.5	62.3	68.3	n/a
XI	3.5	47.7	95.1	70.0	40

a) A piece of rigid foam blocked the mechanism of the thermostatic mixing valve for scalding protection after day 9 of the test period. That is why no draw-offs were possible during the last 3 test days.

[11] Mass flow in the space heat supply loop was reduced gradually by closing a motorized valve when the simulated room temperature increased from 20 to 22 °C.

Figure 7.7 shows the performance factors, the space heat delivered, and the electricity demand for all eleven 12 day Concise Cycle Tests. The performance factors range from 2.7 to 4.8.

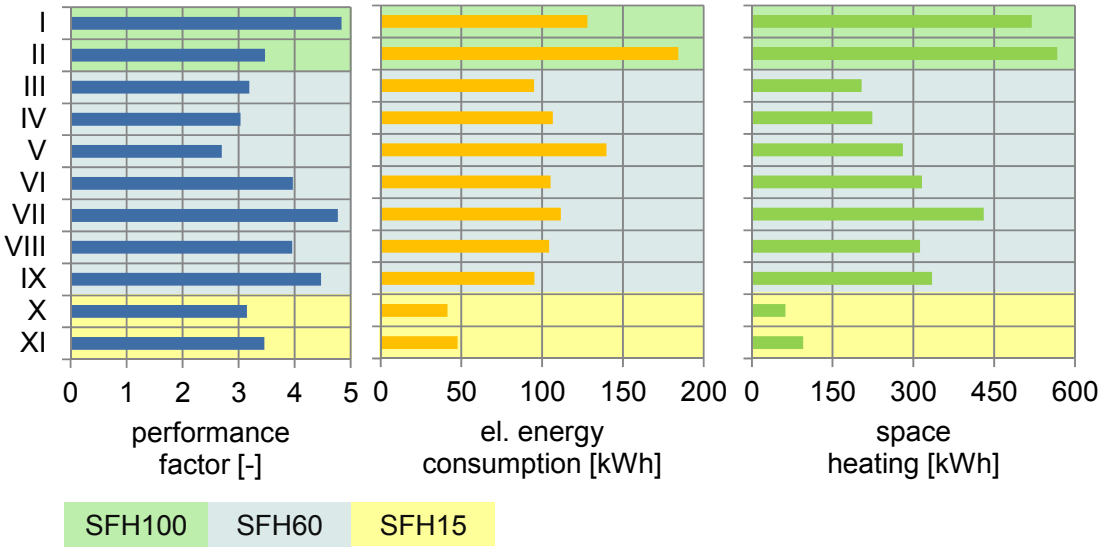

Figure 7.7: Performance factors, electric energy consumption and space heat load of the tested systems during the 12-day test period.

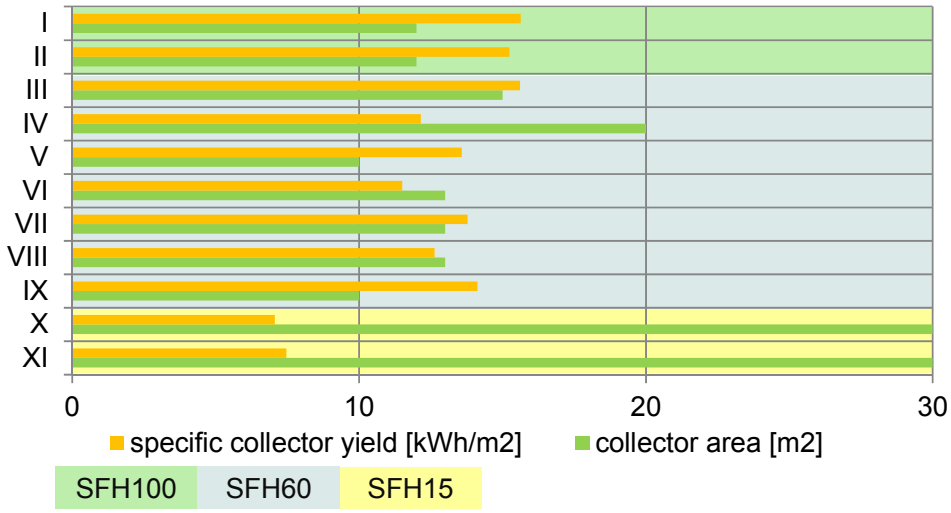

Figure 7.8: Collector area and the specific collector yield of the tested systems during the 12-day test period.

7.2.3 Interpretation of test results

Two of the ground source systems (I for SFH100 and VII for SFH60) reached a system performance factor of 4.8. A more detailed analysis of the results of system VII showed that the result is not as good as the performance factor suggests: On the one hand the comfort requirements for DHW were not met at all times (too low temperatures delivered) and on the other hand the space heating load was much higher than necessary due to a wrong value for a control parameter that led to a continuous operation of the space heat distribution pump

also in the summer period. For this reason, the electric energy demand is higher than for system VI that had a considerably lower performance factor (Figure 7.9). In this case, the performance factor is not the appropriate value for system optimization.

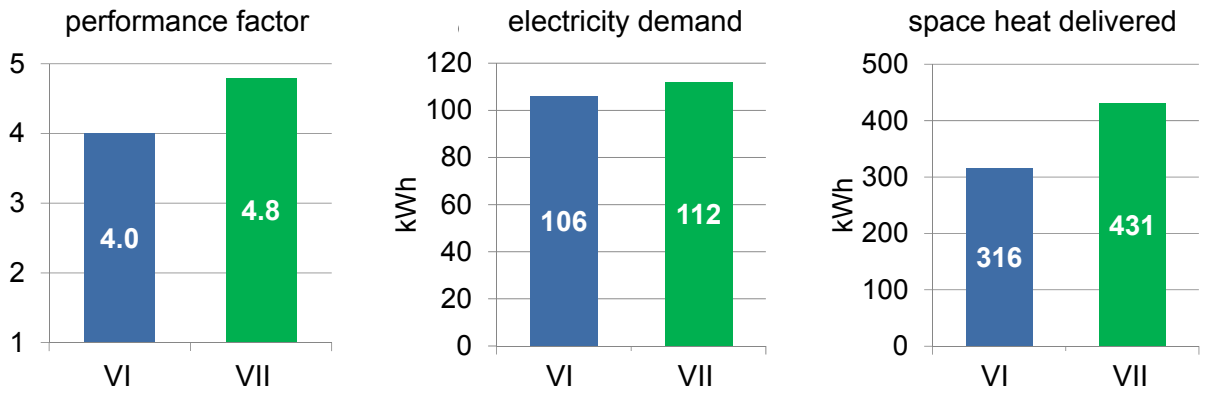

Figure 7.9: Results from the 12-day CCT for systems VI and VII. Both systems were equipped with the same heat pump, storage tank, and collector loop, but used differing control of the space heat distribution. System VII has a higher performance factor and, at the same time, a higher electricity consumption than system VI.

Four of the tested systems (III, IV, X, XI) were able to utilize the collector heat on the source side of the heat pump (in addition to direct charging of the combistore).

Systems III and IV were of the type P/S with dual source heat pump and were tested with the building emulation SFH60. The difference between these two systems was in the type of collector that was chosen for the emulation. System III used 15 m^2 flat plate collectors and reached a performance factor of 3.2, while system IV used 20 m^2 of uncovered selective absorbers and reached a performance factor of 3.0. Also the electric energy demand of system III was 10 % lower than for system IV.

Systems X and XI were of the type P/S with a single source heat pump. This means that the only heat source of the heat pump were the 30 m^2 glazed flat plate collectors in the southern façade of a building with a heat demand of only 15 kWh/(m^2a). The collectors were used to charge a glycol storage on the source side of the heat pump or to charge a combistore directly. The performance factors that were reached within the CCT were between 3.1 and 3.5. However, these are not comparable because of a quite different amount of space heat that was delivered. Calibrated simulation results for system XI show seasonal performance factors of 3.7. The specific collector yield for these systems is comparably low, but one has to keep in mind that the heat demand was also very low and that the collectors in this case have the additional benefit of avoiding other air or ground heat source expenses.

7.2.4 Potential for exergetic system optimization

Many of the tested systems showed considerable potential for exergetic optimization. Figure 7.10 shows storage temperatures and heating power of different connected suppliers and sinks on the fifth test day for a parallel system with flat plate collectors and ground source heat pump. At the beginning of the day, the heat pump is running in space heating mode, charging the space heating zone of the storage intermittently, which can be seen from the heat pump power and the oscillation of the temperature sensor TS5. Between hours 15 and 18, the heat pump is charging the upper part of the combistorage that is reserved for

DHW-preparation. It can be seen that this affects also temperature sensor TS5 that is located in the space heating zone of the combistorage, and even the temperature sensor TS4 below. Thus, the temperature of the space heating zone is lifted to 40 – 50 °C during DHW charging. For the rest of the day, the heat pump does not have to deliver low temperature space heat anymore since heat is taken from the excessively heated space heating zone of the storage and fed to the space heat distribution. As a consequence, heat that was delivered by the heat pump with supply temperatures of 40-50°C is subsequently mixed down in the space heat supply mixing valve to 30 °C that is required for space heating, which is a source of entropy generation and exergetic inefficiency. It should go without saying that running a heat pump at sink temperatures that are 10 – 20 K higher than needed is detrimental for its performance factor.

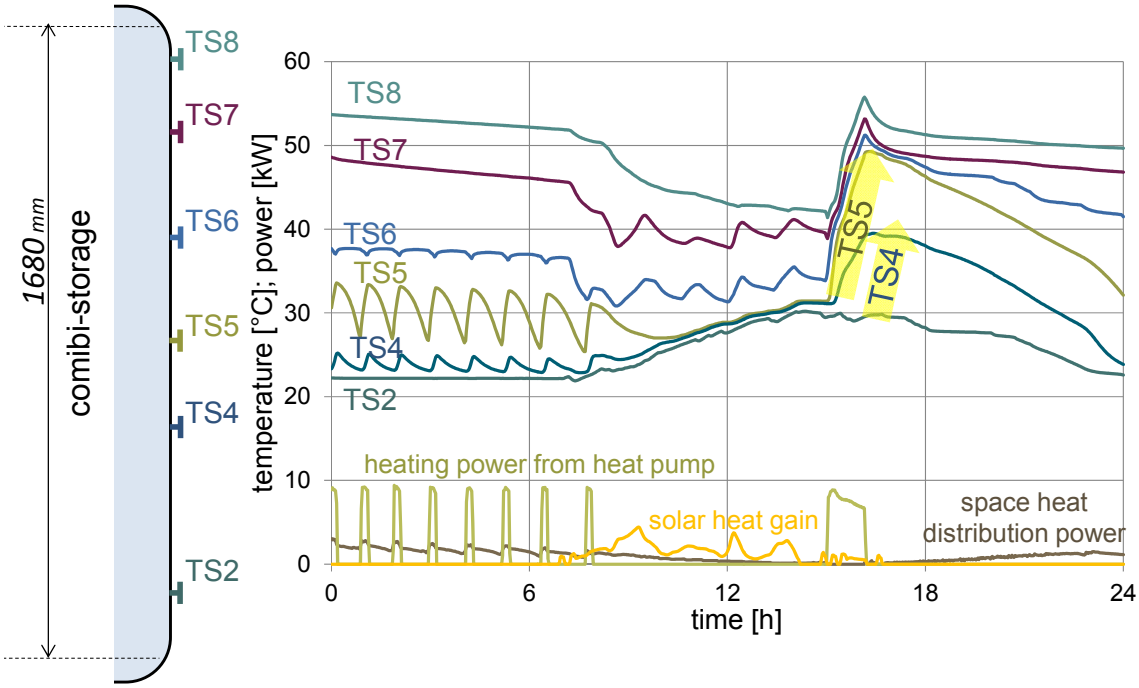

Figure 7.10: Measured temperatures and power on one of the 12 CCT days. TS1 – TS8 = Temperatures measured with contact sensors on the outside surface of the steel tank.

The above mentioned problem is not the only reason for excessive DHW charging of combistorages. Recommendations how to design the integration of combistorage with heat pumps are given in section 6.3. Excessive DHW charging can be detected by the ratio of DHW heat delivered by the heat pump to heat supplied from the storage to the DHW distribution (compare Figure 6.7). Due to the hydraulic compactness of some of the systems, it was not possible to determine this value for all of the tested systems. Table 7.9 shows that for most of the tested systems this ratio was above 100%, and that the difference between the systems is quite large. The ratio is usually correlating with the amount of space heating the system needs to cover. This is shown exemplary by Figure 7.11 where $Q_{WP,DHW}/Q_{DHW}$ is shown day-by-day for a twelve day test, where the summer days are in the middle of the test sequence and days 1-3 and 9-12 correspond to winter days. This is a strong indication that the DHW zone of the storage is disturbed by space heat operation.

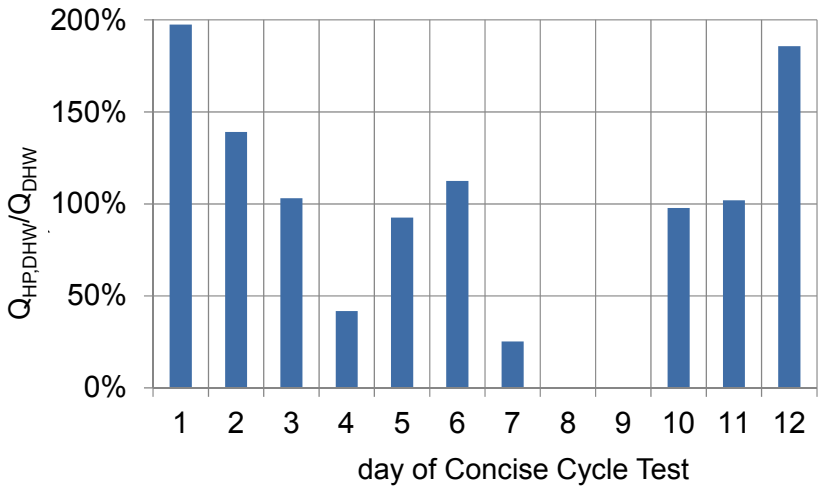

Figure 7.11: Ratio of heat delivered by the heat pump in DHW-mode and heat consumed for DHW on the twelve days of the system tests.

A more general evaluation of the exergetic efficiency of the system is possible by energy-temperature plots presented in Figure 6.17. For each supplier (solar thermal, heat pump) and consumer (space heating, DHW) of the system, the energy transferred during the test is classified and sorted by the supply temperature level. This has been done based on time steps of 1/32 h. The plot then shows the accumulated energy transferred with supply temperatures *below* the temperature on the x-axis.

The interpretation of these curves is shown exemplary for System I: For this system it can be seen that the space heat supplied was just a bit more than 500 kWh, with temperatures in the range of 25 to 35 °C. However, the heat pump was running mostly at a temperature level that was about 8 K above this level. The difference is an indication for exergetic losses. The total amount of DHW delivered was just below 100 kWh, with temperatures between 45 and 50 °C. According to the second slope of the heat pump curve in the temperature range from 40 to 58 °C, about the same amount of heat was delivered by the heat pump for DHW charging.

System V shows an example where the temperature difference between heat pump charging and the heat used for space heating and DHW is lower than in System I, which is an exergetic advantage. However, it is also apparent that substantially more heat has been delivered by the heat pump for DHW charging (temperature range 50 °C – 58 °C) than would be required for covering the DHW demand shown in the blue curve.

System XI on the other hand shows an example for a P/S system with only solar collectors as a heat source of the heat pump for a passive house building.

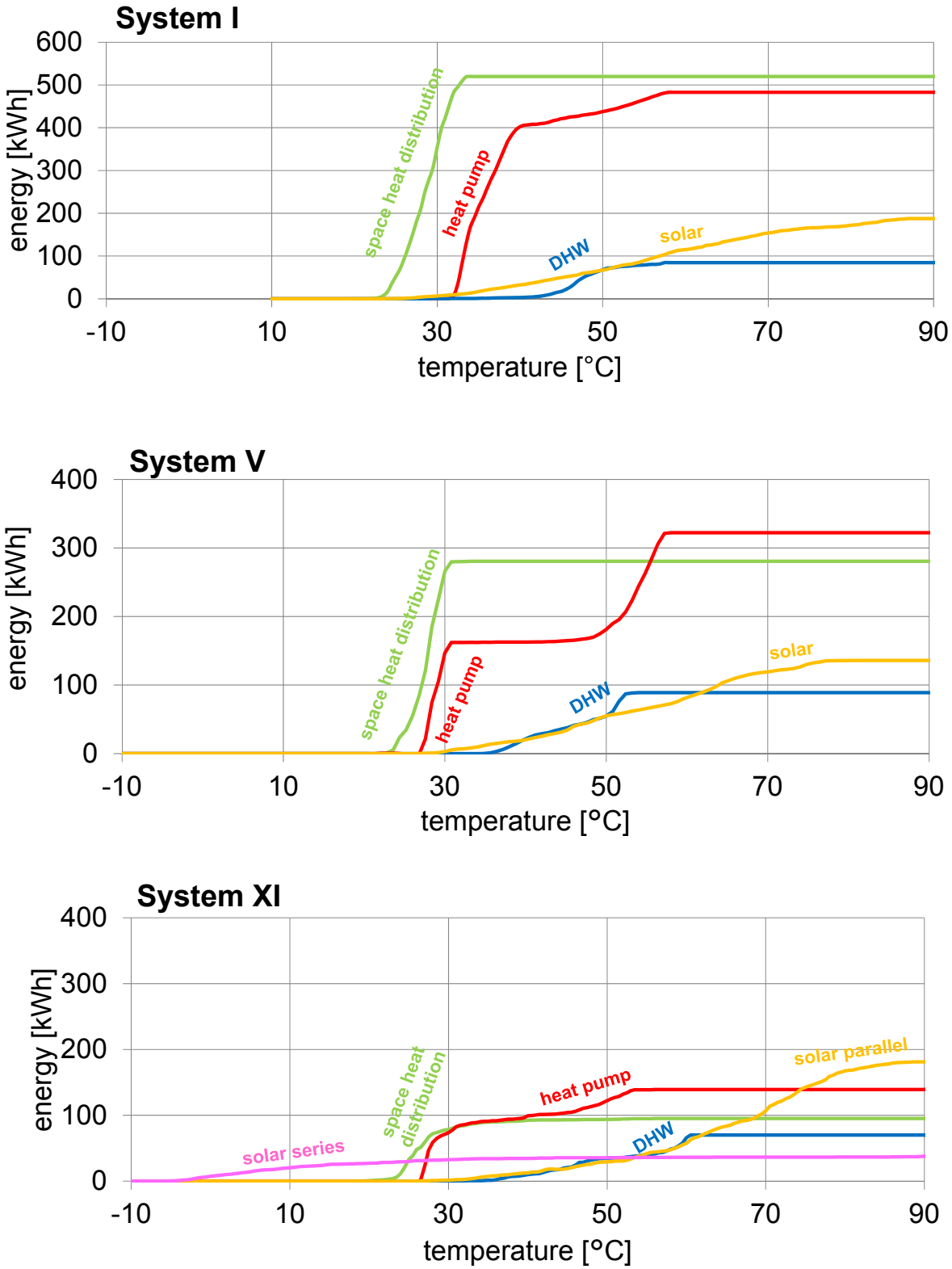

Figure 7.12: Measured data of the accumulated energy over the temperature where the energy was supplied based on twelve day CCT results.

7.2.5 Annual performance figures based on calibrated simulation

Subsequent to the twelve day CCTs, the manufacturers had the choice to commission also annual simulations in order to obtain seasonal performance factors for comparable heat loads. This option was chosen for four of the tested systems: The two systems that had been tested with a design space heat demand of SFH100, one of the systems that had been tested with SFH60, and one of the systems that had been tested with SFH15.

The simulations were performed with the respective design space heat demand from the lab-testing. Exceptions are the systems I and II that were simulated once with a design space heat demand of SFH100, and once with SFH60. The main results of the simulations are shown in Table 7.10.

Table 7.10: Results of annual simulations.

Standard space heat load (Q_{SH}) 100 kWh/(m²a)						
	SPF_{SHP+} [-]	**Q_{SH} [MWh]**	**Q_{DHW} [MWh]**	**$W_{el,tot}$ [MWh]**	**$Q_{HP,DHW}/Q_{DHW}$ [%]**	**Program**
I	4.5	15.5	2.9	4.1	100	TRNSYS
II	3.2	15.5	2.9	5.7	159	TRNSYS
standard space heat load (Q_{SH}) 60 kWh/(m²a)						
	SPF_{SHP+} [-]	**Q_{SH} [MWh]**	**Q_{DHW} [MWh]**	**$W_{el,tot}$ [MWh]**	**$Q_{HP,DHW}/Q_{DHW}$ [%]**	**Program**
I	4.6	11.7	2.9	3.2	100	TRNSYS
II	3.4	11.7	2.9	4.3	151	TRNSYS
V	2.9	11.7	2.8	5.0	166	TRNSYS
standard space heat load (Q_{SH}) 15 kWh/(m²a)						
	SPF_{SHP+} [-]	**Q_{SH} [MWh]**	**Q_{DHW} [MWh]**	**$W_{el,tot}$ [MWh]**	**$Q_{HP,DHW}/Q_{DHW}$ [%]**	**Program**
XI	3.7	2.5	2.2	1.7	n/a	Polysun

Despite of the above indicated room for exergetic improvements, system I achieved the highest seasonal performance factor of 4.6 for SFH60. However, this system was also the only ground source solar and heat pump combination that was used for calibrated annual simulations.

7.3 Discussion and conclusions

7.3.1 Tested systems

With the CCT that were carried out for eleven systems from six manufacturers, covering five different concepts according to the energy flow chart classification, important information was provided for the manufacturers for improving the design, hydraulics, and control of their systems. The recommendations that were given – as far as they do not have to be classified as confidential – were:

- improvements of details for the insulation of the storage and hydraulic connections to the storage that showed to have much larger influence than anticipated by the manufacturer
- improvement of hydraulic integration of heat pump and combistorage
- improvement of storage stratification

- avoidance of natural circulation in hydraulic connections, e.g. across the passive mixing valve for scalding protection in the DHW supply, where natural circulation may heat the uninsulated cold water pipe that is connected to the mixer

A large share of the manufacturers went into a complete re-design of their system concept, changing the storage tank design as well as the hydraulic concept of the system, based on the lessons learnt from the CCT results.

7.3.2 CCT method applied to solar and heat pump systems

Measurements of temperatures and volume flow rates at the boundary of the tested system have allowed to quantify the performance factor of the system within the twelve days test and to compute seasonal performance factors for a whole year based on calibrated annual simulations. Within the tested system's boundary, storage temperatures, as well as temperatures and volume flow rates between the heat pump and the rest of the system, have been measured. These additional measurements were important for a better system understanding and for the detection of potential for system optimization.

For the determination of the exergetic losses within the system hydraulics, the recording of temperature levels and heat delivery from the heat pump condenser and a comparison of these values with the temperatures and quantities of heat delivered to the final use of DHW supply and space heat distribution delivered valuable information.

For systems that use solar collectors as a heat source for the heat pump, the requirements for simulation and emulation of the collector field change significantly compared to the standard collector simulations. Simulation models should be suitable for the simulation of collector operation without solar irradiation, where unglazed collectors may be used as ambient air heat exchangers with free or wind-driven convection on the absorber surface. The models may have to take into account condensation of water vapour when operated below the dew point. For this reason, available collector models had to be extended as shown in section 4.4), and for uncovered absorbers additional measurements were performed to check the suitability of the models and model parameters for this kind of collector operation.

For P/S systems, fast changes in collector inlet temperatures were observed when they switch from parallel to series operation or vice versa. In order to reduce the error of simulation and emulation that arises from incorrect prediction of the inlet temperature for the next time step (based on the inlet temperature measured during the past time step, i.e. ex-ante simulation), two measures proved to be useful:

- the time step for simulation and emulation was reduced from 1/32 h to 1/64 h
- in addition to the ex-ante simulation, an ex-post simulation was performed for the past time step, and the difference between ex-ante and ex-post simulation of this time step was used to correct the power set-point for the next time step (see also Haller et al. 2013d for ex-ante and ex-post simulations).

The collector emulator in the test bench had to be adapted substantially in order to be able to cope with the low temperatures that required an air-tight insulation and a protection of the electric connections of heating elements from condensing water on cold emulator surfaces.

Also for the tests with passive house heat loads several adaptions of the test bench were required in order to cope with the lower mass flow rates in the space heating emulator and in order to reduce the heat losses of the emulator. It also showed that the storage of the system did not fully discharge until the end of the test after it had been heated up in the "summer period" of the test sequence.

The CCT concept that was introduced more than ten years ago (Vogelsanger 2002) followed the approach of letting the installed system act just the way it would in a real installation. This requires that the space heat distribution (pump operation and supply temperature control) is part of the tested system. Consequently, according to the settings of the system controller, a different amount of space heating may be delivered for different control settings – just as would be the case in reality. These differences can be eliminated by the application of a pre-defined space heat load in a calibrated annual simulation (just as has been done for the systems that were also modelled and simulated). However, for systems that were not modelled and simulated, a comparison of the results based on the twelve days test only is extremely difficult because of the different amount of space heat supplied. This short-coming of the test method has been recognized and a method for combining the positive effect of letting the tested system control the space heat distribution, and applying a pre-defined energy target for space heating during the test at the same time, is currently under development.

8 Conclusion

For the distinction of different system concepts, the energy flow chart and the classification as parallel (P), series (S) and regenerative (R) have proved to be of great value and have been adopted by the international research community within and beyond the IEA SHC Task 44 / Annex 38. The introduction of a precise definition of performance figures that are based on the overall system and that include all storage devices was an important step away from the limited view on single components towards the overall system efficiency.

The project SOL-HEAP showed clearly, that the energetic performance of heat pump systems improves significantly by addition of solar heat. The improvements are dependent on the heat pump technology on the one hand, and on the collector area on the other hand. For a typical heat demand in central Europe, it was shown that the seasonal performance factor of the system (SPF_{SHC}) is increasing by 0.07 to 0.1 per m^2 collector area. For example, an air source heat pump system with SPF = 2.9 without solar may increase its performance to SPF = 3.5 with 16 m^2 collector area, while a ground source heat pump may increase its performance from 3.5 to 5.0 with the same collector area.

The increase in system SPF obviously goes along with a decrease in electric energy consumption for the system. Both values are not only dependent on the solar collector area, but also on the climate and the characteristics of the heat load. Electric savings per m^2 of collector area ranged from almost 200 kWh_{el}/m^2 for a system with small solar fraction for the climate and heat load of Davos, down to below 50 kWh_{el}/m^2 for larger collector areas and combisystems in Strasbourg or Helsinki. Electric savings of more than 260 kWh_{el}/m^2 were obtained for DHW systems with daily legionella prevention heating to 60 °C, where heat pump heating was replaced to a large extent by the electric heater.

Monitoring results from a solar and air source heat pump system showed a system SPF (SPF_{SHC}) of 4.4 (5.0 before storage) and thus confirmed the high efficiency that can be achieved with these combinations. The use of a heat tape for keeping the DHW connection between the storage and the DHW distributor warm reduced the SPF from 4.4 to 4.0. The use of heat tapes in combination with solar thermal systems may be seen as a waste of electric energy since the solar thermal system – once installed - provides more than enough heat for DHW at no additional cost during most of the year.

At the beginning of the IEA SHC Task 44 / HPP Annex 38, there were great expectations that system efficiency can be improved by using solar collectors not only in parallel to the heat pump, but also in a series connection to provide heat for the evaporator of the heat pump. Based on a thermodynamic analysis presented in chapter 3, it has been shown that increasing the overall system performance by a series mode of operation instead of a parallel operation of collectors and heat pump is more difficult than anticipated by many. This is consistent with simulation results, laboratory tests, and field tests carried out within T44A38, where no significant increase in system performance was found by using heat from glazed solar collectors in a series connection for a dual source heat pump that can also use another heat source, compared to the system concept where heat pump and collectors are running in parallel. On the other hand, systems that use exclusively solar heat as a source for the heat pump – often equipped with a cold side glycol or ice storage and with unglazed collectors – showed a similar performance as solar and air source heat pump systems, or as ground source heat pump systems without solar. For large sizes of glazed collector areas in combination with a large ice storage, system performance can be in the range of parallel solar and ground source system performance or even above.

Predictive control that uses simple weather forecast may increase the efficiency of an SHP heating system if loading or unloading a storage or thermal capacitance can be controlled based on the forecast. The effect of loading different storages with solar heat based on a perfect daily weather forecast was studied with simulations for systems with storages on both sides of the heat pump: a warm storage on the sink side and an ice storage on the source side. It was shown that for systems with small-sized ice storage and collector field an increase of the SPF_{SHP+} up to 16% can be achieved by predictive control. If the components are large-sized the effect of including weather forecast seems to be negligible.

For all system concepts exergetic efficiency of the storage and of the hydraulic integration play an important role for the overall performance of the system. Exergetic losses may be a result of poor storage stratification or of unfavourable solutions for hydraulic connections and control. Thus, even a system that is composed of excellent components may still perform poorly when the overall design for the hydraulic integration and control is not appropriate. This has been seen both in system simulations as well as in laboratory tests. Recommendations for the proper integration of solar combistorages into systems with heat pumps have been given in section 6.3.

Measurements on heat pumps and on solar absorbers have shown that quite large errors may result from the application of models outside the range that was used for the determination of the parameters for the model. In particular, the extrapolation of COP values of heat pumps towards higher source temperatures and towards lower temperature difference between source and sink was found to produce too optimistic results compared to what was achieved in measurements. Existing solar collector models had to be extended for the operation below the dew point of the air, and for operation as air heat exchangers. The combination of low mass flow rates with small heat gains from the ambient air required to simulate the collector field with more thermal capacitance nodes along the fluid path than for normal collector simulations.

The Concise Cycle Test method has successfully been adapted for the testing of systems that include ground source or air source heat pump systems. Eleven CCTs were carried out for systems provided by six different manufacturers covering five different solar and heat pump concepts according to the energy flow chart classification. These hardware-in-the-loop tests gave detailed information about the dynamic behaviour of the systems in different seasons of the year. The kind of information that is generated is usually only obtained by field testing over a whole year. In comparison to field testing, the CCT method has the advantages of being faster and less costly, providing more measured points with an accuracy and logging frequency that is quite higher than is usually achieved in field testing. Furthermore, CCT measurements are repeatable and thus the results can be compared to other results from CCT where the same boundary conditions for climate and heat load have been applied, whereas repeatability is not achievable at all in field testing. These CCT results were valuable for gaining insight into the exergetic performance of the systems and for the determination of potentials for improving the systems. In particular, storage design, hydraulic integration, and control were aspects where the manufacturers of the systems have re-designed their systems after testing in order to improve the overall system performance.

9 Abbreviations and Symbols

9.1 Abbreviations

CCT	Concise Cycle Test
COP	coefficient of performance
DHW	domestic hot water
HP	heat pump
HPP	Heat Pump Programme (of the IEA)
IEA	International Energy Agency
P	parallel
PF	performance factor
R	regenerative
S	series
S	solar collector
SFH	single family home
SFH100	bulding with 100 kWh/(m2a) SH demand in a ref. climate (Strasbourg for T44A38)
SFH15	bulding with 15 kWh/(m2a) SH demand in a ref. climate (Strasbourg for T44A38)
SFH45	bulding with 45 kWh/(m2a) SH demand in a ref. climate (Strasbourg for T44A38)
SH	space heating
SHC	Solar Heating and Cooling Programme (of the IEA)
SHP	solar and heat pump system
skS	sink storage
Sol	solar irradiation
SPF	seasonal performance factor
SPF	Institut für Solartechnik SPF
srS	source storage
TRY	test reference year
T44A38	IEA SHC Task 44 / HPP Annex 38
W	ground water

9.2 Symbols

See also list of abbreviations

A	area, m^2
a_1	linear heat loss coefficient, W/m^2K
a_2	quadratic heat loss coefficient, W/m^2K^2
b_0	factor for IAM calculation, -
C_{eff}	effective specific heat capacity of the filled collector, J/m^2K
COP	coefficient of performance in terms of heat output divided by electricity input, -
$c_{w,F'}$	influence of wind speed on $F'(\tau\alpha)$, s/m

c_{IR} long wave radiation exchange factor, -

$c_{w,hl}$ wind speed factor, J/m^{3}K

$F'(\tau\alpha)$ effective transmission-absorption product multiplied with the collector efficiency factor, -

$f_{save,el}$ fractional electricity savings compared to a reference system without solar

G solar irradiance, W/m^2

H solar irradiation, J/m^2

K incident angle modifier, -

L long wave irradiance, W/m^2

$\dot{m}$ mass flow rate, kg/s

P power, W

PF performance factor in terms of heat output divided by electricity input, -

Q heat or solar energy, J

$\dot{Q}$ heat transfer rate, W

S entropy, J/K

SPF see Abbreviations, -

T absolute temperature, K

t time, s

U heat transfer coefficient, W(m^{2}K)

u_w wind speed, m/s

V volume, m^3

W work, J

x specific heat loss, W/m^2

greek symbols

ε long wave emissivity, -

γ incident angle, °

η efficiency, -

ϑ temperature, °C

ϑ_m mean collector temperature, °C

σ Stefan-Boltzman constant, W/m^{2}K^4

9.3 Subscripts

abs absorbed

amb ambient

b beam

coll solar thermal collector

cond condenser / condensation gains

Ctr additional controllers that cannot be attributed to HP or SC alone

d diffuse

day restricted by daily limits

dem demand

EH	electric heater elements (direct electric heating) that are not included yet in HP or SC
el	electricity
$evap$	evaporator of the heat pump
$flow$	supply line / flow line
in	inlet
$irrad$	irradiance or irradiation on the collector plane
lat	latent heat
lim	limit
L	long wave radiation exchange
loc	for a given geographical location
mix	fully mixed reference
OFF	during times without collector operation
ON	during times with collector operation
out	outlet
par	parallel heat use (P)
pen	penalty (for not meeting required temperatures to maintain comfort level)
pot	potentially useable for the evaporator of the heat pump
PU	pumps that are not included yet in HP or SC, also including a primary DHW pump for an external DHW heat exchanger if present, but not the space heat distribution pumps
PU,SH	space heat distribution pump
S	short wave irradiance
$save,el$	fractional electric savings
SC	Solar circuit – anything needed to run the solar circuit (pumps, controller - if additional to heat pump controller, valves, air ventilators for hybrid collectors, etc.)
sim	simulated
ser	series heat use (S)
SHP	solar and heat pump system, including all storages and all electricity consumers, without the space heat distribution pump
$SHP+$	solar and heat pump system, including all storages and all electricity consumers, including also the space heat distribution pump
sim	simulated
sol	solar
St	storage
$supply$	supply of (useful) heat
sys	system
uc	uncovered collector (= uncovered absorber)

10 Bibliography

Afjei, T. & Wetter, M., 1997. TRNSYS Type - Compressor heat pump including frost and cycle losses - Version 1.1 - Model description and implementing into TRNSYS.

ANSI/ARI, 1999. Standard 540-1999 “Positive Displacement Refrigerant Compressors and Compressor Units.”

Bertram, E., Glembin, J., Scheuren, J. & Rockendorf, G., 2010. Condensation Heat Gains on Unglazed Solar Collectors in Heat Pump Systems. In: Proc. of the EuroSun 2010 Conference, Graz, Austria.

Bertsch, S., 2009. “Quasidynamischer Wärmepumpen-Simulator”, Computer - Code in EES (Engineering Equation Solver).

Bundesamt für Gesundheit BfG, 2009. Legionellen und Legionellose.

Carbonell, D., Philippen, D., Haller, M.Y. & Frank, E., 2014. Development and Validation of a Mathematical Model for Ice Storages with Heat Exchangers That Can Be De-Iced. In: Proc. of the ISES Solar World Congress 2013, Cancun, Mexico.

Cengel, Y.A., 2003. Heat transfer: a practical approach. McGraw-Hill, Boston.

Citherlet, S., Bony, J. & Nguyen, B., 2008. SOL-PAC - Analyse des performances du couplage d’une pompa à chaleur avec une instnallation solaire thermique pour la rénovation - Rapport final. Swiss Federal Office of Energy (SFOE).

Dott, R., Afjei, T., et al., 2013a. Models of Sub-Components and Validation for the IEA SHC Task 44 / HPP Annex 38 - Report C2 Part C: Heat Pump Models - A technical report of subtask C - Final Draft.

Dott, R., Haller, M., Ruschenburg, J., Ochs, F. & Bony, J., 2013b. The Reference Framework for System Simulations of the IEA SHC Task 44 / HPP Annex 38 - Report C1 Part B: Buildings and Space Heat Load - Final Revised. FHNW, Muttenz, Switzerland.

Frank, E., 2007. Modellierung und Auslegungsoptimierung unabgedeckter Solarkollektoren für die Vorerwärmung offener Fernwärmenetze. PhD Thesis, Universität Kassel, Fachbereich Maschinenbau.

Frank, E., Haller, M., Herkel, S. & Ruschenburg, J., 2010. Systematic Classification of Combined Solar Thermal and Heat Pump Systems. In: Proc. of the EuroSun 2010 Conference, Graz, Austria.

Freeman, T.L., Mitchell, J.W. & Audit, T.E., 1979. Performance of combined solar-heat pump systems. Solar Energy, 22(2), p.125–135.

Haberl, R., Haller, M.Y. & Frank, E., 2013. Combining heat pumps with combistores: detailed measurements reveal demand for optimization. In: SHC conference 2013 - accepted for publication, Freiburg, Germany.

Haberl, R., Haller, M.Y., Konersmann, L. & Frank, E., 2011. Solar & Pellet Heating: Specifications for High Efficiency System Design. In: Proc. of the ISES Solar World Congress 2011, Aug. 28 - Sep. 2, Kassel, Germany.

Haberl, R., Konersmann, L. & Frank, E., 2009. PelletSolar-2 - Systemoptimierung von Pelletfeuerungen in Kombination mit thermischen Solaranlagen basierend auf dynamischen Simulationen und Messungen im Prüfstand. Bundesamt für Energie BFE, Bern.

Haller, M. & Frank, E., 2012. System-Jahresarbeitszahl grösser 4.0 mit Luft-Wasser Wärmepumpe kombiniert mit Solarwärme. In: 22. OTTI Symposium Thermische Solarenergie, 9.-11. Mai 2012, Kloster Banz, Bad Staffelstein, Germany.

Haller, M. & Vogelsanger, P., 2005a. Combisystem Performance Investigation. In: J. C. Hadorn, Ed. Thermal Energy Storage for Solar and Low Energy Buildings - State of the Art by the IEA Solar Heating and Cooling Task 32. IEA-SHC, pp. 41–45.

Haller, M. & Vogelsanger, P., 2005b. Kombi-Kompakt+ Schlussbericht, korrigierte Version von 2005. Bundesamt für Energie BFE, Bern.

Haller, M.Y., 2010. Combined Solar and Pellet Heating Systems - Improvement of Energy Efficiency by Advanced Heat Storage Techniques, Hydraulics, and Control. PhD Thesis, Graz University of Technology, Graz, Austria.

Haller, M.Y., 2014. System Simulation Reports for the IEA SHC Task 44 / HPP Annex 38 - A technical report of subtask C - Report C3 – Final.

Haller, M.Y., Dott, R., Ruschenburg, J., Ochs, F. & Bony, J., 2013a. The Reference Framework for System Simulations of the IEA SHC Task 44 / HPP Annex 38 - Report C1 Part A: General Boundary Conditions - Final Revised. Report C1 Part A, Institut für Solartechnik SPF, Hochschule für Technik HSR, Rapperswil, Switzerland.

Haller, M.Y. & Frank, E., 2010. Kombination von Wärmepumpen mit solarthermischen Kollektoren - Konzepte und Fragestellungen. In: CD - Konferenzbeiträge 16. Status-Seminar “Forschung und Bauen im Kontext von Energie und Umwelt”, 2./3. Sep., BRENET - Nationales Kompetenznetzwerk Gebäudetechnik und erneuerbare Energien, ETH Zürich, 1–6.

Haller, M.Y. & Frank, E., 2011a. On the Potential of Using Heat from Solar Thermal Collectors for Heat Pump Evaporators. In: Proc. of the ISES Solar World Congress 2011, Aug. 28 - Sep. 2, Kassel, Germany.

Haller, M.Y. & Frank, E., 2011b. Steigert die Nutzung von Solarkollektoren als Wärmequelle für Wärmepumpen die System-Arbeitszahl? In: 21. Symposium Thermische Solarenergie, 11. - 13. Mai, OTTI Regensburg, Bad Staffelstein, Germany, CD.

Haller, M.Y., Haberl, R., Mojic, I. & Frank, E., 2013b. Hydraulic integration and control of heat pump and combi-storage: Same components, big differences. In: SHC conference 2013 - accepted for publication, Freiburg, Germany.

Haller, M.Y., Haberl, R., Mojic, I. & Frank, E., 2013c. Solare Kombispeicher mit Wärmepumpen: Scheinbare Details entscheiden über die Performance! In: 23. Symposium Thermische Solarenergie, 24.-26. April 2013, OTTI e. V., Regensburg, Kloster Banz, Bad Staffelstein, Germany.

Haller, M.Y., Haberl, R., Persson, T., Bales, C., Kovacs, P., Chèze, D. & Papillon, P., 2013d. Dynamic whole system testing of combined renewable heating systems – The current state of the art. Energy and Buildings, 66, p.667–677.

Haller, M.Y., Yazdanshenas, E., Andersen, E., Bales, C., Streicher, W. & Furbo, S., 2010. A method to determine stratification efficiency of thermal energy storage processes independently from storage heat losses. Solar Energy, 84(6), p.997–1007.

Hantzsche, F., 2011. Untersuchung unabgedeckter Kollektoren für den Einsatz in Solarthermie-Wärmepumpen-Systemen. Bachelor Thesis, Institut für Solartechnik SPF of the University of Applied Sciences HSR & Fakultät für Maschinenbau und Verfahrenstechnik der Hochschule Offenburg, Raperswil & Offenburg.

Heimrath, R. & Haller, M., 2007. Project Report A2 of Subtask A: The Reference Heating System, the Template Solar System - A Report of IEA SHC Task 32: Advanced Storage Concepts for So-

lar and Low Energy Buildings.

Heinz, A. & Haller, M., 2013. Appendix A3 - Description of TRNSYS Type 877 by IWT and SPF. In: . In: Models of Sub-Components and Validation for the IEA SHC Task 44 / HPP Annex 38 - Part C: Heat Pump Models - FINAL - A technical report of subtask C Report C2 Part C.

Hirsch, H., 2010. Latentwärmespeicher auf Wasser/Eis-Basis mit horizontaler Wärmeübertragungsfläche. Bachelor Thesis, FH Nordhausen, Germany & Institut für Solartechnik SPF, Switzerland.

Huber, A., 1999. Hydraulische Auslegung von Erdwärmesondenkreisläufen. Bundesamt für Energie BFE, Bern.

Huber, A. & Schuler, O., 1997. Berechnungsmodul für Erdwärmesonden. im Auftrag des Bundesamtes für Energiewirtschaft, Bern.

Isakson, P. & Eriksson, L.O., 1994. MFC 1.0Beta Matched Flow Collector Model for simulation and testing - User's manual. Royal Institute of Technology, Stockholm, Sweden.

Jordan, U. & Vajen, K., 2000. Influence of the DHW Load Profile on the Fractional Energy Savings: A Case Study of a Solar Combi-System with TRNSYS Simulations. Solar Energy, 69(1-6), p.197–208.

Jordan, U., Vajen, K., Streicher, W. & Letz, T., 2003. Performance of Solar Combisystems. In: W. Weiss, Ed. Solar Heating Systems for Houses - A Design Handbook for Solar Combisystems. James & James, London, pp. 125–162.

Konersmann, L., Haller, M. & Vogelsanger, P., 2007. PelletSolar - Leistungsanalyse und Optimierung eines Pellet-Solarkombinierten Systems für Heizung und Warmwasser. im Auftrag des Bundesamt für Energie BFE, Bern.

Logie, W., Frank, E., Haller, M.Y. & Rommel, M., 2010. Investigation of Immersed Coil Heat Exchangers in regard to Heat Transfer and Storage Stratification. In: Proc. of the EuroSun 2010 Conference, Graz, Austria.

Malenkovic, I., 2013. Definition of Main System Boundaries and Performance Figures for Reporting on SHP Systems. Report Deliverable B1, IEA SHC Task 44 / HPP Annex 38 - Solar and Heat Pump Systems.

Malenkovic, I., 2011. Proposal for the discussion on performance figures for solar and heat pump systems – Deliverable B1 v2.

MeteoSchweiz, 1999. Bundesamt für Meteorologie und Klimatologie. Available at: http://www.meteoschweiz.admin.ch/web/de.html [Accessed December 7, 2010].

Miara, M., Günther, D., Kramer, T., Oltersdorf, T. & Wapler, J., 2011. Wärmepumpen Effizienz - Messtechnische Untersuchung von Wärmepumpenanlagen zur Analyse und Bewertung der Effizienz im realen Betrieb. Fraunhofer ISE, Freiburg, Germany.

Morrison, G.L., 1994. Simulation of Packaged Solar Heat-Pump Water Heaters. Solar Energy, 53(3), p.249–257.

Nipkow, J., Suter, J.-M. & Mathez, S.A., 2011. Neue Norm SIA 385/1, gültig ab 1. Mai 2011: Anlagen für Trinkwarmwasser in Gebäuden - Grundlagen und Anforderungen - Warmwasser: höherer Anteil in Wärmebilanz. HK-Gebäudetechnik, 11(5), p.78–79.

Palyvos, J., 2008. A survey of wind convection coefficient correlations for building envelope energy systems' modeling. Applied Thermal Engineering, 28(8-9), p.801–808.

Perers, B., 2010. An Improved Dynamic Solar Collector Model Including Condensation and Asymmet-

ric Incidence Angle Modifiers. In: Proc. of the EuroSun 2010 Conference, Graz, Austria.

Perers, B. & Bales, C., 2002. A Solar Collector Model for TRNSYS Simulation and System Testing - A Technical Report of Subtask B of the IEA-SHC - Task 26.

Philippen, D., Haller, M.Y. & Frank, E., 2011. Einfluss der Neigung auf den äusseren konvektiven Wärmeübergang unabgedeckter Absorber. In: 21. Symposium Thermische Solarenergie, 11. - 13. Mai, OTTI Regensburg, Bad Staffelstein, Germany, CD.

Philippen, D., Haller, M.Y., Frank, E. & Brunold, S., 2012a. Entwicklung einer hocheffizienten Solarthermie- Wärmepumpen-Heizung mit Eisspeicher. In: 17. BRENET Status-Seminar "Forschen für den Bau im Kontext von Energie und Umwelt" - 13./14. September 2012, ETH-Zürich.

Philippen, D., Haller, M.Y., Logie, W., Thalmann, M., Brunold, S. & Frank, E., 2012b. Development of a heat exchanger that can be de-iced for the use in ice stores in solar thermal heat pump systems. In: Proc. of the EuroSun 2012 Conference, Rijeka and Opatija, Croatia.

Poppi, S. & Bales, C., 2013. Influence of hydraulics and control of thermal storage in solar assisted heat pump combisystems. In: SHC conference 2013 - accepted for publication, Freiburg, Germany.

Ruschenburg, J., Herkel, S. & Henning, H.-M., 2013. A statistical analysis on market-available solar thermal heat pump systems. Solar Energy, 95, p.79–89.

Sporn, P. & Ambrose, E.R., 1955. The Heat Pump And Solar Energy. In: Proc. of the World Symposium on Applied Solar Energy, The Association for Applied Solar Energy, Stanford Research Institute, Menlo Park California, Phoenix, US, 159–170.

TREN D1, 2002. Tren D1 D(2002) M/324 - Mandate to Cen and Cenelec for the Elaboration and Adoption of Measurement Standards for Household Appliances: Water-Heaters, Hot Water Storage Appliances and Water Heating Systems.

Trinkl, C., Zörner, W. & Hanby, V., 2004. A Review on Solar-Assisted Heat Pump Systems for Domestic Heating. In: Proc. of the EuroSun 2004 Conference, Freiburg, 1, 734 – 743.

Vogelsanger, P., 2002. The Concise Cycle Test Method - A Twelve Day System Test - A Report of IEA SHC - Task 26. International Energy Agency Solar Heating and Cooling Programme.

Wetter, M. & Huber, A., 1997. TRNSYS Type 451 - Vertical Borehole Heat Exchanger EWS Model Version 2.4. Zentralschweizerisches Technikum Luzern & Huber Energietechnik.

Zimmermann, S., 2012. Einfluss der Speicherschichtung auf die Jahresarbeitszahl von WP-Solar Systemen. Bachelor Thesis, Institut für Solartechnik SPF, University of Applied Sciences HSR, Rapperswil, Switzerland.

Annex A Publications and presentations

A.1 Conference proceedings

Carbonell, D., Haller, M.Y., Philippen, D. & Frank, E., 2014. Simulations of Combined Solar Thermal and Heat Pump Systems for Domestic Hot Water and Space Heating. Energy Procedia, 48, p.524–534.

Frank, E., Haller, M., Herkel, S. & Ruschenburg, J., 2010. Systematic Classification of Com-bined Solar Thermal and Heat Pump Systems. In: Proc. of the EuroSun 2010 Confe-rence, Graz, Austria.

Haberl, R., Haller, M.Y., Reber, A. & Frank, E., 2014. Combining Heat Pumps with Combistores: Detailed Measurements Reveal Demand for Optimization. Energy Procedia, 48, p.361–369.

Haberl, R., Haller, M.Y., Reber, A. & Frank, E., 2013. Solare Kombispeicher mit Wärmepumpen: Labormessungen der Jahresleistung zeigen Optimierungspotential. In: 23. Symposium Thermische Solarenergie, 24.-26. April 2013, OTTI e. V., Regensburg, Kloster Banz, Bad Staffelstein, Germany.

Haller, M. & Frank, E., 2010. Kombination von Wärmepumpen mit solarthermischen Kollekto-ren - Konzepte und Fragestellungen. In: CD - Konferenzbeiträge 16. Status-Seminar "Forschung und Bauen im Kontext von Energie und Umwelt", BRENET - Nationales Kompetenznetzwerk Gebäudetechnik und erneuerbare Energien, ETH Zürich, 1-6.

Haller, M. & Frank, E., 2012. System-Jahresarbeitszahl grösser 4.0 mit Luft-Wasser Wärmepumpe kombiniert mit Solarwärme. In: 22. OTTI Symposium Thermische Solarenergie, 9.-11. Mai 2012, Kloster Banz, Bad Staffelstein, Germany.

Haller, M., Frank, E., Trinkl, C. & Zörner, W., 2010. Systematische Gliederung der Systemkombination von solarthermischen Anlagen mit Wärmepumpen. In: 20. OTTI Sympo-sium Thermische Solarenergie, Bad Staffelstein, Germany.

Haller, M., Haberl, R. & Frank, E., 2013. Integration von Kombispeichern in Solar-Wärmepumpenanlagen. In: News aus der Wärmepumpen-Forschung - 19. Tagung des BFE-Forschungsprogramms “Wärmepumpen und Kälte,” Burgdorf, Switzerland.

Haller, M.Y. & Frank, E., 2011a. On the Potential of Using Heat from Solar Thermal Collec-tors for Heat Pump Evaporators. In: Proc. of the ISES Solar World Congress 2011, Aug. 28 - Sep. 2, Kassel, Germany.

Haller, M.Y. & Frank, E., 2011b. Steigert die Nutzung von Solarkollektoren als Wärmequelle für Wärmepumpen die System-Arbeitszahl? In: 21. Symposium Thermische Solar-energie, 11. - 13. Mai, OTTI Regensburg, Bad Staffelstein, Germany, CD.

Haller, M.Y., 2011. Entwicklung von Prüfverfahren für Anlagen mit Kombination aus Wärmepumpen und Solarthermie. In: VDI-Fachkonferenz Wärmepumpen 2011 - Umweltwärme effizient nutzen, 7. - 8. Juni 2011, Frankfurt, VDI Wissensforum GmbH, Düsseldorf, Germany, 159-167.

Haller, M.Y., Bertram, E., Dott, R., Afjei, T., Ochs, F. & Hadorn, J.-C., 2012. Review of component models for the simulation of combined solar and heat pump heating systems. In: Solar Heating and Cooling (SHC) Conference 2012, San Francisco.

Haller, M.Y., Haberl, R., Mojic, I. & Frank, E., 2014. Hydraulic Integration and Control of Heat Pump and Combi-storage: Same Components, Big Differences. Energy Procedia, 48, p.571–580.

Haller, M.Y., Haberl, R., Mojic, I. & Frank, E., 2013. Solare Kombispeicher mit Wärmepumpen: Scheinbare Details entscheiden über die Performance! In: 23. Symposium Thermische Solarenergie, 24.-26. April 2013, OTTI e. V., Regensburg, Kloster Banz, Bad Staffelstein, Germany.

Philippen, D., Haller, M.Y. & Frank, E., 2011. Einfluss der Neigung auf den äusseren konvektiven Wärmeübergang unabgedeckter Absorber. In: 21. Symposium Thermische Solarenergie, 11. - 13. Mai, OTTI Regensburg, Bad Staffelstein, Germany, CD.

A.2 Journal paper with contributions from this project

Haller, M.Y., Haberl, R., Persson, T., Bales, C., Kovacs, P., Chèze, D. & Papillon, P., 2013. Dynamic whole system testing of combined renewable heating systems – The current state of the art. Energy and Buildings, 66, p.667–677.

A.3 Bachelor and Master Thesis

Gemperle, S., 2010. Analyse einer solarthermisch unterstützten Luft-Wasser-Wärmepumpenheizung. Bachelor Thesis, Institut für Solartechnik SPF, University of Applied Sciences HSR, Rapperswil-Jona, Switzerland.

Hirsch, H., 2010. Latentwärmespeicher auf Wasser/Eis-Basis mit horizontaler Wärmeübertragungsfläche. Bachelor Thesis, FH Nordhausen, Germany & Institut für Solartechnik SPF, Switzerland.

Hantzsche, F., 2011. Untersuchung unabgedeckter Kollektoren für den Einsatz in Solarthermie-Wärmepumpen-Systemen. Bachelor Thesis, Institut für Solartechnik SPF of the University of Applied Sciences HSR & Fakultät für Maschinenbau und Verfahrenstechnik der Hochschule Offenburg, Raperswil & Offenburg.

Zimmermann, S., 2012. Einfluss der Speicherschichtung auf die Jahresarbeitszahl von Wärmepumpen-Solar Systemen, Bachlorarbeit an der Hochschlule für Technik HSR, Institut für Solartechnik SPF.

A.4 Presentations without publication

Other than T44A38 meetings

Date	***Event & Place***	***Title***	***Presenter & Authors***
2013-04-08	Industry Workshop of the IEA SHC Task 44 / HPP Annex 38, Mechelen, Portugal	Hydraulic Integration of Heat Pumps with Combistores	M. Haller, R. Haberl, I. Mojic, A. Reber
2012-03-21	SPF Industrietag, Rapperswil, Switzerland	Kombination von Solarthermie mit Wärmepumpen	M.Haller, D. Philippen R. Haberl
2012-03-29	Swissolar ERFA WP-Solar on, Muttenz, Switzerland	Kombination von Solarthermie mit Wärmepumpen	M.Haller, D. Philippen R. Haberl
2012-04-04	Swissolar ERFA WP-Solar, Buchs, Switzerland	Kombination von Solarthermie mit Wärmepumpen	M.Haller, D. Philippen R. Haberl
2013-01-23	Sonnen-Symposium, Graz, Austria	Kombination von Solarthermie mit Wärmepumpen	M.Haller
2013-03-14	SPF Industrietag, Rapperswil, Switzerland	Anbindung von Wärmepumpen an Kombispeicher	M.Haller, R. Haberl
2013-04-18	SolPumpEff Abschluss-Workshop "Solarthermie und Wärmepumpenkombinationen - Heizsysteme der Zukunft?", Wels, Austria	Solare Kombispeicher mit Wärmepumpe – Details entscheiden über die Performance	M.Haller, R. Haberl

International T44A38 meetings (without presentations for Subtask C lead)

Date	*Event & Place*	*Title*	*Presenter & Authors*
2010-04-29	Meeting 1, Bolzano, Italy	Systematic classification of combined systems	E. Frank, M. Y. Haller
2010-04-29	Meeting 1, Bolzano, Italy	Development of a holistic system test method for Hp-solar systems (CCT) in combination with a suitable climatic chamber for the SPF system test rig	M. Y. Haller
2010-04-29	Meeting 1, Bolzano, Italy	Advanced semi-physical TRNSYS Heat Pump Model	M. Y. Haller
2011-04-07	Meeting 3, Barcelona, Spain	Monitoring of a parallel solar and heat pump system	M. Y. Haller
2011-04-07	Meeting 3, Barcelona, Spain	Combined Solar and Heat Pump Systems: A Thermodynamic Analysis	M. Y. Haller
2011-04-07	Meeting 3, Barcelona, Spain	Influence of the inclinationon the energy transfer of uncovered collectors	D. Philippen
2011-10-19	Meeting 4, Marseilles, France	Type 877 - A new heat pump model for TRNSYS	A. Heinz, M.Y. Haller
2013-04-08	Meeting 6, Mechelen, Belgium	Hydraulic Integration of Heat Pumps with Combistores	M.Y. Haller, R. Haberl, I. Mojic, A. Reber

Annex B Boundary conditions for system simulations

The base climates used for the simulation framework are Strasbourg (moderate), Helsinki (cold) and Athens (warm). In addition to these, Davos is used for an extreme mountainous climate and Montreal for an extreme continental climate (see Figure 10.1).

The permission granted by Meteotest (Switzerland) to use the corresponding Meteonorm climate data-sets for work within T44A38 is gratefully acknowledged.

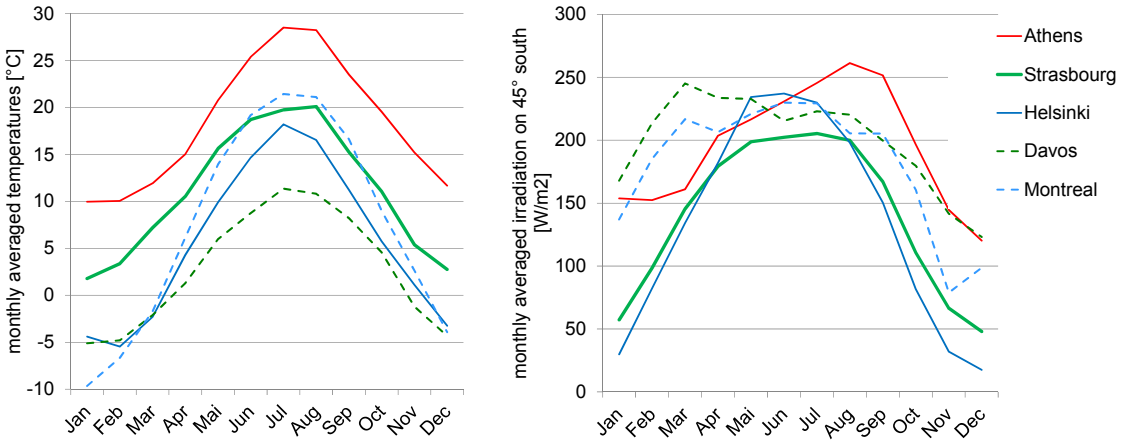

Figure 10.1: Monthly average values for ambient temperature and solar irradiation on the 45° inclined surface for the climates chosen for T44A38.

B.1 Building load and DHW demand

The building load is based on the simulation of a one-zone building (Dott et al. 2013b) that was derived from previous IEA SHC Tasks 26 & 32. Three different thermal energy performance levels have been used. For easy identification, these buildings have been labelled according to their rounded heating demand in the climate of Strasbourg in kWh/(m^{2}a), as SFH15, SFH45, and SFH100. The annual energetic balance of these buildings for the climate of Strasbourg is shown in Figure 10.2, and a comparison for SFH45 placed in different climates is shown in Figure 10.3. Low temperature (floor heating) systems have been assumed for SFH15 and SFH45, and a radiator heating system with higher temperatures has been assumed for SFH100[12]. Table 10.1 shows for the three climates of Strasbourg, Helsinki, and Athens the nominal supply and return temperatures of the hydronic heat distribution system, together with the design heating demand.

The supply temperature of the heat distribution system is controlled depending on to the 24 h averaged ambient air temperature, and the room temperature set point that is always 20 °C. Thermostatic valves are assumed in all distribution loops for the reference case, reducing the

[12] The simulation of air-based heat distribution system is excluded here due to a lack of contributions to T44A38 from countries where these systems are predominantly used.

mass flow rate when the room temperature rises, and the heat distribution system is completely off when the 12 h averaged ambient temperature rises above the limit for the heating season.

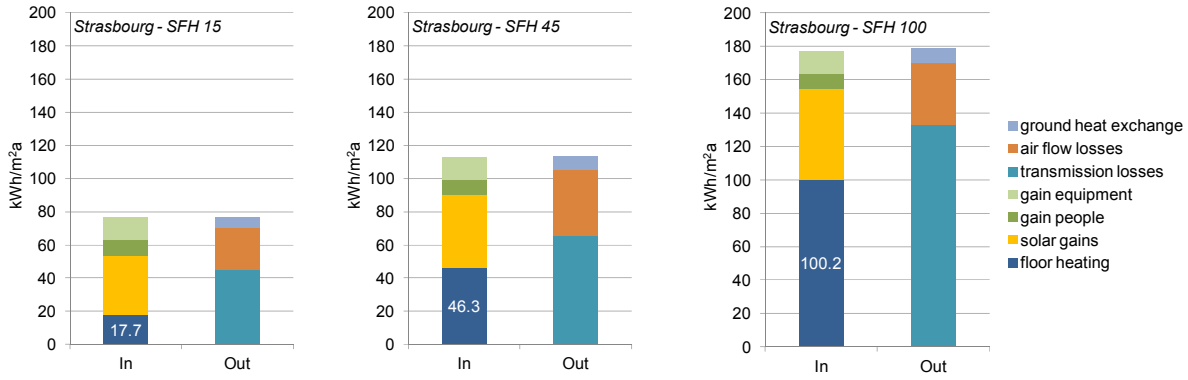

Figure 10.2: Resulting building energy balances for the three different houses at the climate of Strasbourg.

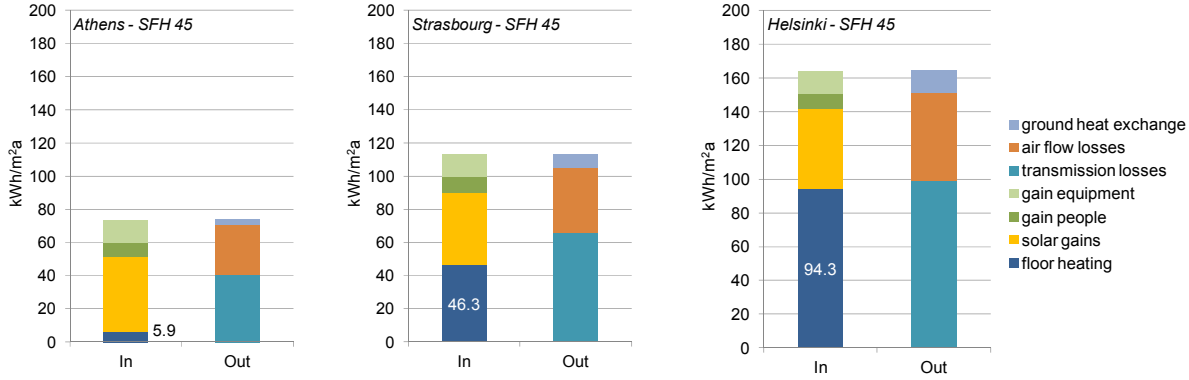

Figure 10.3: Resulting building energy balances of the SFH 45 at three different locations.

Table 10.1: Building dependent heating system parameters: design heat load, in- and outlet temperatures, and heating season limit.

			building		
climate	***value***		***SFH15***	***SFH45***	***SFH100***
all	ambient temperature limit for heating season	°C	12	14	15
ST	space heating power at design conditions	W	1'792	4'072	7'337
	supply / return temperature at design conditions	°C	35 / 30	35 / 30	55 / 45
AT	space heating power at design conditions	W	0	1'310	3'382
	supply / return temperature at design conditions	°C	35 / 30	35 / 30	55 / 45
HE	space heating power at design conditions	W	3'097	6'315	10'931
	supply / return temperature at design conditions	°C	35 / 30	40 / 35	60 / 50

Seasonal performance factors can be improved considerably in simulation by assuming lower supply and return systems of the space heating system only, without improving the system that delivers the heat. For this reason, a key question for the benchmarking of the central heating unit(s) is which was the temperature level required for satisfying the heat demand. Figure 10.4 answers this question by showing for each climate and heat load the cumulative energy delivered to the space heat distribution, versus the maximum temperature of the supply and return line. These curves have been obtained from the hourly averaged heat supply

to the space heat distribution system and the hourly averaged values of the inlet and outlet temperatures of the space heat distribution system. For each temperature on the x-axis of the plot the y-axis value is obtained by integrating the heating power of all hours of the year where the temperature of space heat distribution supply or return was below the respective value. From these plots it can be derived that, e.g. for SFH 100 in the climate of Strasbourg the space heating load is 14 MWh/a, and about 6 MWh are delivered with supply temperatures below 40 °C and return temperatures below 25 °C.

For the comparison of solar and heat pump system performance, these are the most important curves (besides the share and temperature requirements of DHW on the total demand) that two different simulations have to match in order to be comparable!

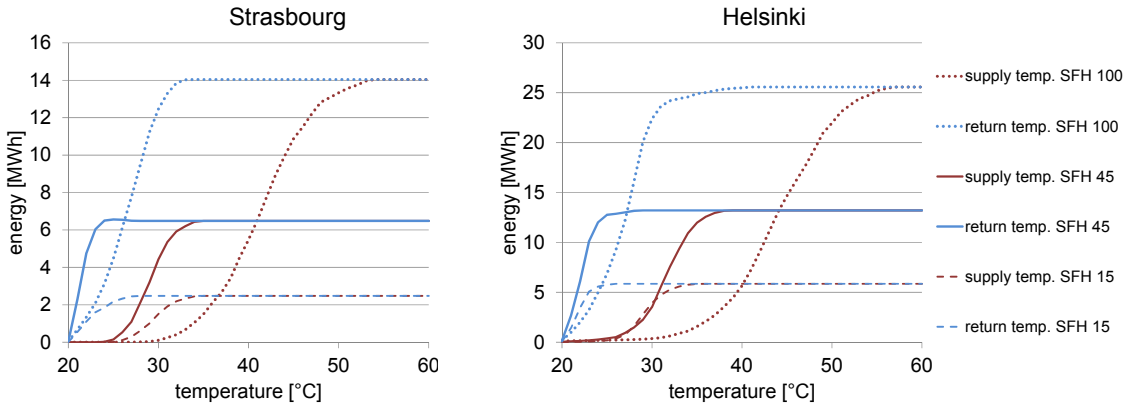

Figure 10.4: Energy-temperature-plots showing cumulative energy demand of the building vs. maximum supply and return temperatures for the two locations Strasbourg and Helsinki.

The domestic hot water load is based on the EU mandate M/324 tapping cycle M (TREN D1 2002, p.324). In order to be suitable for the use in annual simulations, adaptations have been made in order to introduce one bath tub tapping per week, the dependency of hot water demand on the cold water temperature of each location and annual fluctuations. The resulting DHW demand is for Strasbourg 2076 kWh/a, for Helsinki 2398 kWh/a, and for Athens 1648 kWh/a.

In order to assure that the simulated systems are comparable also in terms of comfort provided which manifests in the temperatures of the room and in the DHW temperatures, an "electric energy consumption penalty" is added to the electric consumption of the system whenever the room temperature drops below 19.5 °C or the 2 min. averaged DHW temperature drops below 45 °C. Details on this procedure can be found in Report C3 of T44A38 (Haller 2014).

B.2 Other boundary conditions

For the simulation of ground heat exchangers, reference ground properties are defined together with standard heat exchanger design (e.g. number and lengths of probes) for the climates of Strasbourg and Helsinki. The standard simulation uses vertical borehole heat exchangers with double-U pipes, 0.18 m borehole diameter 0.026 m inner pipe diameter, thermal conductivity of the ground and of the filling material are 2 W/(mK) for the base case.

The number and length of the boreholes are different for each building and each climate as shown in Table 10.2.

Table 10.2: Number and length of borehole heat exchangers for the different locations and buildings.

		Strasbourg			***Helsinki***		
		SFH15	***SFH45***	***SFH100***	***SFH15***	***SFH45***	***SFH100***
Max. heat extraction	kW	3.5	4.2	7.0	3.5	5.6	10.5
borehole(s)	m	49	84	2 x 90	75	2 x 95	4 x 95